

## Mechanical Snakes

### Path-Following Instruments for Minimally Invasive Surgery

Henselmans, Paul

#### DOI

[10.4233/uuid:6e67ef39-843c-43a5-bd39-02f24ab23c18](https://doi.org/10.4233/uuid:6e67ef39-843c-43a5-bd39-02f24ab23c18)

#### Publication date

2020

#### Document Version

Final published version

#### Citation (APA)

Henselmans, P. (2020). *Mechanical Snakes: Path-Following Instruments for Minimally Invasive Surgery*. [Dissertation (TU Delft), Delft University of Technology]. <https://doi.org/10.4233/uuid:6e67ef39-843c-43a5-bd39-02f24ab23c18>

#### Important note

To cite this publication, please use the final published version (if applicable). Please check the document version above.

#### Copyright

Other than for strictly personal use, it is not permitted to download, forward or distribute the text or part of it, without the consent of the author(s) and/or copyright holder(s), unless the work is under an open content license such as Creative Commons.

#### Takedown policy

Please contact us and provide details if you believe this document breaches copyrights. We will remove access to the work immediately and investigate your claim.

# **MECHANICAL SNAKES**

**Path-Following Instruments for Minimally Invasive Surgery**

**Paulus Wilhelmus Johannes HENSELMANS**

Title: *Mechanical Snakes: Path-Following Instruments for Minimally Invasive Surgery*

Author: *Paul W.J. Henselmans (p.henselmans@gmail.com)*

Cover illustration by: *Stephan Timmers*

ISBN: 9789464022131

This research was funded by the Netherlands Organization for Scientific Research (NWO), project 12137

An electronic version of this dissertation is available at <http://repository.tudelft.nl>

Copyright 2019, P.W.J. Henselmans

*All right reserved. No part of this book may be reproduced by any means, or transmitted without the written permission of the author. Any use or application of data, methods and/or results etc. occurring in this report will be at the user's own risk.*

# **MECHANICAL SNAKES**

**Path-Following Instruments for Minimally Invasive Surgery**

## **PROEFSCHRIFT**

ter verkrijging van de graad van doctor  
aan de Technische Universiteit Delft,  
op gezag van de Rector Magnificus prof. dr. ir. T.H.J.J. van der Hagen  
voorzitter van het College voor Promoties,  
in het openbaar te verdedigen op  
vrijdag 15 mei 2020 om 10:00 uur

door

**Paulus Wilhelmus Johannes HENSELMANS**

werktuigkundig ingenieur, Technische Universiteit Delft, Nederland  
geboren te Geldrop, Nederland

Dit proefschrift is goedgekeurd door de promotoren.

**Samenstelling promotiecommissie bestaat uit:**

Rector Magnificus	voorzitter
Prof. dr. ir. P. Breedveld	Technische Universiteit Delft, promotor
Dr. ir. G. Smit	Technische Universiteit Delft, copromotor

**Onafhankelijke leden:**

Prof. dr. P. Valdastrì	Universiteit van Leeds, Verenigd Koninkrijk
Prof. dr. W.J.H.J. Meijerink	Radboud Universiteit Nijmegen
Prof. dr. ir. J.L. Herder	Technische Universiteit Delft
Prof. dr. J. Dankelman	Technische Universiteit Delft
Dr. E. van der Poorten	Katholieke Universiteit Leuven, België
Prof. dr. H.E.J. Veeger	Technische Universiteit Delft, reservelid

# TABLE OF CONTENTS

<b>SUMMARY</b>	<b>IX</b>
<b>SAMENVATTING</b>	<b>XIII</b>
<b>Chapter 1 - Introduction</b>	<b>1</b>
1.1 Surgical technology	2
1.2 From open surgery to minimally invasive surgery	2
1.3 Challenges of minimally invasive surgery	4
1.4 Steerable instruments & flexible endoscopes	6
1.5 Follow-the-leader instruments	9
1.6 Mechatronic versus mechanical control	14
1.7 Goal of this thesis	15
1.8 Approach and outline	15
1.9 References	17
<b>Chapter 2 - HelixFlex: Squid-inspired mechanical snake</b>	<b>21</b>
Abstract	22
2.1 Introduction	23
2.1.1 <i>Endoscopic endonasal surgery</i>	23
2.1.2 <i>Steerable instruments</i>	24
2.1.3 <i>Multi-steerable instruments</i>	26
2.1.4 <i>Objectives and requirements</i>	27
2.2 New approach: multi-actuation	30
2.3 Multi-actuation: from 2D to 3D	34
2.4 HelixFlex prototype	37
2.5 Prototype evaluation	39
2.6 Discussion	41
2.7 Conclusion	45
2.8 References	46
<b>Chapter 3 - HelicoFlex: Mechanical snake through minimum assembly</b>	<b>51</b>
Abstract	52
3.1 Introduction	53
3.2 Conceptual design	55
3.2.1 <i>Design requirements</i>	55
3.2.2 <i>Design choices</i>	56

3.3	Proof of concept: HelicoFlex	58
3.4	Additive manufacturing the HelicoFlex	60
3.5	HelicoFlex performance	62
3.6	Discussion	63
3.7	Conclusion	68
3.8	References	68
<b>Chapter 4 - MemoFlex I: Path-following using a single spatial track</b>		<b>73</b>
	Abstract	74
4.1	Introduction	75
4.2	State of the art	76
	4.2.1 <i>Instruments using a virtual track</i>	76
	4.2.2 <i>Instruments using a physical track</i>	77
4.3	A new approach	78
4.4	Proof of concept	81
	4.4.1 <i>Master design</i>	81
	4.4.2 <i>Slave design</i>	83
	4.4.3 <i>Proof of concept prototype: MemoFlex I</i>	84
4.5	Performance test	84
4.6	Discussion	87
	4.6.1 <i>NOTES</i>	88
	4.6.2 <i>Future developments</i>	88
4.7	Conclusion	89
4.8	References	89
<b>Chapter 5 - MemoFlex II: Path-following using multiple planar tracks</b>		<b>93</b>
	Abstract	94
5.1	Introduction	95
	5.1.1 <i>State of the art</i>	95
	5.1.2 <i>Advantages and disadvantages</i>	96
	5.1.3 <i>Goal</i>	97
5.2	Mechanism design	97
	5.2.1 <i>Mechanical Follow-the-Leader concept in 2D</i>	97
	5.2.2 <i>Mechanical Follow-the-Leader concept in 3D</i>	99
	5.2.3 <i>Cable-configuration in the 3D shaft</i>	99
	5.2.4 <i>Full 3D concept</i>	100
5.3	Experimental setup	102
	5.3.1 <i>Reverse engineering the tracks</i>	104
	5.3.2 <i>Experimental measurements</i>	104
5.4	Results	105
5.5	Further optimization of the system	107
5.6	Discussion	109

5.6.1	<i>Performance</i>	109
5.6.2	<i>An individual track per cable</i>	110
5.6.3	<i>Model-based engineering of the tracks</i>	110
5.6.4	<i>The MemoFlex II in a medical setting</i>	111
5.7	Conclusion	112
5.8	References	112
<b>Chapter 6 - MemoSlide: Programmable mechanism for path-following</b>		<b>117</b>
	Abstract	118
6.1	Introduction	119
6.1.1	<i>State of the art</i>	120
6.1.2	<i>Problem statement and goal</i>	122
6.2	Mechanism design	122
6.2.1	<i>Miniaturization of the shaft with the cable-ring mechanism</i>	122
6.2.2	<i>Cable control for Follow-the-Leader motion</i>	124
6.2.3	<i>The alternating memory mechanism</i>	125
6.3	Proof of concept prototype	126
6.4	Functional evaluation	129
6.5	Discussion	130
6.5.1	<i>The range of the MemoSlide</i>	130
6.5.2	<i>Design choices</i>	130
6.5.3	<i>The MemoSlide as a surgical instrument</i>	131
6.6	Conclusion	134
6.7	References	135
<b>Chapter 7 - Discussion &amp; conclusions</b>		<b>139</b>
7.1	Main findings of this study	140
7.2	Limitations of this study	141
7.3	Mechanical versus mechatronic path-following	142
7.4	Clinical implementation	144
7.5	Medical and industrial applications	146
7.6	Recommendation for future research	148
7.7	Conclusions	150
7.8	References	151
<b>Acknowledgments</b>		<b>154</b>
<b>Curriculum vitae</b>		<b>157</b>
<b>Publications</b>		<b>158</b>



# SUMMARY

Surgical procedures are inherently invasive as they require the surgeon to cut into the body to create a surgical pathway towards the diseased area, resulting in surgical trauma for the patient. The field of Minimally Invasive Surgery (MIS) strives to reduce surgical trauma by minimizing the size and number of incisions. The used instrumentation plays an important role in this pursuit. Instrumentation that is currently in use is either straight and rigid, demanding a straight surgical pathway, or flexible, allowing for multi-curved surgical pathways. The currently existing flexible instruments, such as, for example, a catheter guided by the blood vessel wall, rely on external support and guidance from the anatomical environment. The ability to follow multi-curved surgical pathways without the need for anatomical guidance extends the reach of surgery and is especially useful in less accessible areas such as, for example, the human skull base. The skull base is a dense anatomical area that, next to important structures such as the pituitary gland, supports a network of fragile nerves and blood vessels. In such a delicate anatomical environment, flexible instruments cannot find the necessary external support and guidance. This implies a need for instrumentation that is not only flexible, but also steerable. A logical next step is the development of steerable snake-like instruments that can follow multi-curved pathways through the body without the need for external support or guidance from the anatomical environment. This kind of functionality is new in surgery and a topic of research in multiple research institutes around the world. Nevertheless, solutions that are thin, stiff and affordable are not yet available.

Similar to a biological snake that continuously adapts the shape of its entire body as it moves forward, the shape of a snake-like instrument also needs to be fully controllable. In practice, this will require multiple elements of the instrument to be controlled simultaneously. Humans are not particularly good in this kind of multi-tasking, while robots may excel at such tasks. Therefore, when trying to solve control problems concerning snake-like motion, a natural tendency exists to search for robotic solutions. Medical instrumentation does, for obvious reasons, have to meet high-quality standards. As a consequence, medical-grade robotics tend to be very expensive. The objective of this thesis is, therefore, to explore the possibilities for mechanically-controlled solutions for path-following cable-driven instruments that are suitable for surgical applications.

The work is divided into two parts; Part I (Chapters 2 and 3) focuses on the construction of cable-driven snake-like instruments and in Part II Chapters 4, 5 and 6) mechanically-controlled solutions for such cable-driven instruments to perform path-following motion, are explored.

## **PART I: CABLE-DRIVEN MECHANICAL SNAKES**

In Part I inspiration was found in the tentacle of Loliginid squid, which attains its flexibility by using multi-directional muscle structures. In Chapter 2, these muscle structures have been translated into a multi-directional cable-configuration for steering a surgical instrument. This cable-configuration consists partially of cables that follow a straight route along the instrument. These cables can deform the instrument into a single bend. The cable-configuration also includes cables that follow a helical route along the instrument. These cables can deform the instrument into an S-shaped curve. By the simultaneous use of straight and helical cables, intermediate shapes are achieved and the instrument can be steered in a way that resembles the fluent motion of a tentacle. The result is a novel handheld steerable instrument called HelixFlex which supports a Ø5.8 mm thick and 60 mm long steerable shaft. The direction and position of the tip of the shaft can be independently controlled in four degrees of freedom (DOFs); a functionality that can prove useful during, for example, transnasal (through the nose) surgery.

The intricate designs of cable-driven snake-like instruments typically result in demanding fabrication and assembly processes. In Chapter 3 the use of 3D-printing is explored for simplifying the production of such instruments. This resulted in the development of a helical structure that is compliant, yet axially and torsion stiff. Moreover, the structure can be 3D-printed from a single piece of material without the need for printed support. This structure was incorporated into a handheld prototype called HelicoFlex. The instrument's Ø8 mm thick and 60 mm long shaft is steered by manually deforming its handle. The shaft consists of five steerable segments, providing a total of ten DOFs. Moreover, the shaft supports four inner lumens that make it possible to guide fiber optics for vision and multiple tools (e.g. flexible graspers and surgical knives) for performing surgical interventions. Evaluation of the HelicoFlex shows that each shaft-segment can be individually controlled in two planes, and C-curves, S-curves and more complex 3D-shapes can be created. Although the HelicoFlex itself contains a total of five steerable segments, a 192 mm long shaft with sixteen segments was successfully 3D-printed as well. This shaft is steerable in 32 DOFs, making more complex shapes possible. Based on the level of steerability, this shaft-design seems very suitable for path-following motion along multi-curved pathways.

## **PART II: MECHANICALLY-CONTROLLED PATH-FOLLOWING**

In Chapter 4 a concept of a mechanical control strategy is presented for following fixed surgical pathways that are determined before the surgical procedure. This concept is based on a 3D-track (for example, a steel rod) that is shaped in the form of the desired

path and is placed outside the patient. The 3D-track is inserted into a mechanism that captures the track's 3D shape. A snake-like instrument, positioned inside the patient's body, is connected to this mechanism via cables in such a way that it copies the shape of the 3D-track. By moving the entire instrument forward, the shape of the 3D-track is captured and simultaneously mimicked by the snake-like instrument. In this way, the snake-like instrument follows the desired path inside the body of the patient. The concept was embodied in the MemoFlex I prototype which supports a Ø5 mm thick and 112 mm long shaft that is steerable in 28 DOFs. The MemoFlex I shows the feasibility of mechanically-controlled path following. Accurately capturing the shape of a 3D-track did, however, prove mechanically challenging, especially with a mechanism composed out of rigid links. Moreover, the use of a single 3D-track means that antagonistic steering cables must be directly coupled to one another and cannot be independently controlled, resulting in backlash and hysteresis in the system.

In Chapter 5, the lessons learned from the MemoFlex I led to a revised concept for mechanically-controlled path-following wherein the single 3D-track is split into four 2D-tracks. In this way, control over the antagonistic cables is separated, which makes it possible to (partially) compensate for the play and hysteresis in the system. This concept was successfully implemented in the MemoFlex II prototype, which also incorporates the 3D-printed Ø8 mm shaft design from Chapter 3. A 192 mm long shaft that is steerable in 32 DOFs can be supported, yet more satisfying path-following behavior was achieved using an 84 mm long shaft with 14 DOFs. The MemoFlex II outperforms the MemoFlex I, following pre-determined paths more accurately and showing more fluency in its motion.

The fixed nature of the 2D-tracks of the MemoFlex II requires them to be determined before the mechanism starts moving, thus before the surgical procedure. In Chapter 6 the possibility of making the 2D-tracks on-demand programmable, thus during the surgical procedure, is explored. This resulted in an innovative mechanism that captures a control algorithm for cable-driven path-following, enabling the user to change the direction of the snake-like instrument head at any time during the motion. Using the mechanism, the user's steering-action is stored in a mechanical memory-bank and, as the instrument moves forward, the stored steering-actions are passed on backward along the instrument. In this way, the snake-like instrument will follow the path that is initiated by its tip. The mechanism was implemented in the MemoSlide prototype; a mechanical memory-bank capable of creating a discretely programmable 2D-track on-demand. Although the MemoSlide itself is not yet connected to a snake-like instrument and is also too large to be successful in a surgical setting, it does show that on-demand mechanically-controlled path-following is a feasible solution.

This work ends with a discussion, reflecting on the proposed concepts for path-following snake-like instrumentation for minimally invasive surgery. Although control over such instrumentation is most often realized with robotics technology, this thesis shows that mechanical control strategies for path-following are possible for following fixed pathways, and feasible for following variable pathways that are created on-demand. Although the mechanically-controlled solutions might not yet be able to reach an equal level of precision or versatility as their robotic counterparts, they may deliver satisfactory performance at, presumably, lower production costs.

# SAMENVATTING

Chirurgische ingrepen hebben een invasief karakter, omdat de chirurg door middel van incisies een chirurgisch pad moet vrijmaken tot het te opereren gebied. Dit resulteert in letsel voor de patiënt. Het veld van minimaal invasieve chirurgie streeft ernaar om dit letsel zoveel mogelijk te reduceren, door het aantal en de grootte van de incisies te verkleinen. Hierbij speelt de gebruikte instrumentatie een belangrijke rol. De huidige instrumentatie is ofwel recht en rigide waardoor het pad naar het te opereren gebied rechtlijnig moet zijn, ofwel flexibel waardoor het instrument kronkelige paden af kan leggen terwijl het ondersteund en geleid wordt door het lichaam van de patiënt. Een voorbeeld van een dergelijk flexibel instrument is een katheter die langs de bloedvatwand wordt geleid. Het kunnen afleggen van kronkelige paden kan het bereik van een operatie vergroten. Dit kan met name van meerwaarde zijn bij moeilijk begaanbare gebieden in het lichaam, zoals bijvoorbeeld de hersenbasis. Dit is een gebied met een hoge anatomische dichtheid waarin zich belangrijke organen en een netwerk van fragiele zenuwbanen en bloedvaten bevinden. Deze delicate omgeving biedt weinig steun voor de geleiding van flexibele instrumenten. De instrumenten zouden daarom niet enkel flexibel maar ook stuurbaar moeten zijn. Dit vraagt om de ontwikkeling van stuurbare slangachtige instrumenten die zonder externe ondersteuning of geleiding de benodigde kronkelige chirurgische paden kunnen afleggen. Dergelijke functionaliteit is nieuw in de chirurgie en wordt momenteel wereldwijd door meerdere onderzoeksgroepen onderzocht. Ondanks deze inspanningen zijn oplossingen voor slangachtige instrumenten die zowel dun, stijf als betaalbaar zijn nog niet beschikbaar.

Zoals een slang continu zijn gehele lichaam vervormt wanneer het dier zich voortbeweegt, moet ook de vorm van een slangachtig instrument op soortgelijke wijze gecontroleerd kunnen worden. In de praktijk betekent dit dat meerdere onderdelen van het instrument tegelijkertijd aangestuurd dienen te worden. Robots zijn aanzienlijk beter in dergelijke multitasking dan mensen. Vrijwel alle wereldwijde onderzoeken op dit gebied richten zich dan ook op gerobotiseerde systemen. Aan medische apparatuur wordt echter hoge eisen gesteld en mede hierdoor kunnen de kosten voor medische robotica snel oplopen. Dit onderzoek is dan ook gericht op de ontwikkeling en beoordeling van mechanische besturingssystemen voor kabel-aangedreven slangachtige chirurgische instrumenten die zich over kronkelige paden moeten kunnen voortbewegen.

Het proefschrift is opgesplitst in twee delen. In Deel I (Hoofdstukken 2 en 3) wordt de constructie van kabel-aangedreven slangachtige instrumenten onderzocht. In Deel II (Hoofdstukken 4 tot en met 6) worden de mechanische besturingssystemen voor de voortbeweging van dergelijke kabel-aangedreven instrumenten behandeld.

## DEEL I: KABEL-AANGEDREVEN MECHANISCHE SLANGEN

In Hoofdstuk 2 worden tentakels van de Loliginid-inktvis als inspiratiebron gebruikt voor de constructie van kabel-aangedreven stuurbare instrumenten. Tentakels verlenen hun flexibiliteit aan multidirectionele spierstructuren. Deze spierstructuren zijn vertaald in een multidirectionele kabelconfiguratie, welke onder andere kabels bevat die recht langs het instrument zijn geplaatst. Deze maken een C-vormige beweging mogelijk. Daarnaast bevat de kabelconfiguratie ook kabels die een helixvormige route om het instrument volgen. Deze maken een S-vormige beweging mogelijk. Door het gelijktijdig gebruik van beide soorten kabels kunnen ook tussenvormen worden gerealiseerd, waardoor het instrument kan worden aangestuurd op een manier die overeenkomt met de vloeiende beweging van een tentakel. Het resultaat is een manueel bestuurbaar instrument genaamd HelixFlex, met een Ø5.8 mm dikke en 60 mm lange stuurbare schacht. De richting en de positie van het uiteinde van de schacht kunnen onafhankelijk van elkaar in vier vrijheidsgraden worden bestuurd; een functionaliteit die onder andere nuttig kan zijn bij het bereiken van de hypofyse via transnasale (via de neus) chirurgie.

De doorgaans ingewikkelde ontwerpen van kabel-aangedreven instrumenten resulteren in veeleisende fabricage- en montageprocessen. In Hoofdstuk 3 wordt daarom onderzoek gedaan naar de inzet van 3D-printing voor een versimpeling van het productieproces van kabel-aangedreven slangachtige instrumenten. Het resultaat is een flexibele, maar axiaal- en torsiestijve structuur die uit één stuk materiaal 3D-geprint kan worden, zonder het gebruik van extra ondersteunend materiaal. Deze structuur is opgenomen in een slangachtig instrument, genaamd HelicoFlex. Dit instrument bevat een Ø8 mm dikke en 60 mm lange schacht welke kan worden aangestuurd door het handvat manueel te vervormen. De schacht bestaat uit vijf stuurbare segmenten en kan daarmee in totaal in tien vrijheidsgraden worden vervormd. Verder heeft het instrument vier interne kanalen waardoor chirurgische hulpmiddelen, zoals grijpertjes en schaaftjes, naar het te opereren gebied kunnen worden geleid. Evaluatie van de HelicoFlex laat zien dat elk schacht-segment individueel in twee vlakken kan worden bestuurd. Hierdoor kan het instrument onder andere C-vormen, S vormen en complexere 3D vormen aannemen. Hoewel de HelicoFlex is uitgevoerd met vijf stuurbare schacht-segmenten, is er ook een 192 mm lange schacht met zestien segmenten 3D geprint. Deze schacht is bestuurbaar in 32 vrijheidsgraden en kan zodoende nog complexere vormen aannemen dan de eerste variant. Door deze mate van stuurbaarheid lijkt het schacht-ontwerp dan ook erg geschikt voor het volgen van kronkelige paden.

## **DEEL II: MECHANISCHE BESTURINGSSYSTEMEN VOOR HET VOLGEN VAN PADEN**

In Hoofdstuk 4 wordt een concept van een mechanisch besturingssysteem gepresenteerd voor het volgen van paden die vóór de operatie zijn vastgesteld. Dit concept gaat uit van een 3D-spoor, gerepresenteerd door een verbogen metalen stang. De vorm van dit 3D-spoor wordt, buiten het lichaam van de patiënt, door een mechanisme afgetast. Een slangachtig instrument is door middel van kabels aan dit aftastende mechanisme verbonden, en kan zo de vorm van het 3D-spoor kopiëren. Door nu het gehele instrument voorwaarts te bewegen, wordt de vorm van het 3D-spoor afgetast en tegelijkertijd door het slangachtige instrument gekopieerd. Op deze manier kan het slangachtige instrument het vooraf bepaalde pad door het lichaam afleggen. De haalbaarheid van dit concept is aangetoond in een prototype genaamd MemoFlex I. De MemoFlex I bevat een  $\varnothing 5$  mm en 112 mm lange schacht die in 28 vrijheidsgraden gestuurd kan worden. Het nauwkeurig aftasten en kopiëren van het 3D-spoor bleek een flinke uitdaging, onder andere vanwege het feit dat de rigide schakels in het mechanisme het vloeiend aftasten van het 3D-spoor bemoeilijkten. Daarnaast betekende het gebruik van één enkel 3D-spoor dat antagonistische stuurkabels met elkaar gekoppeld zijn en hierdoor niet onafhankelijk van elkaar bestuurd kunnen worden, wat resulteerde in speling en hysteresis in het systeem.

De bevindingen uit Hoofdstuk 4 hebben geleid tot een herziening van het mechanische besturingssysteem van de MemoFlex I. In Hoofdstuk 5 wordt een nieuw concept onderzocht, waarbij het 3D-spoor is opgesplitst in vier 2D-sporen. Dit heeft tot gevolg dat antagonistische kabels niet langer aan elkaar gekoppeld zijn, waardoor de mogelijkheid ontstaat om (gedeeltelijk) te compenseren voor speling en hysteresis in het systeem. Dit concept is succesvol uitgewerkt in een prototype genaamd MemoFlex II, waarin ook gebruik wordt gemaakt van het 3D-geprinte schacht-ontwerp uit Hoofdstuk 3, uitgebreid tot 16 individueel bestuurbare segmenten. Het prototype kan een  $\varnothing 8$  mm dikke en 192 mm lange schacht met maximaal 32 vrijheidsgraden besturen, maar de meest bevredigende resultaten worden behaald met een 84 mm lange schacht met 14 vrijheidsgraden. De MemoFlex II presteert beter dan de MemoFlex I in het volgen van vooraf vastgestelde kronkelige paden, en vertoont daarnaast ook een meer vloeiende beweging.

De vooraf vastgestelde 2D-sporen van de MemoFlex II dienen vóór de beweging, dus vóór de operatie, te worden vastgesteld. In Hoofdstuk 6 wordt de mogelijkheid onderzocht om de 2D-sporen ad hoc, dus tijdens de operatie, instelbaar te maken. Om dit te bewerkstelligen is een algoritme voor het volgen van een instelbaar pad vastgelegd in een mechanisme. Met dit mechanisme kan de gebruiker de tip van een slangachtig instrument besturen, waarna deze stuuractie wordt opgeslagen in een mechanische geheugenbank. Op het moment dat het slangachtige instrument wordt voortbewogen,

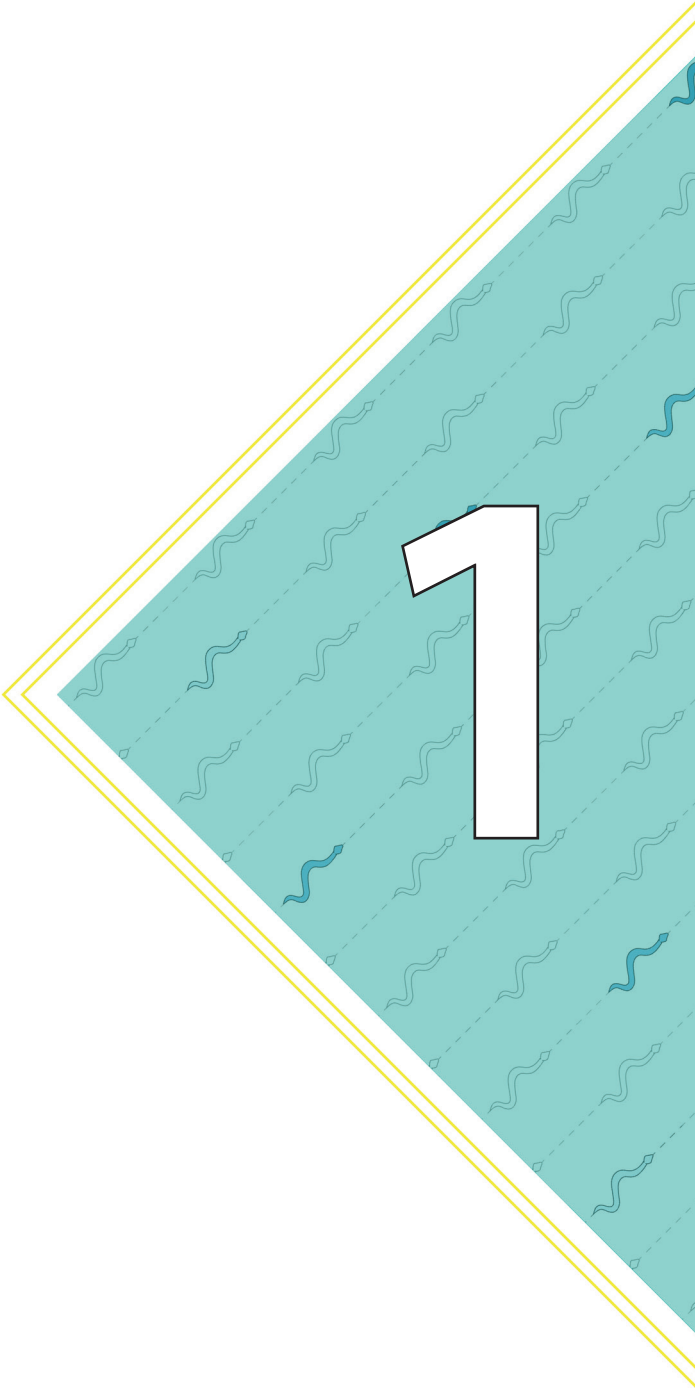
zal de eerder gegeven stuuractie aan de tip naar achteren door het instrument worden doorgegeven. Op deze manier legt het slangachtige instrument het pad af dat door de kop is ingezet. Dit mechanisme is geïmplementeerd in een vernuftig prototype genaamd MemoSlide; een mechanische geheugenbank waarmee de gebruiker een stapsgewijs-instelbaar 2D-spoor kan creëren. Hoewel de MemoSlide nog niet is gekoppeld aan een slangachtig instrument, en ook nog te groot is om succesvol te kunnen zijn in een chirurgische setting, toont het wel de haalbaarheid van mechanisch besturingssysteem aan voor het volgen van paden die ad hoc worden gecreëerd.

Dit proefschrift wordt afgesloten met een discussie waarin wordt gereflecteerd op de eerdergenoemde ontwikkelde concepten van slangachtige instrumentatie voor minimaal invasieve chirurgie. Terwijl de besturing van dergelijke instrumentatie vooralsnog vaak gepaard gaat met robotica, toont dit proefschrift de succesvolle inzetbaarheid van mechanische besturingssystemen aan. De mogelijkheid tot het volgen van vooraf vastgestelde paden is hierbij bewezen, en het volgen van instelbare paden blijkt plausibel. Hoewel de mechanische besturingssystemen nog niet in staat zijn om een even hoog niveau van precisie of veelzijdigheid te bereiken als hun robotachtige tegenhangers, kunnen ze wel bevredigende prestaties leveren tegen, naar verwachting, veel lagere productiekosten.





# INTRODUCTION



## 1.1 SURGICAL TECHNOLOGY

Technology has always played a vital role in the development of surgery, often standing at the forefront of surgical breakthroughs. These breakthroughs are often the result of a symbiotic interaction between surgeons and engineers. On one side, advances in technology developed by the engineer present the surgeon with new possibilities, extending the reach of surgery. On the other side, it is the surgeon who develops new procedures and pushes the boundaries of that technology, often finding new ways of utilizing the available instrumentation.

Surgery is an inherently invasive procedure, as becomes apparent when looking at its definition given by the Cambridge online dictionary:

*Surgery: The treatment of injuries or disease in people or animals by cutting open the body and removing or repairing the damaged part [1].*

By “cutting open the body”, a surgical pathway is created through which the targeted area can be reached. As will be explained in the following sections, the invasiveness of a surgical procedure closely relates to the surgical pathway that is taken. The choice for a particular pathway is in turn influenced by the available technology. The purpose of the technology that is presented in this thesis is to reduce the invasiveness of surgical interventions by extending the possibilities in surgical pathways.

## 1.2 FROM OPEN SURGERY TO MINIMALLY INVASIVE SURGERY

Since the beginning of surgery there has always been a quest for the optimal balance between the inherent trauma caused by surgery, and the impairment the operation is meant to repair. Surgery is inherently invasive, as in order to gain access to the diseased area, a pathway needs to be created. Moreover, once arrived at the diseased area the instruments require a certain workspace. This workspace has to be available or otherwise created. Creating a pathway and workspace near the diseased area is damaging to the patient, as is especially apparent during traditional open surgical procedures. In these procedures, the surgeon must be able to look directly at the diseased area, dictating a straight and broad surgical pathway. Moreover, the techniques for cutting and suturing are based on the dexterity of the surgeon's hands. The surgeon, therefore, needs to be able to reach the hands close to the operated area. To provide sufficient view and workspace to maneuver the hands, large incisions are necessary. Larger incisions relate to higher chances of infection and longer recovery times [2-4]. In some cases, the invasiveness of

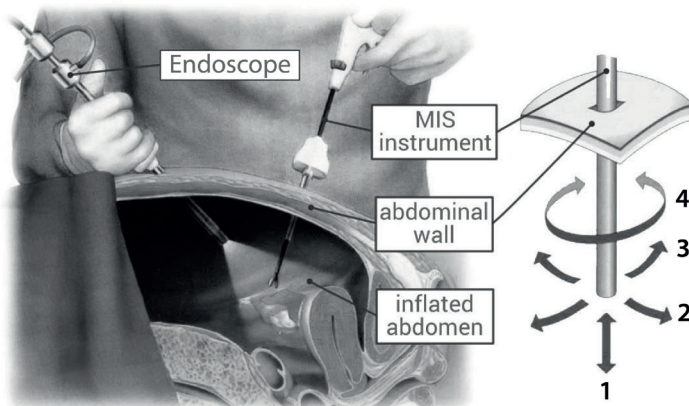


Figure 1.1: Minimally invasive surgery (MIS) Left: Laparoscopy, a minimally invasive procedure in the abdomen. Right: The four degrees of freedom of a MIS instrument [9].

the procedure can be so immense that recovering from the surgical trauma related to the pathway takes the longest time. An example is the maxillary swing approach where the upper jaw and parts of the nose are temporarily moved aside, for the resection of tumors at the nasopharynx (back of the throat) [5].

Minimally Invasive Surgery (MIS) strives to limit the invasiveness of surgical procedures by reducing the necessary access and workspace to a minimum. MIS involves the use of long and slender instruments that are inserted through small incisions in the body [6]. Such instruments typically consist of a straight shaft (max Ø5 mm) with on one side a handle and on the other an end-effector, e.g. a grasper, curette or scissors. An example is presented in Figure 1.1, which shows a minimally invasive procedure called laparoscopy in the abdomen. The largest difference as compared to open surgery is that, instead of relying on a direct line of sight, the diseased area is visualized on a screen using an endoscope. An endoscope is basically a small camera on a slender stick that can be used to visualize the diseased area from up close. As compared to open surgery, the surgical trauma is significantly reduced due to the smaller sizes of the incisions. Since the introduction of the first high-resolution endoscope in 1982, MIS has replaced many of the traditional open surgical procedures. For example, nowadays 90% of the cholecystectomies (removal of the gall bladder) in the Netherlands are carried out using MIS [7, 8].

MIS leads to faster recovery times and less scar tissue [2]. The most obvious beneficiary of MIS is, therefore, the patient. Society, however, benefits as well as the faster recovery times reduce the costs of hospitalization and stimulate a swifter re-entry of the patient into society [10]. The fact that both the patient and society benefit from MIS explains its rapid acceptance since the '80s.

### 1.3 CHALLENGES OF MINIMALLY INVASIVE SURGERY

1

Apart from the upsides for the patient and society, a downside of MIS includes the severe restrictions it places on the maneuverability of the instrumentation. First of all, the small incisions restrict the sideways motions of the instruments. As a result, the positioning of the instrument's end-effector is reduced from six degrees of freedom (DOFs) during open surgery to the four DOFs indicated in Figure 1.1. Secondly, the incision acts as a fulcrum point. As a consequence the two sideways angular DOFs are reversed, i.e. movement of a surgeon's hand to the right results in the end-effector moving to the left, and vice versa. Finally, the fulcrum point makes the instrument act as a lever of which the ratio changes as the instrument slides in and out of the body, i.e. the angular movements of the surgeon's hands are amplified or reduced at the end-effector based on this continuously changing ratio. Next to problems with instrument maneuverability, another major disadvantage is that the surgeon now has to monitor the instrument movements on a screen, challenging depth perception and hand-eye coordination [9]. For these reasons, MIS is more demanding for a surgeon than traditional open surgery.

It was in the '80s that laparoscopy became the first field of surgery wherein MIS was broadly accepted. This was not an arbitrary choice as the abdomen can be inflated with gas, which expands the available workspace. This additional workspace increases instrument maneuverability, which makes the abdomen very well suited for MIS. Moreover, the additional workspace means that incisions can be placed further apart, allowing for the diseased area to be approached from multiple angles.

MIS is more challenging in denser anatomic areas that cannot be inflated. Firstly, the limited workspace leaves less room for instrument maneuverability. Secondly, the density of the area often limits the choice for angles of approach. This is taken to the extreme during endonasal (entry through the nose) surgery at the skull base, first reported on in 1997 by H.D Jho and R.L. Carrau [11]. The skull base is the area just beneath the brain where the spinal cord leaves the brain. This area houses important structures, one of which is the pituitary gland that regulates hormone secretion and is also called the master gland of the endocrine system. The pituitary gland is cradled by the sella turcica, which is positioned above a cavity called the sphenoidal sinus. The pituitary gland is surrounded by delicate and important structures such as the optic chiasm (crossing of the optic nerves) and the cavernous sinus which houses a network of cranial nerves and the internal carotid arteries (Figure 1.2). Traditionally, the pituitary gland was reached using an open surgical approach such as a bifrontal craniotomy, which requires the temporal removal of a bone plate from the forehead and pushing aside the brain for access (Figure 1.3, top left). During the endonasal transsphenoidal approach for removing adenomas of the pituitary gland, the instruments are inserted through one or two nostrils, as illustrated in

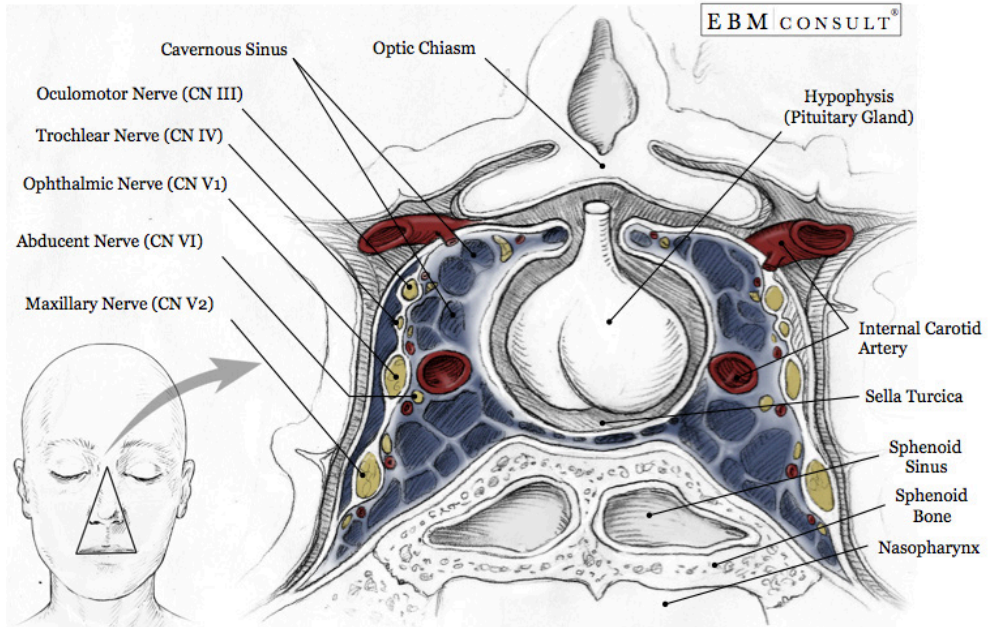


Figure 1.2: Frontal cross view of the pituitary gland that sits in the sella turcica, surrounded by the optic chiasm and cavernous sinus that houses numerous nerves and the internal carotid arteries (courtesy of Evidence-based Medicine Consult [12]).

Figure 1.3 (top right & bottom). First, the cavity of the nose has to be prepared to create access for the instruments, which means moving or removing parts of the conchae (bone plates inside the nose that increase surface area). After passing the narrow nasal cavity, holes are drilled through the bony wall of the sphenoid sinus and the floor of the sella turcica. This is a very precise task, as the hole must be drilled near the carotid arteries and damaging them can have fatal consequences. Next, resection of the adenoma can begin, which is again a very precise task as, for example, merely touching the optic chiasm can already lead to (partial) loss of vision. Through the surgical pathway from nose to pituitary gland, the instruments are restricted by the nostrils and the two holes in the bony walls of the sphenoidal sinus and sella turcica. These restrictions make changing the direction of the end-effector close to impossible. As a result of the highly limited sideways movement of the end-effector, the maneuverability is nearly restricted to only two DOFs: a translation and rotation around the longitudinal axis of the instrument shaft. Moreover, the nostrils only allow for a single angle of approach. Next to that, there is a maximum number of instruments that fit the nostrils, which usually means only two instruments can be used at one time. The dense anatomical environment of the skull base thus particularly hampers the maneuverability of standard rigid MIS instrumentation.

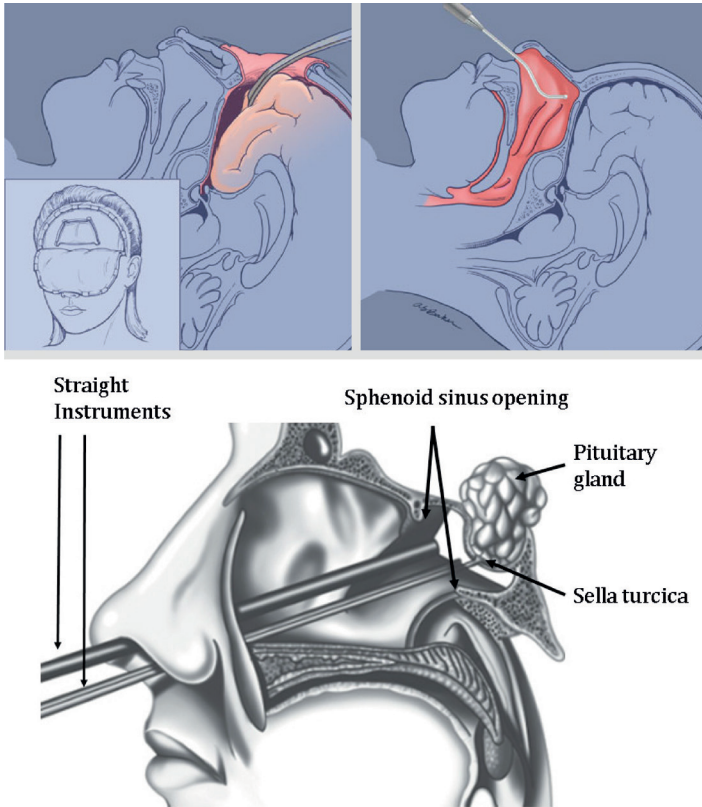


Figure 1.3: Surgical approaches to the pituitary gland. Top left: Bifrontal craniotomy, an open surgical procedure (adapted from [13]). Top right & bottom: The endonasal transsphenoidal approach (adapted from [14]).

#### 1.4 STEERABLE INSTRUMENTS & FLEXIBLE ENDOSCOPES

One way of handling the severe restrictions on instrument maneuverability is to include some sort of steerability close to the instrument's end-effector. In this way, the end-effector can be re-directed while its rigid shaft remains in place. There are several handheld steerable instruments on the market, for example the LaproFlex (Amsterdam, the Netherlands, DEAM) or SILS hand instruments (Minneapolis, Minnesota, USA, Medtronic) [15, 16]. The best known steerable instrument is the EndoWrist, which is incorporated in the Da Vinci surgical robotic system (Sunnyvale, California, USA, Intuitive Surgical) as illustrated in Figure 1.4. The Da Vinci system consists of one or even two surgeon consoles and four robotic arms that position the instruments. The EndoWrist has two planar joints that are placed perpendicular to each other at the end of the rigid shaft. This allows the

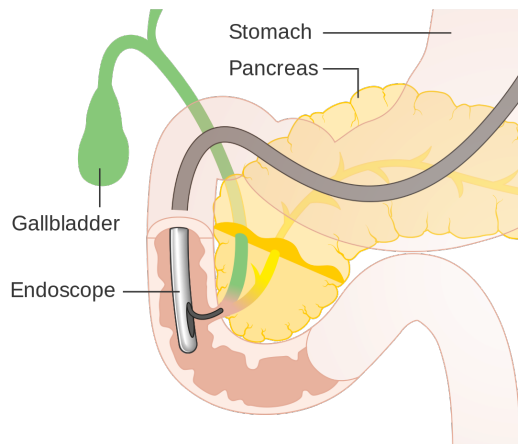


Figure 1.4: Left, the Da Vinci surgical system (Sunnyvale, California, USA, Intuitive Surgical): a robotic master-slave system containing multiple robotic arms that maneuver the instruments, and one or two surgeon consoles. (© 2016, Intuitive Surgical, Inc. (CC BY-SA 3.0, <https://creativecommons.org/licenses/by-sa/3.0>). Right, the steerable instrument called the EndoWrist incorporated in the Da Vinci system. The two degrees of freedom of the joint mimic the maneuverability of a human wrist (adapted from [17]).

end-effector to be redirected in two DOFs. The name EndoWrist refers to the intention of retrieving the dexterity of the surgeon's wrist close to the diseased area; a feature that was initially lost in the transition from open to minimally invasive surgery.

Steerable instruments increase the dexterity at the tip of their shafts, yet the body of their shafts remains rigid and primarily straight. As a result, the path from incision to diseased area must be a straight line. A straight path is, however, not always an option. This is especially the case in the field of Natural Orifice Transluminal Endoscopic Surgery (NOTES): a specialized form of MIS first reported on in 2004 [18]. During NOTES, natural orifices in the body, such as the nose, mouth, anus or vagina are used as entry-points. After entry through a natural orifice, the instruments must be navigated through the curvy natural lumen of the body to reach the diseased area. NOTES therefore often involves the use of flexible endoscopes that, next to a steerable tip, also contain a flexible shaft. In this way, the curvy lumen can be passed by actively steering the tip in the desired direction, while the flexible shaft is guided by the surrounding anatomy.

Figure 1.5 presents an example of a flexible endoscope being used during a NOTES procedure for removing gallstones from the bile duct called Endoscopic Retrograde Cholangiopancreatography (ERCP). During ERCP, the endoscope is inserted through the mouth and guided by the esophagus towards the stomach and through the duodenum (first part of the small intestine). Once in position, a small tube is extended from the



*Figure 1.5: Endoscopic Retrograde Cholangio-Pancreatography (ERCP), a NOTES procedure in which a flexible endoscope called a duodenoscope is inserted through the mouth and guided by the gastrointestinal tract towards the bile duct to remove gall stones [19]. 'Detailed diagram of an endoscopic retrograde cholangio pancreatography (ERCP)'; by Cancer Research UK, licensed under CC BY-SA 4.0.*

endoscope tip into the ampulla of Vater (a duct that splits into the bile and pancreatic duct), where it is used to stretch open the bile duct. Instruments such as baskets can eventually be used to enclose and remove the gallstones.

During ERCP, the anatomical environment supports the weight and guides the motion of the flexible endoscope. When going from the mouth down to the pharynx (throat), for example, the shaft is pushed against the posterior wall of the oropharynx (back of the throat), which forces it to change direction and follow the lumen towards the stomach. This type of motion is possible when the anatomical environment is strong enough to endure these forces.

There are situations in which the surrounding anatomy is too weak or fragile to supply sufficient support for the guidance of flexible instruments. This is, for example, the case in endonasal skull base surgery where the delicate anatomic environment is too fragile to provide any support or guidance to a flexible instrument. This lack of environmental support can, for example, make it difficult to reach behind a corner during an endonasal procedure. Lesions near the pituitary gland with parasellar extensions (reaching outside the sella turcica) behind the carotid arteries can, for this reason, remain out of reach [20]. In cases where the anatomical environment cannot be used for supplying the instrument with support or guidance, the instrument's flexible shaft itself should be able to support its weight and guide its motion.

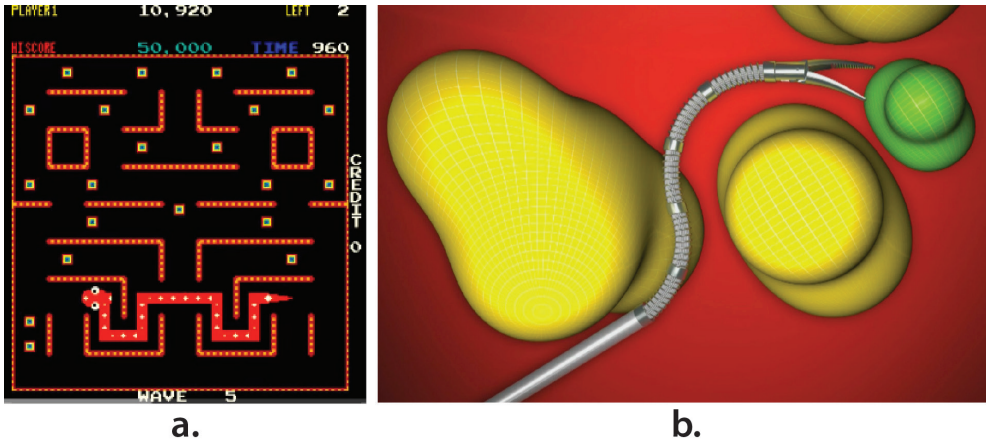


Figure 1.6: Follower-The-Leader (FTL) motion. a) 1980's Videogame called Nibbler wherein a snake performs FTL-motion for steering through a maze (1982, Chicago, Chicago, Rock-Ola). b) Schematic representation of a surgical instrument using FTL-motion to reach a target [adopted from [21]].

## 1.5 FOLLOW-THE-LEADER INSTRUMENTS

For a flexible shaft to be called self-supported and self-guided, it should be able to maneuver itself along multi-curved paths in free space. This type of motion is called Follow-The-Leader (FTL) motion and is best compared with a videogame called Snake that used to be popular in the '90s. A Snake-version called Nibbler (1982, Chicago, Chicago, Rock-Ola) is illustrated in Figure 1.6a. In this game, the player steers the head of a virtual snake through a maze, while the snake's body follows the route that is traced by the head. This way of motion reduces the required access down to the width of the snake, which is the absolute minimum width that the path can have. Minimizing the required access is exactly what minimally invasive surgery strives to achieve. Being able to steer an instrument through a dense anatomical environment using FTL-motion can significantly reduce the required access compared to conventional straight-line approaches. FTL-motion is therefore very suitable for minimizing the invasiveness of a surgical procedure. As schematically illustrated in Figure 1.6b, FTL-motion would allow an instrument to avoid obstacles and reach its target by following a tortuous multi-curved path.

FTL-motion requires control over the shape of the shaft. This entails some sort of steerability of the shaft, i.e. the shaft must include segments with a controllable shape. As a path becomes more tortuous by including multiple bends, the shaft will require a higher level of steerability by using more segments. How to accurately control the DOFs of all these segments for the shaft to perform FTL-motion is one of the major challenges in the development of FTL-instruments. Human beings are not particularly good at



Figure 1.7: Snake-like robots. Left: ACM-R3 snake robot developed at the Tokyo Institute of Technology © [2009] IEEE [22]. Right: Uncle Sam, a snake robot developed at the Robotics Institute of Carnegie Mellon University. 'Snake robot at the Robotics institute', image by Jiuguang Wang, [www.robo.guru](http://www.robo.guru), licensed under CC BY-SA 2.0.

simultaneously controlling high numbers of DOFs, while robots can excel at such tasks. When faced with a control problem that involves a high number of DOFs, there is a natural tendency to search for a robotic solution.

There is an entire field of robotics focused on snake-like robots, some examples presented in Figure 1.7. These robots typically consist of a chain of jointed segments, similar to the vertebrae of a biological snake. Each segment is coupled to an individual actuator, often an electric motor embedded inside the segment. By controlling the movements of the segments in a coordinated fashion, these robots strive to mimic the motion and maneuverability of biological snakes. Generally, these robots are used for exploring and monitoring tasks during pipe inspection or in hazardous and rugged terrain or confined spaces in collapsed buildings after an earthquake.

Although the snake-like robots of Figure 1.7 have the flexibility to perform FTL-motion, their advanced constructions are not particularly suitable for surgical purposes. Because the actuators are embedded inside the segments, the diameters of these snake-like robots are far too large for surgical applications. Secondly, these snake-like robots are self-propelled devices designed to travel stand-alone over long distances in an environment that supports their weight and motion. For surgical applications, the snake-like structure should not be stand-alone but at one side connected to a stable base, fixed to the operation table, from which it can extend.

One way of achieving FTL-motion from a stable base is through a method that will be referred to as shape-shifting. A hypothetical shape-shifting robotic snake is visualized in Figure 1.8. The setup consists of a segmented shaft that is connected to a stable base, which can translate to provide the required forward and backward motion of the

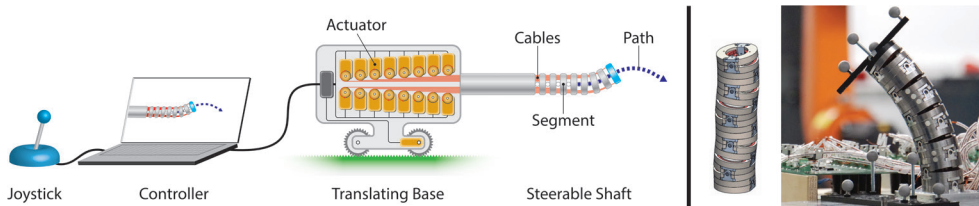


Figure 1.8: Shape-shifting mechanisms. Left: Hypothetical snake-like robot for surgery. The segmented shaft is connected a translating base, which can move backward and forward and holds a series of electric actuators (yellow). The segments are connected to the actuators via cables. The surgeon only has to steer the direction of the first segment via the joystick, while the computer controls the preceding segments to perform Follow-The-Leader motion. Right: Shape-shifting mechanism consisting of actuators embedded in the shaft © [2016] IEEE [23].

instrument. Electric actuators (yellow in the figure) are placed inside the translating base and connect to the shaft segments via cables. Because the actuators are situated outside of the instrument shaft, the shaft can be miniaturized to the small size required for surgery. The electric actuators are controlled by a computer and a joystick. With the joystick, the surgeon can control the direction of the first segment of the shaft (blue in the figure). While maneuvering this segment along a path through the anatomy, the computer ensures that the preceding segments follow the path that is traced by this first segment. In this way, the surgeon only has to manually control the direction of the first segment, while the computer handles the complex task of simultaneously controlling the preceding segments to ensure FTL-motion. The right part of Figure 1.8 shows an instrument especially designed for FTL-motion from a stable base proposed by Tappe et. al hat has its actuators embedded in the shaft [23]. Although embedding the actuators eliminates the need for a transmission mechanism like cables, it also increases the diameter of the shaft, in his case up to  $\text{\O}30$  mm. Every snake-like instrument placed on a translating based can, in theory, perform shape-shifting FTL-motion [24].

Another way of achieving FTL-motion is based on a telescoping mechanism. Instead of moving the entire instrument forward as a whole, FTL-motion is in this case achieved by telescopically extending the tip of the shaft, while the rest of the shaft holds its position and shape. The best known telescoping mechanisms are concentric tube robots, first developed by Webster et al. at Vanderbilt University and since then extensively researched by others (Figure 1.9 top left) [25]. These robots are based on concentrically placed pre-curved tubes and translating and rotating the tubes relative to each other influences their overall shape. FTL-motion can be achieved by choosing the right combination of pre-curved tubes. However, only specific, relatively simple paths can be followed due to the predetermined nature of the pre-curved tubes [26]. For this reason, Neumann et al. replaced the pre-curved tubes with highly flexible tubes that are connected via cables to an extra set of actuators (Figure 1.9 top right) [27]. This allows for more control over

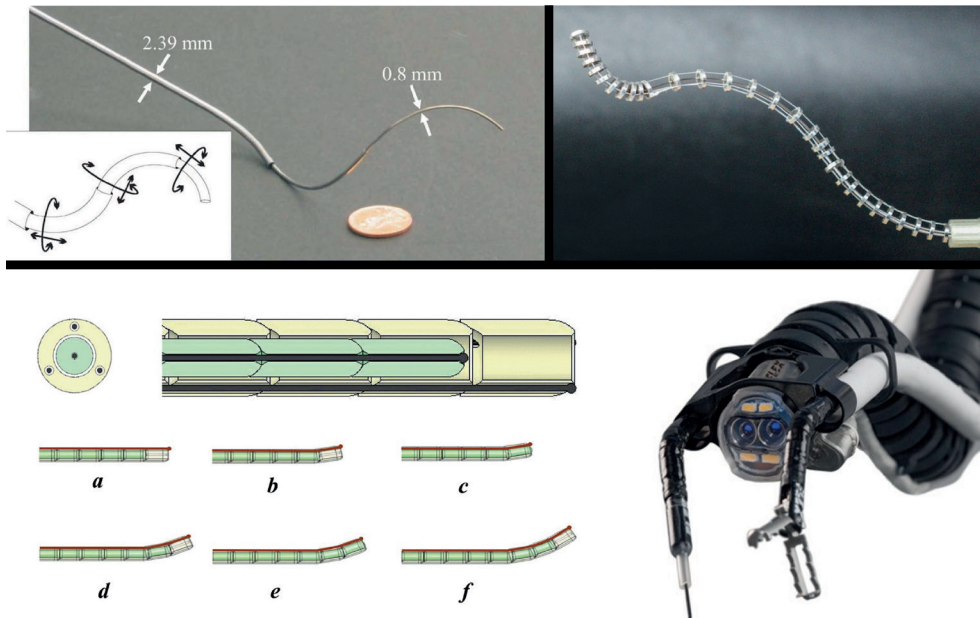


Figure 1.9: Top left: Concentric tube robot, a telescoping mechanism consisting of pre-curved tubes © [2009] IEEE [25]. Top right: Telescoping mechanism consisting of flexible tubes connected with steering cables © [2016] IEEE [27]. Bottom left: Alternating telescoping mechanism consisting of two arms that alternate between a flexible and locked state [28]. Bottom right: The Flex System (Raynham, Massachusetts, Medrobotics), an endoscope based on the alternating telescoping mechanism capable of Follow-The-Leader motion, supporting two instruments at the side [32]. Image by Medrobotics (Raynham, USA), adapted from [32], licensed under CC BY-NC-ND 4.0.

the shape of the shaft with more complex FTL-motion as a result. A drawback is that the additional components for connecting and guiding the cables cannot be fully retracted and stack-up at the instrument's tip. This stack of components will sway along with the motion, requiring a broader surgical pathway and limiting the maximum number of sections. Degani et al. presented an FTL-solution using an alternating telescoping mechanism based on two concentric arms that can independently advance and alternate between a flexible and locked state (Figure 1.9 bottom) [28]. FTL-motion is achieved by letting the arms alternate between flexible and locked, while the locked arm memorizes the current shape of the shaft and serves as a guide for the flexible arm that advances and is steered in a new direction.

FTL-motion is relatively new in surgery. In 2015 Remacle et al. reported on the first surgical application of a commercialized FTL-system that is based on the alternating telescoping mechanism called the Flex System (Raynham, Massachusetts, Medrobotics) (also published under the name highly articulated robotic probe (HARP) or the CardioaARM), illustrated in the bottom of Figure 1.9 [28, 29]. The Flex System was designed for transoral (through

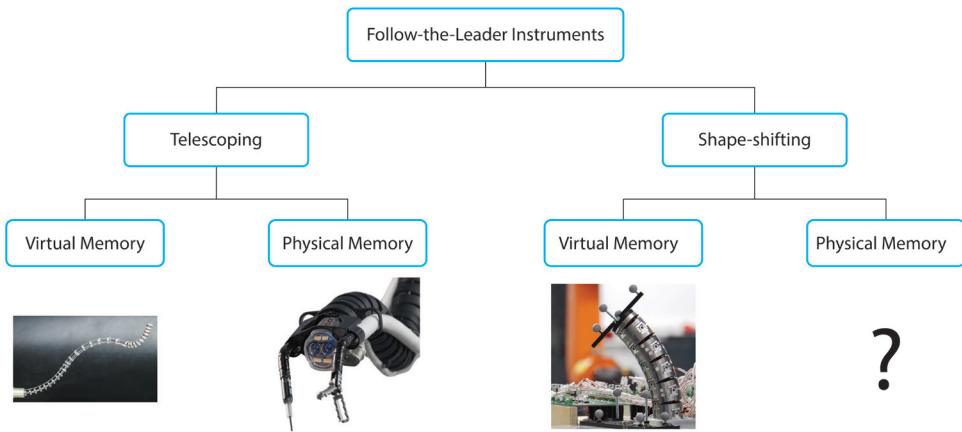


Figure 1.10: Categorization of Follow-the-Leader instrumentation. First level distinguishes between telescoping mechanisms and shape-shifting mechanisms. Second level distinguishes between virtual and physical memory.

the mouth) procedures involving the oropharynx and hypopharynx and the larynx (part of the throat and voice box). The Flex System contains a central endoscope that is capable of FTL-motion and supports two additional instruments at its side. The first clinical trials with the Flex System show promising results for extending the reach of transoral surgical procedures [30, 31]. Aside from the Flex System, no medical instruments that can perform FTL-motion are commercially available.

The discussed FTL-instruments are categorized in Figure 1.10. The first level is based on the distinction between shape-shifting and telescoping mechanisms. The second level of categorization is based on how the instrument memorizes the path to be followed. A distinction is made between “Virtual Memory”, e.g. digital information stored on a computer or controller, and “Physical Memory”, e.g. geometrical information stored in the deformation of a single element or the combined configuration of multiple elements [33].

All the instruments in the Virtual Memory groups require electromechanical actuators to transfer the digital path-information into motion, which makes them, by default, mechatronic systems. For the instruments in the Physical Memory groups, this transfer from digital information to motion is not required, meaning that these instruments do not necessarily have to include mechatronic components. In these instruments, the motion could also be generated manually or by a mechanical energy source, for example, a spring-loaded mechanism. Nevertheless, all currently known FTL-instruments known contain electromechanical actuators. Furthermore, no shape-shifting instruments that use a physical memory mechanism were found in the literature.

## 1.6 MECHATRONIC VERSUS MECHANICAL CONTROL

1

Although a robotic (mechatronic) solution seems best suited to control the multitude of segments required for FTL-motion, there are a couple of drawbacks to using mechatronics in a surgical setting. Firstly, robotics require additional components such as actuators, sensors, and controllers. As every component in a system affects the overall reliability of the system, the addition of mechatronic components may increase the chance of system failure. Failure of robotic surgical systems like stalling or unintended movement of the instruments have been reported and can have severe effects on the well-being of the patient [34].

A second downside of using mechatronics in a surgical setting is that surgical robotics tend to be very expensive, especially as compared to conventional manual techniques [35-38]. A laparoscopic procedure with the Da Vinci surgical system is, for example, almost four times as expensive as a similar conventional manual procedure [37]. This can partly be explained by the additional mechatronic components that the Da Vinci robot requires. Medical grade mechatronic components have to meet specific requirements (ISO 13485). They, for example, have to meet higher reliability standards as compared to standard industrial components. As a result, medical-grade mechatronics are not particularly low cost. Moreover, to ensure a certain level of reliability and prevent failure, robotic surgical systems require a level of maintenance and service [39]. The Da Vinci robot (Figure 1.4), which has a lower mechatronic complexity than the hypothetical setup of Figure 1.8, has a cost price of near 2.3 million euro and additional yearly service costs of 10% of the purchasing price [35, 38]. The Flex System of Figure 1.9 has a price tag of close to 1 million dollars [40]. Next to the purchase costs, surgical robots can also be costly to operate. As the robotic system itself is not sterile, it needs to be wrapped in sterile drapes before every operation. This not only involves the costs of the drapes but also requires additional time for preparing the system for surgery [17]. As a result, robotic surgery can be more time consuming than conventional manual techniques [17, 41]. Another cost factor that needs to be considered is the additional training of the surgical staff, for example on how to act in case of system failure.

The last decade has seen a rise in robotic surgery, with the promise of enhancing the capabilities of surgeons, yet clear clinical benefits of robotic surgery above conventional manual techniques are still under discussion [35, 36, 42, 43]. Next to that, robotic systems tend to be more expensive than non-robotic solutions, and ensuring their reliability can be challenging. This triggered the following question; can a mechanism control the high number of segments required to perform FTL-motion?

## 1.7 GOAL OF THIS THESIS

The field of MIS is constantly evolving with the primary goal of reducing the invasiveness of a procedure to limit the surgical trauma for the patient. A logical next step in this pursuit is the introduction of follow-the-leader (FTL) instruments that can follow tortuous paths without support or guidance from the environment, weaving their way through intricate and delicate anatomical surroundings. Such a motion requires control over a high number of DOFs, which typically calls for a robotic solution. Surgical robotics, however, tend to be less reliable and more expensive than non-robotic alternatives. This thesis, therefore, sets out to explore the possibilities for non-robotic mechanically-controlled FTL-solutions.

The goal of this thesis is:

*To explore new mechanically-controlled Follow-The-Leader solutions suited for surgical purposes.*

This research strives to (partly) fill in the perceived knowledge-gap concerning shape-shifting FTL-instruments that are based on physical memory systems, specifically focusing on cable-driven snake-like mechanisms. This work is part of an ongoing study that has the ultimate goal of realizing end-solutions for surgical FTL-motion, and in particular for endonasal approaches to the skull base [44]. The main focus of this thesis is the development of general platform technology, rather than on specific clinical applications of this technology.

## 1.8 APPROACH AND OUTLINE

The outline of this thesis is visually represented in Figure 1.11. The body of the work is divided into two main categories; cable-driven mechanical snakes (Chapter 2 & 3) and mechanically-controlled path-following (Chapters 4, 5 & 6). Chapter 2 presents a novel way of enhancing the steerability at the tip of the shaft. Inspiration was found in the muscle structures of a squid tentacle. This led to an exploration into the use of multi-directional cable-layers, which resulted in a manually actuated steerable segment that is controllable in four DOFs. Chapter 3 describes the development of an innovative compliant hyper-redundant shaft, with special attention to its producibility. Typically, a hyper-redundant shaft is an intricate mechanism that, due to a multitude of parts, tends to be challenging to fabricate and assemble. This chapter explores the use of additive manufacturing, leading to a hyper-redundant shaft that is fabricated and assembled with

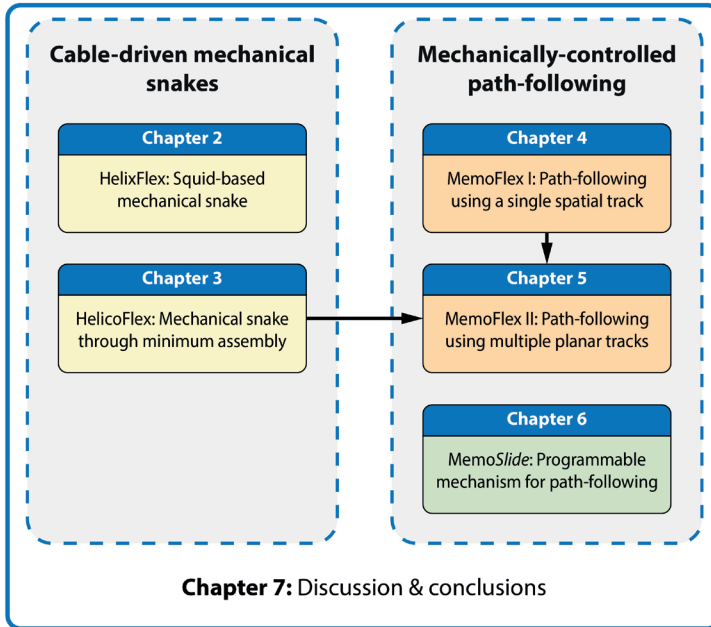


Figure 1.11: Thesis outline. Part I consists of Chapter 2 & 3 and concerns cable-driven mechanical snakes (yellow). Part II presents mechanically-controlled path-following, wherein Chapters 4 & 5 concern fixed paths (orange) and Chapter 6 concerns adaptable paths (green).

relative ease. Chapter 4 presents our first attempt towards a fully mechanical instrument capable of FTL-motion. It involves a mechanical master-slave system that captures the shape of a fixed multi-curved physical 3D track and copies it to a hyper-redundant slave. In this way, the slave follows a predetermined path through 3D space. Chapter 5 combines the findings of Chapters 3 & 4 into a new concept. The single fixed 3D track of Chapter 4 is replaced by four fixed 2D tracks. Moreover, the compliant shaft of Chapter 3 is implemented. The result is a mechanism that can follow a predetermined path with significantly higher accuracy as compared to its older brother of Chapter 4. Chapter 6 is completely focused on the control aspect of a cable-driven FTL-instrument, presenting a manually-driven mechanical memory-bank that embodies the control algorithm as required for FTL-motion. This mechanism can create adaptable 2D tracks. Combined with the mechanism of Chapter 5, it presents the possibility of a mechanically-controlled FTL-instrument capable of creating the path on-demand. Finally, the presented work is summarized and further discussed in Chapter 7.

## 1.9 REFERENCES

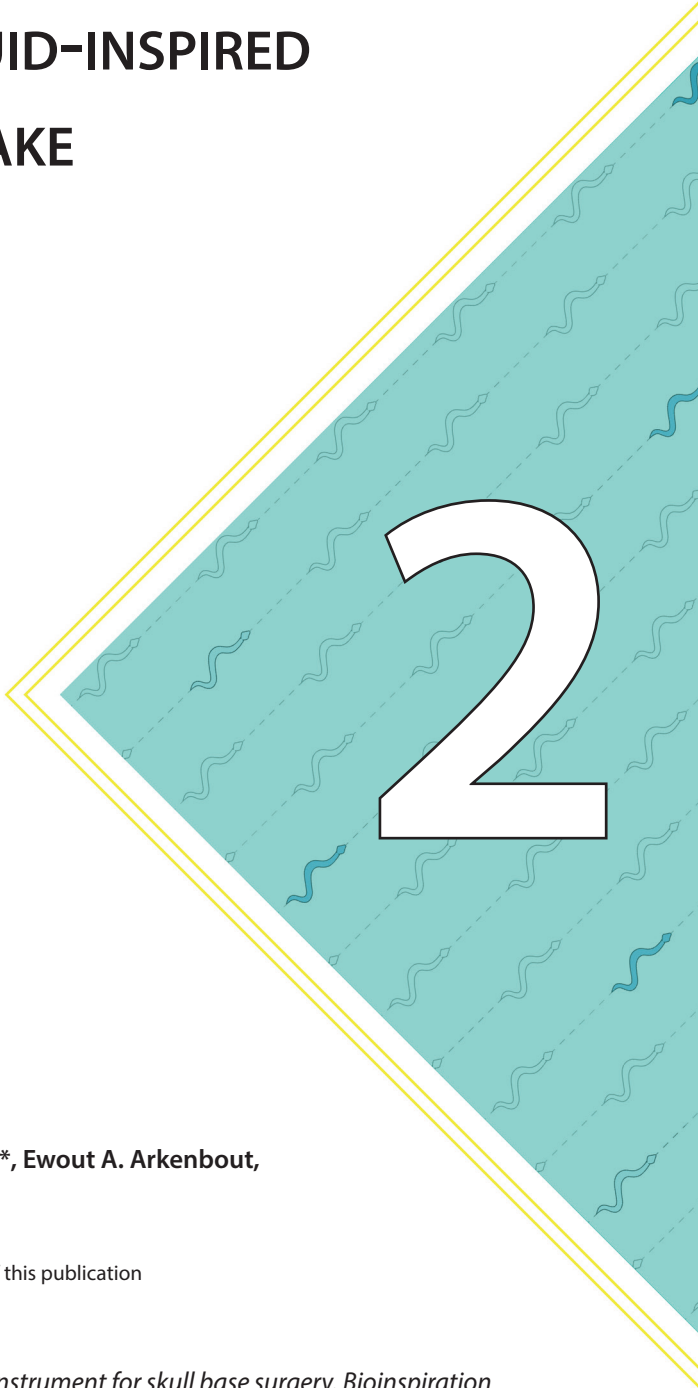
1. "Surgery." 2019. In Cambridge Dictionary. Retrieved Okt 31, 2019, from <https://dictionary.cambridge.org>.
2. Ljungqvist, O., M. Scott, and K.C. Fearon, Enhanced Recovery After Surgery A Review. *Jama Surgery*, 2017. 152(3): p. 292-298.
3. Mack, M.J., Minimally Invasive and Robotic Surgery. *JAMA*, 2001. 285(5): p. 568-572.
4. Liem, M.S.L., et al., Comparison of Conventional Anterior Surgery and Laparoscopic Surgery for Inguinal-Hernia Repair. *New England Journal of Medicine*, 1997. 336(22): p. 1541-1547.
5. Wei, W.L., K.H. Lam, and J.S.T. Sham, New approach to the nasopharynx: The maxillary swing approach. *Head & Neck*, 1991. 13(3): p. 200-207.
6. Hunter, D.J.S., Spight, D.H., Atlas of Minimally Invasive Surgical Operations. 1 ed. Vol. 1. 2018: McGraw Hill Professional.
7. St. Peter, S. and G. Holcomb, History of minimally invasive surgery. *Endoscopic Surgery in Infants and Children*, 2009: p. 1-5.
8. Centraal Bureau voor Statistiek. Operaties in het ziekenhuis; soort opname, leeftijd en geslacht, 1995-2010 [Database]. StatLine. 2011 [cited 24 Okt 2019] Available from: <https://opendata.cbs.nl/statline/>. [Accessed ]
9. Breedveld, P., et al., Theoretical background and conceptual solution for depth perception and eye-hand coordination problems in laparoscopic surgery. *Minimally Invasive Therapy & Allied Technologies*, 1999. 8(4): p. 227-234.
10. Epstein, A.J., et al., Impact of Minimally Invasive Surgery on Medical Spending and Employee AbsenteeismSurgery, Medical Spending, and AbsenteeismSurgery, Medical Spending, and Absenteeism. *JAMA Surgery*, 2013. 148(7): p. 641-647.
11. Jho, H.D. and R.L. Carrau, Endoscopic endonasal transsphenoidal surgery: experience with 50 patients. *J Neurosurg*, 1997. 87(1): p. 44-51.
12. EBM Consult. Cavernous Sinus Anatomy. 2019; Available from: <https://www.ebmconsult.com/articles/anatomy-cavernous-sinus>.
13. Fan, C., Manual control for medical instruments in minimally invasive surgery, dissertation, Delft University of Technology, Delft, the Netherlands, 2014. Available from <https://repository.tudelft.nl>.
14. Gerboni, G., et al., HelixFlex: bioinspired maneuverable instrument for skull base surgery. *Bioinspir Biomim*, 2015. 10(6): p. 066013. 15.
15. DEAM. [www.deam.com](http://www.deam.com) [Internet]. Amsterdam: DEAM; 2019 [cited 2019-11-26]. Availale from: [www.deam.com](http://www.deam.com)
16. Medtronic. [www.medtronic.com](http://www.medtronic.com) [Internet]. Minneapolis: Metronics;2019 [cited 2019-11-26]. Availale from: <https://www.medtronic.com/covidien/en-us/products/hand-instruments-ligation/sils-hand-instruments.html>
17. Higuchi, T. and M. Gettman, Robotic Instrumentation, Personnel and Operating Room Setup. 2011. p. 15-30.
18. Moreira-Pinto, J., et al., Natural orifice transluminal endoscopy surgery: A review. *World journal of gastroenterology*, 2011. 17(33): p. 3795-3801.
19. UK, C.R., Detailed diagram of an endoscopic retrograde cholangio pancreatography (ERCP). 2014, Wikimedia Commons.

20. Lee, S.-H., et al., Parasellar Extension Grades and Surgical Extent in Endoscopic Endonasal Transsphenoidal Surgery for Pituitary Adenomas : A Single Surgeon's Consecutive Series with the Aspects of Reliability and Clinical Validity. *Journal of Korean Neurosurgical Society*, 2016. 59(6): p. 577-583.
21. Henselmans, P.W.J., G. Smit, and P. Breedveld, Mechanical Follow-the-Leader motion of a hyper-redundant surgical instrument: Proof-of-concept prototype and first tests. *Proceedings of the Institution of Mechanical Engineers, Part H: Journal of Engineering in Medicine*, 2019. 233(11): p. 1141-1150.
22. Hirose, S. and H. Yamada, Snake-like robots [Tutorial]. *IEEE Robotics & Automation Magazine*, 2009. 16(1): p. 88-98.
23. Tappe, S., et al., Kinematics and dynamics identification of a hyper-redundant, electromagnetically actuated manipulator. 2016 IEEE International Conference on Advanced Intelligent Mechatronics (AIM), Banff, AB, 2016: pp. 601-607.
24. Burgner-Kahrs, J., D.C. Rucker, and H. Choset, Continuum robots for medical applications: a survey. *IEEE Transactions on Robotics*, 2015. 31(6): p. 1261-1280.
25. Webster III, R.J., J.M. Romano, and N.J. Cowan, Mechanics of pre-curved-tube continuum robots. *IEEE Transactions on Robotics*, 2009. 25(1): p. 67-78.
26. Gilbert, H.B. and R.J. Webster. Can concentric tube robots Follow-the-Leader? in *Proceedings - IEEE International Conference on Robotics and Automation*. 2013.
27. Neumann, M. and J. Burgner-Kahrs. Considerations for Follow-the-Leader motion of extensible tendon-driven continuum robots. in 2016 IEEE International Conference on Robotics and Automation (ICRA). 2016.
28. Ota, T., et al., A Highly Articulated Robotic Surgical System for Minimally Invasive Surgery. *The Annals of Thoracic Surgery*, 2009. 87(4): p. 1253-1256.
29. Remacle, M., et al., Transoral robotic surgery (TORS) with the Medrobotics Flex System: first surgical application on humans. *Eur Arch Otorhinolaryngol*, 2015. 272(6): p. 1451-5.
30. Sethi, N., et al., Transoral robotic surgery using the Medrobotic Flex<sup>®</sup> system: the Adelaide experience. *Journal of Robotic Surgery*, 2019.
31. Persky, M.J., et al., Transoral surgery using the Flex Robotic System: Initial experience in the United States. *Head and Neck*, 2018. 40(11): p. 2482-2486.
32. Moura, D.T.H.d., H. Aihara, and C.C. Thompson, Robotic-assisted surgical endoscopy: a new era for endoluminal therapies. *VideoGIE*, 2019. 4(9): p. 399-402.
33. Loeve, A., P. Breedveld, and J. Dankelman, Scopes too flexible and too stiff. *IEEE Pulse*, 2010. 1(3): p. 26-41.
34. Alemzadeh, H., et al., Adverse events in robotic surgery: A retrospective study of 14 years of fda data. *PLoS ONE*, 2016. 11(4).
35. Higgins, R.M., et al., Cost analysis of robotic versus laparoscopic general surgery procedures. *Surgical Endoscopy*, 2017. 31(1): p. 185-192.
36. Jayne, D., et al., Effect of Robotic-Assisted vs Conventional Laparoscopic Surgery on Risk of Conversion to Open Laparotomy Among Patients Undergoing Resection for Rectal Cancer: The ROLARR Randomized Clinical Trial Robotic-Assisted vs Conventional Laparoscopic Surgery for Rectal Cancer, *JAMA*, 2017. 318(16): p. 1569-1580.
37. Childers, C.P. and M. Maggard-Gibbons, Estimation of the Acquisition and Operating Costs for Robotic Surgery, *Letters. JAMA*, 2018. 320(8): p. 835-836.
38. Jeong, I.G., et al., Association of Robotic-Assisted vs Laparoscopic Radical Nephrectomy

- With Perioperative Outcomes and Health Care Costs, 2003 to 2015 Outcomes and Costs of Robotic-Assisted vs Laparoscopic Radical Nephrectomy. *JAMA*, 2017. 318(16): p. 1561-1568.
39. Schuler, P.J., Robotic Surgery - Who is The Boss? *Laryngo- rhino- otologie*, 2018. 97(S 01): p. S231-S278.
  40. Belfiore, M., Flexible surgical robot, in *Bloomber Businessweek*. 2016.
  41. Delaney, C.P., et al., Comparison of robotically performed and traditional laparoscopic colorectal surgery. *Dis Colon Rectum*, 2003. 46(12): p. 1633-9.
  42. Köckerling, F., Robotic vs. Standard Laparoscopic Technique - What is Better? *Frontiers in surgery*, 2014. 1: p. 15-15.
  43. Roh, H.F., S.H. Nam, and J.M. Kim, Robot-assisted laparoscopic surgery versus conventional laparoscopic surgery in randomized controlled trials: A systematic review and meta-analysis. *PloS one*, 2018. 13(1): p. e0191628-e0191628.
  44. Breedveld, P., Bio-Inspired Maneuverable Dendritic Devices for Minimally Invasive Surgery, NWO Vici-grant, Project 12137. 2013..



# HELIXFLEX: SQUID-INSPIRED MECHANICAL SNAKE



2

**Giada Gerboni\*, Paul W.J. Henselmans\*, Ewout A. Arkenbout,  
Wouter R. van Furth, Paul Breedveld**

\*Authors contributed equally to the realization of this publication

Published as:

*HelixFlex: bioinspired maneuverable instrument for skull base surgery. Bioinspiration  
& Biomimetics, 2015. 10(6): p. 066013.*

**ABSTRACT**

Endoscopic endonasal surgery is the current 'gold standard' for operating on pituitary gland tumors and is gaining a for treatment of other skull base lesions. Still, endoscopic surgical treatment of most skull base pathologies, including certain pituitary tumors, is severely impaired by current instruments' lack of maneuverability. Gaining access to, and visibility of, difficult to reach anatomical corners without interference with surrounding neurovascular structures or other used instruments, is a challenge. In this context, there is the need for instruments that can provide a stable shaft position, while both the orientation and the position of the end-effector can be controlled independently from each other. Current instruments that allow for this level of maneuverability are usually mechanically complex, and hence less suitable for mass production. This study introduces a cable-driven actuation technique wherein multiple cable routes are integrated into a single segment. This technique, referred to as multi-actuation, enhances the maneuverability of a steerable segment while reducing the complexity of its construction. Multi-actuation has been successfully integrated and tested in a handheld prototype instrument called HelixFlex. HelixFlex contains a 4 degrees of freedom steerable 5.8 mm (diameter) shaft that shows promising results concerning its maneuverability.

## 2.1 INTRODUCTION

Surgery is an inherently invasive procedure as it requires a pathway to be created towards the impaired area. Larger surgical pathways increase the chance of post-surgery infections as well as recovery time and scar tissue. The field of minimally invasive surgery (MIS) therefore aims to reduce the width of surgical pathways by minimizing the required size of the incision. A prime example of MIS is a laparoscopic procedure, wherein the surgeon enters the abdomen through small incisions in the skin [1]. Vision is obtained by an endoscope, and the required end-effectors (graspers, scissors, curettes, etc) are placed on long slender shafts. As a result, the size of the incisions can be reduced. Natural Orifice Transluminal Endoscopic Surgery (NOTES) is an even less invasive approach wherein natural orifices, such as the anus, mouth or nostrils are used as the surgical entry point into the body [2].

2

### 2.1.1 ENDOSCOPIC ENDONASAL SURGERY

Endoscopic Endonasal Surgery (EES) is a NOTES procedure that uses the nostrils as the surgical entry point for reaching areas in the skull. A prime example of EES is the resection of pituitary gland adenomas [3]. Although this minimally invasive approach is becoming the standard, the complete removal of very large or invasive adenomas of the pituitary gland cannot always be achieved [4–8]. As a result, residual parts of the tumor are often treated by radiation therapy, or by returning to more invasive classical open surgery (craniotomy) [9, 10]. The main reason why complete removal by EES is not always a possibility becomes apparent when a one takes a closer look at the EES procedure.

An EES procedure targeting a pituitary tumor starts by passing the instruments through one or both nostrils and opening the frontal bony wall of the sphenoidal sinus. Subsequently, also the floor of the sella turcica is partially removed before entering the sella that cradles the pituitary gland (Figure 2.1) [4, 11]. The resulting surgical pathway is confined by multiple physical limits and is therefore often referred to as a ‘narrow’ corridor [12]. The pituitary gland is located at the end of this corridor, where it is surrounded by highly delicate neural structures and important vascular structures, such as the optic chiasm and the carotid arteries [13]. Removal of adenomas that are in-line with the mentioned corridor is relatively straight forward, while adenomas that extend behind the delicate neurovascular structures are more difficult to reach. In these cases, the surgeon needs to be able to see and reach around the corner of the corridor, without touching its walls to avoid damaging the delicate surroundings [6, 14, 15]. Currently used instruments are long and rigid as depicted in Figure 2.1. As it is impossible to reach behind the corner of the corridor with these straight rigid instruments, some adenomas remain partly unresectable. The limitations of current rigid instruments in other EES procedures, such as olfactory groove

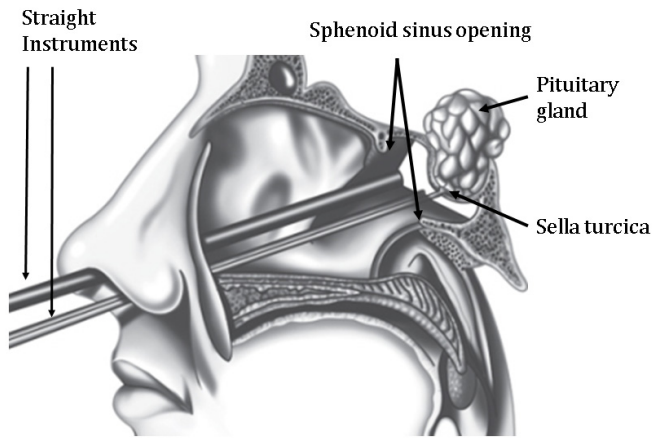


Figure 2.1: Endoscopic Endonasal Surgery (EES), a minimally invasive approach to the pituitary gland.

meningioma, is even more noticeable since the approach is under an angle [16]. Moreover, in EES procedures beyond the skull base, e.g. craniopharyngioma in the third ventricle, the entire tumor lies behind the optic nerve and often remains out of reach [17].

Other research groups have already identified the lack of instrument maneuverability in EES approaches [18–20]. Schneider et al. presented a list of functional requirements for robotic systems suitable for EES procedures, describing an ideal instrument to be small, flexible and strong, yet not specifying concrete values [21]. There is a clear need for flexible instruments that can maneuver their end-effector relative to the shaft, throughout this communication these instruments will be referred to as steerable instruments.

### 2.1.2 STEERABLE INSTRUMENTS

Steerable instruments are equipped with a steerable segment attached to the end of their rigid shafts, allowing for the re-orientating of the end-effector (Figure 2.2, left). A steerable segment is a jointed or compliant structure and contains some sort of actuation technique [22]. A variety of actuation techniques have already been proposed, including hydraulic, pneumatic, magnetic, pushrod or shape memory alloy principles. The most common actuation technique is, however, based on cables or tendons [23].

The best known cable-driven steerable instrument is the EndoWrist, capable of 2 degrees of freedom (DOFs) and incorporated in the Da Vinci® System (developed by Intuitive Surgical Inc., Sunnyvale, CA, USA) [24]. The EndoWrist's mechanism is either constructed out of a miniaturized pulley system (Figure 2.3, left) or incorporates multiple stacked joints (Figure 2.3, right) [25, 26].

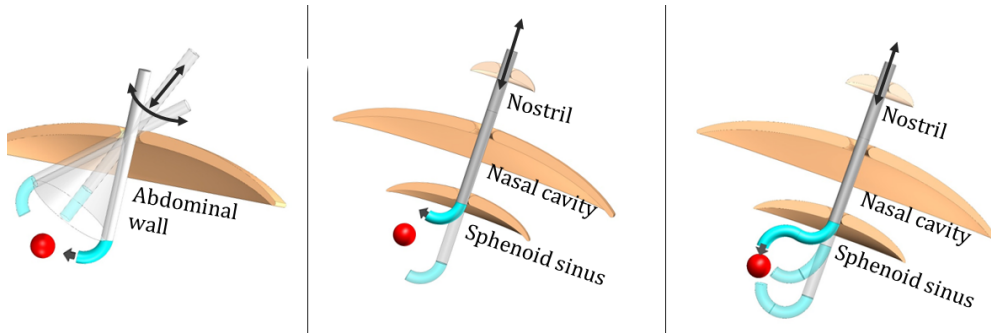


Figure 2.2: Instrument restriction. Left: steerable instrument as used in laparoscopy. The shaft can be re-positioned and re-orientated towards the target (red ball). Centre: steerable instrument to be used in EES. Constraints on the shaft result in an insufficient reach of the end-effector. Right: representation of a multi-steerable instrument to be used in EES. The additional maneuverability allows for the re-orientation and re-positioning of the end-effector.

Even though 2-DOFs steerable instruments are useful in laparoscopy, they are not suitable for EES procedures [24]. During laparoscopy, the instrument's shaft is only restricted at the access point into the abdomen and can be maneuvered inside a conical workspace (Figure 2.2, left) [18]. During EES, however, there is no longer a conical workspace, like the nostrils, nasal cavity and hole through the sphenoidal sinus severely restrict the movement of the shaft (Figure 2.2, center). In this situation, the surgeon will not be able to sufficiently re-orientate and re-position the end-effector. A steerable instrument suitable for EES should not only be able to re-orientate its end-effector but also allow control over the position (Figure 2.2, right).



Figure 2.3: Two versions of the EndoWrist developed by Intuitive Surgical Inc. Left:  $\varnothing 8$  mm pulley mechanism (adapted with permission from [44], copyright IEEE 2005). Right:  $\varnothing 5$  mm stacked multi jointed version.

### 2.1.3 MULTI-STEERABLE INSTRUMENTS

A multi-steerable instrument is a steerable instrument with enhanced steering capabilities [27]. Examples of surgical multi-steerable instruments are; the hyper-redundant CardioArm developed by Ota et al. [28, 29], the two arms of the telerobotic system for MIS of the throat by Simaan et al. [30] and the cable-driven robot of Li et al. [31]. The flexible shafts of these instruments consist of multiple steerable segments stacked on top of each other, thus increasing steerability. Next to a single deflection, these shafts are also capable of deforming into S-shaped curves which affect the position of the end-effector while keeping its orientation intact, thus making it possible to both re-orientate and re-position the end-effector relative to the shaft.

2

An alternative, and worth mentioning approach to building multi steerable instruments at a very small size is represented by the cannula robot of Webster et al. that was specially designed for endonasal surgical procedures targeting the skull base [32, 33]. The shaft of this robot consists of multiple pre-curved concentric tubes that can be rotated and translated relative to each other [34]. By modeling the behavior of this mechanism it is possible to control the shape of the articulated series of cannulas [35].

Next to these man-made solutions, hydrostatic skeletons found in nature, as for example trunks, tongues, and tentacles, have been a form of inspiration for creating robots and instruments with multi-steerable functionality [36]. Kier explains that conventional hydrostatic skeletons typically include a volume of incompressible fluid that is enclosed by a cylindrical musculature. This musculature contains three different muscle arrangements all placed perpendicular to the longitudinal axis; circular, radial and transverse. The contraction of these muscle fibers causes a decrease in diameter and an increase of pressure of the incompressible fluid, resulting in the elongation of the hydrostatic skeleton [37]. Additional longitudinal muscle fibers serve as the antagonist members by shorting the hydrostatic skeleton. The varying differential pressure caused by local contraction of the different muscle fibers along the length and circumference of the hydrostatic skeleton gives it its highly dexterous maneuverability [38]. The use of differential pressures for steering a flexible arm inspired the work of Ranzani et al., who developed a soft surgical manipulator driven by fluid pressure that deforms an elastomeric based structure [39]. Such soft manipulators have the potential to be inherently safe thanks to their high compliance in case of contact with organs, yet should also include a stiffening mechanism or performing surgical tasks with the end-effector [40]. Kier describes that many hydrostatic skeletons also incorporate such a stiffening mechanism by reinforcing its walls with layers of crossed-fiber helical connective tissue that control and limit shape change [38]. A mechanical approach to such a stiffening mechanism using braided structures of helical elements running both clockwise (CW) and counterclockwise (CCW) is for example also used in flexible endoscopes [41].

All mentioned multi-steerable instruments have the required maneuverability for EES. Moreover, they are all robotic systems. Consequently, these solutions require additional mechatronic components such as actuators, sensors, and controllers. As a result, they will be relatively expensive compared to the currently used handheld instrumentation [42]. Moreover, considering EES procedures, robotic systems tend to be quite bulky and will inevitably reduce the available workspace in front of the nose for the insertion of other instruments.

#### 2.1.4 OBJECTIVES AND REQUIREMENTS

The goal of this study is to develop a multi-steerable instrument for EES that is manually actuated. For one, as currently handheld instruments are already being used, we believe that a handheld multi-steerable instrument will be easier adapted into the current surgical procedures. Secondly, the exclusion of a robotic system makes the instrument cheaper and less bulky. And thirdly, because the user is heavily involved in the control loop of the instrument, he/she can actively adapt to any distortion between the control input and the resulting motion of the end-effector.

In search of a suitable cable-based actuation technique, previous work of our group studied a special type of hydrostatic skeleton called a muscular hydrostat. Muscular hydrostats lack the volume of fluid present in the described conventional hydrostatic skeletons and instead are fully based on highly dense muscle structures [43]. An example of a muscular hydrostat can be found in the tentacle of Loliginid squid, illustrated in Figure 2.4, left. Its longitudinal muscle bundles were the inspiration for the cable-ring mechanism [44]. This mechanism incorporates a ring of cables that are enclosed by two springs, as illustrated in Figure 2.4, right. A useful characteristic of this configuration is that the cables keep each other in-line without the need for additional guidance. Furthermore, a multi-steerable instrument can be created by fixating some of the cables at an intermediate point along the flexible shaft, as illustrated with two segments in Figure 2.5. MultiFlex is a multi-steerable handheld instrument that incorporates this principle and contains a cable-ring of 20 cables, Figure 2.6 [45]. By fixating groups of four cables, that are evenly spaced along the circumference, at intermediate fixation points along the length of the shaft, the shaft of MultiFlex is effectively divided into five independently steerable segments. The result is a highly articulate  $\varnothing 5$  mm shaft.

However, using intermediate fixation points in multi-steerable instruments, like MultiFlex, makes fabrication particularly challenging. The reason is that, at these fixation points, only the cables of the related segment should be fixated, while an obstruction-free passage has to remain for the cables belonging to the following segments. Strong and obstruction-free

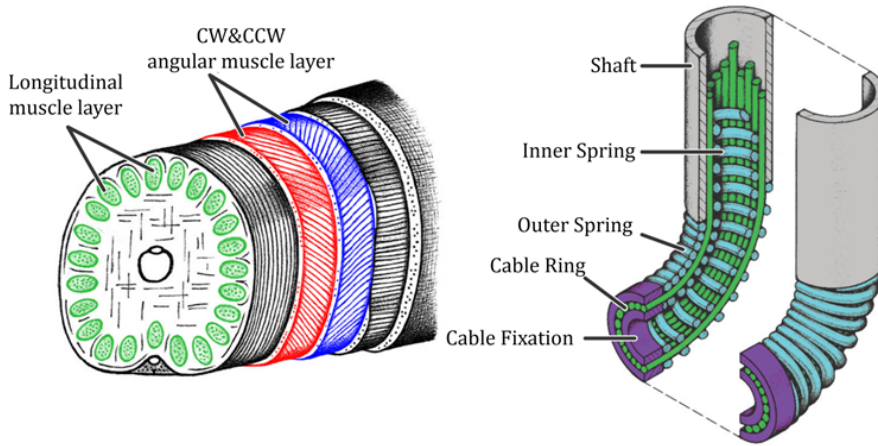


Figure 2.4: Left: Lolliginid squid tentacle containing longitudinal and angular muscle layers. Right: cable-ring mechanism, by placing a ring of cables between an inner and outer spring, the cables are fully enclosed and aligned (adapted with permission from [44], copyright IEEE 2005).

fixation of individual cables at a miniature scale, for example by clamping, gluing, soldering or laser welding, requires very high precision in manufacturing and assembly processes, leading to increased complexity and low effectiveness-cost ratio unfitting for successful commercialization.

Apart from the exclusion of intermediate fixation points, there are more general requirements that the instrument must meet to be usable during EES. First, there is the size of the instrument, which can be defined by the diameter and length of the steerable shaft. Because the steerable instruments are intended to replace the current rigid ones, its diameter should not surpass the current standard of 3 mm. The required length of the steerable segment, instead, is more difficult to be defined and determines the reachable workspace of the end-effector relative to the rigid part of the shaft. This dimension is, therefore, related to the size of the specific surgical workspace; in the case of pituitary surgery, it is strongly related to the dimensions of the sella turcica that cradles the pituitary gland. The dimensions of the sella turcica, however, are patient-specific and can vary significantly. Zada et al. reported that, for healthy adults, the sellar face (which relates to the workspace's height) ranges from 6.7 to 19.8mm and the length of the planum sphenoidal (which relates to the workspace's width) ranges from 6.4 to 28.8 mm [46]. Moreover, adenomas can extend well beyond the sella turcica further into the skull base. An educated guess would be that a length of around 30 mm would be sufficient to reach the majority of the adenomas.

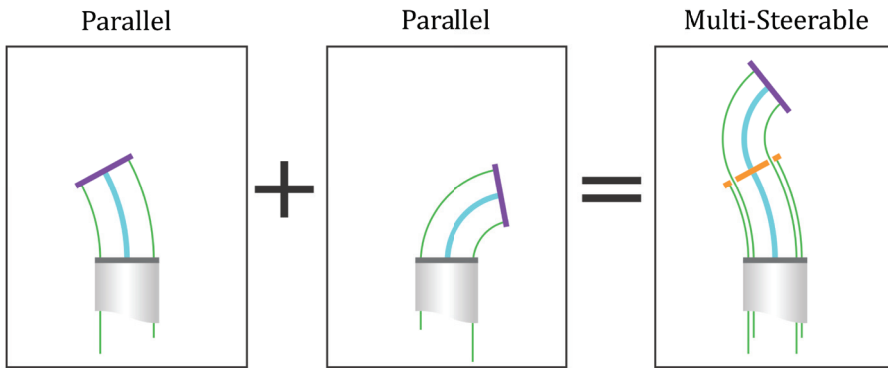


Figure 2.5: 2D view of two segments with parallel-routed cables combined into a multi-steerable shaft construction. The orange line represents an intermediate cable-fixation point.

2



Figure 2.6: MultiFlex by the BITE-group of TU Delft: a multi-steerable handheld instrument composed out of five steerable segments stacked in series. The instrument uses the cable-ring mechanism and contains 16 intermediate cable fixation points (four of which are indicated by circles).

The steerable shaft must have a certain stiffness as it must be able to withstand the forces that are exerted on the end-effector during tissue resection. An indication of these forces is given by Bekeny et al. who studied the forces that are present on a curette during resection of a pituitary adenoma [47]. They reported average forces of 0.1 to 0.5 N in the x, y and z directions during tumor resection and a peak force of 2.12 N during collisions with bony structures.

An intuitive and accurate manner of controlling the end-effector's movement is important for surgical instruments. Even though in manually actuated instruments the user is involved in the control loop, a non-intuitive mapping between user input and the resulting motion of the end-effector will put unnecessary strain on the surgeon. Furthermore, the presence of hysteresis should be avoided as it will cause a delay in the motion of the end-effector relative to the control input.

This paper we present a fundamentally new approach to cable steering of a flexible shaft. The mentioned requirements, even though relevant for an instrument ready for EES, will be taken as reference, but not all of them will be exactly addressed in this specific study. This study is primarily focused on the working principles behind the proposed cable actuation technique.

## 2.2 NEW APPROACH: MULTI-ACTUATION

As intermediate cable-fixations need to be avoided, all cables should preferably be fixated at one single point along the length of the shaft. In that case, however, it is no longer possible to divide the length of the shaft into different steerable segments. To get the desired multi-steerable maneuverability from a single steerable segment, the functionality of that steerable segment should, therefore, be enhanced. Looking again at the muscular hydrostat of a Loliginid squid (Figure 2.4, left), one can see that, apart from the longitudinal muscle bundles that lay parallel to the central axis of the tentacle, it also contains angular muscle layers. This configuration inspired the idea of using multi-directional cable-configurations in a single steerable segment. These cables will inflict different deformation modes, thus expanding the functionality of a single steerable segment.

To explore the different deformation modes, the segment is modeled as a two-dimensional (2D) cantilever beam, see Figure 2.7 (top). The fixed left side of the beam represents the fixation of the steerable segment with the rigid part of the shaft. A non-deformable rib is

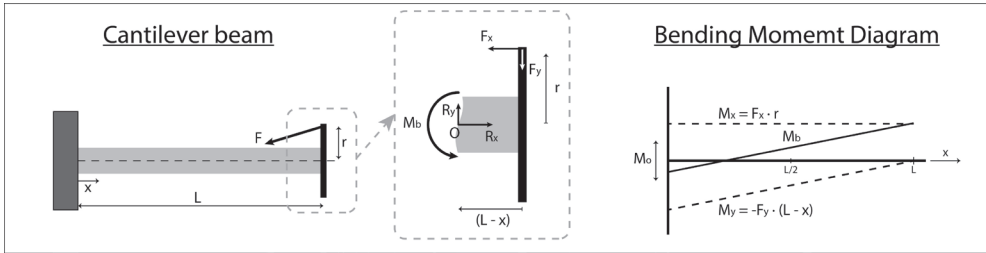


Figure 2.7: Left: cantilever beam representing a steerable segment. The left fixed side of the beam represents the fixation of the steerable segment with the rigid part of the shaft.  $F$  is the cable force and is decomposed  $F_x$  and  $F_y$ . Right: bending moment diagram including moments  $M_x$ ,  $M_y$  and  $M_b$  as calculated by equations 2.1a, 2.1b and 2.1c, respectively.

attached to the free end of the beam, and forces placed on this rib represent the pulling forces of the actuation cables. The direction of the force determines the angle of the cable, and based on this angle the cable force  $F$  is divided into the force components  $F_x$  and  $F_y$ .

Calculated from the fixed end of the beam, the two force components will result in different bending moments  $M_x$  and  $M_y$  along the central axis of the beam. The resulting bending moment along the beam  $M_b(x)$ , see Figure 2.7 (left), can be derived based on the moment balance around point  $O$ :

$$M_x(x) = F_x \cdot r \quad (2.1a)$$

$$M_y(x) = -F_y \cdot (L - x) \quad (2.1b)$$

$$\sum_{x=0}^L M_o(x) = 0; \quad M_b(x) + M_x(x) + M_y(x) = 0, \quad (2.1c)$$

where  $L$  is the segment length,  $x$  is the position along the beam, and  $r$  represents the distance from the cable fixation point to the central axis. Figure 2.7 (right) shows the bending moment diagram, wherein it can be seen that moment  $M_x$  is constant while moment  $M_y$  varies linearly along the length of the beam. As the overall bending moment ( $M_b$ ) is directly proportional to the deflection of the beam, this diagram can be used to study the deflection modes of the beam.

For a cable directed parallel to the central axis, force  $F_y$  will be zero, causing a constant bending moment  $M_x$  that results in a constant bending radius (Figure 2.8, left). By placing the cable at an angle, the transverse force  $F_y$  will no longer be zero, and the overall bending moment  $M_b$  will become linearly varying. An interesting deformation occurs when the cable is routed diagonally, thus passing through the beam's center (Figure 2.8, right). The force components  $F_x$  and  $F_y$  can, in this case, be described by:

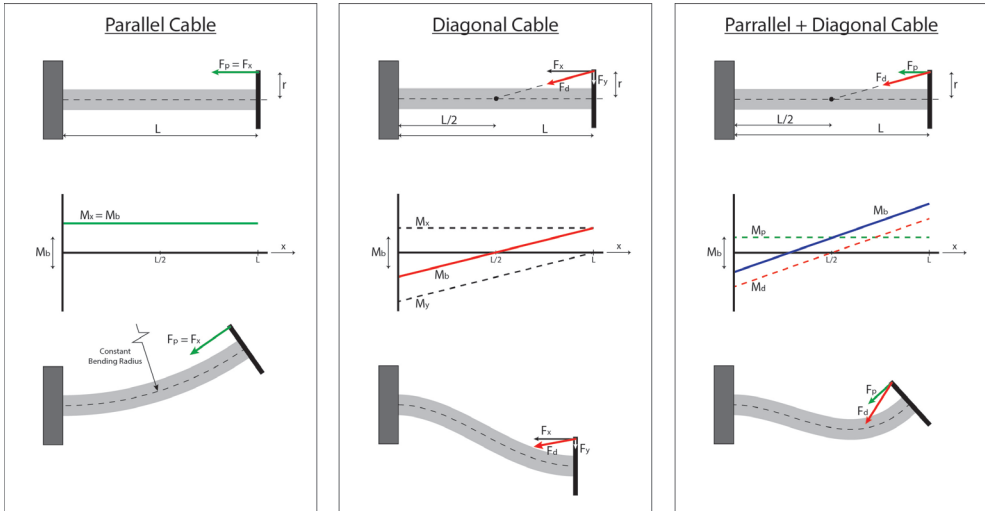


Figure 2.8: Left: parallel actuation cable causing a constant  $M_b$  resulting in a constant curvature deformation mode. Middle: diagonal actuation cable causing  $M_b$  to cross the x-axis at  $L/2$  resulting in an S-shaped deformation mode. Right: multi-directional cable-configuration with a parallel and diagonal cables causing a linearly varying  $M_b$  and corresponding deformation mode.

$$F_x = -F \cdot \frac{\frac{L}{2}}{\left(\frac{L}{2}\right)^2 + r^2} \quad (2.2a)$$

$$F_y = -F \cdot \frac{r}{\left(\frac{L}{2}\right)^2 + r^2} \quad (2.2b)$$

Filling in this into (2.1c) gives:

$$M_b(x) = -F \cdot \frac{\frac{L}{2}}{\left(\frac{L}{2}\right)^2 + r^2} + F \cdot \frac{r}{\left(\frac{L}{2}\right)^2 + r^2} \cdot (L - r) \quad (2.3)$$

Moment  $M_b$  (2.3) will thus cross the x-axis at  $L/2$ , as (Figure 2.8, middle). Cable force  $F$  determines the slope, and the segment will deform in an S-shaped curve (Figure 2.8, right).

By applying both a parallel and diagonal cable force, the  $M_b$  becomes a skewed line in the moment diagram of which the height and slope can be independently regulated (Figure 2.8, right). The corresponding deflection mode can be considered a transition between the two distinctive deflection modes caused by the individual parallel and diagonal routed cables. The use of such multi-directional cable-configuration in a

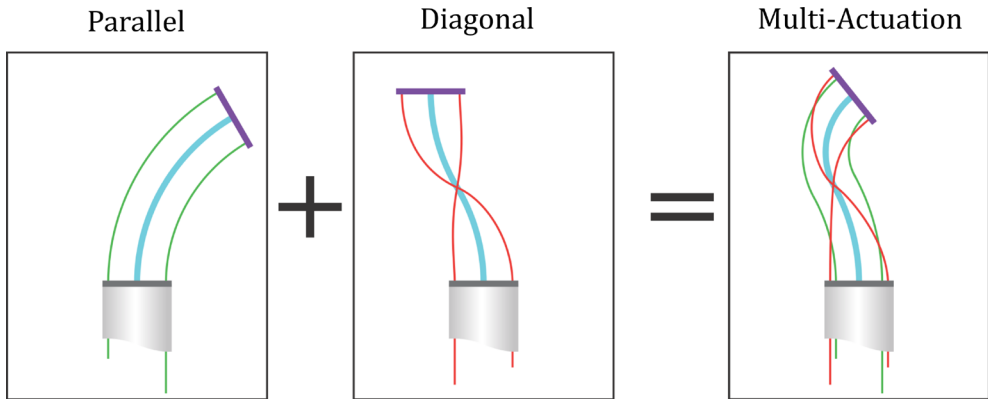


Figure 2.9: A 2D schematic representation of a multi-actuated steerable segment with two parallel and two diagonal cables. This cable configuration is capable of a 2 DOFs bending motion, allowing the alteration of both the orientation and position of the tip in a single plane.

single steerable segment will be referred to as multi-actuation. To be actionable in two directions, a multi-actuated steerable segment should at least include two parallel and two diagonal cables as illustrated in Figure 2.9.

The theoretical workspace of a multi-actuated segment contains all deformation modes that are described by a constant or linearly varying bending moment. A number of these deformation modes and their corresponding bending moment diagrams are illustrated in Figure 2.10. Deformation modes 1 and 4 depict the deformations that are induced by the use of only parallel or diagonal cables, respectively. Deformation modes 2, 3, 5 and 6 show some of the possible shapes that make use of both parallel and diagonal cables. Moreover, Figure 2.11 illustrates that different deformation modes can be used to reach the same end-position while having a different orientation (case a) or reach different end-positions while having an equal orientation (case b). This shows that the combination of parallel and diagonal cables allows for the desired independent control of both the orientation and position of the tip. Note that an axial translation of the shaft is required for reaching the same tip position with different deformation modes, as denoted in Figure 2.11 (case (a)).

The described beam theory is only applicable to small deformations (<10 deg.), thus it only served as a design tool to aid in the decision for the most favorable cable-configuration for a multi-actuated segment. This model will therefore not be used to accurately predict the behavior and/or optimize the mechanics of the actual multi-actuated instrument.

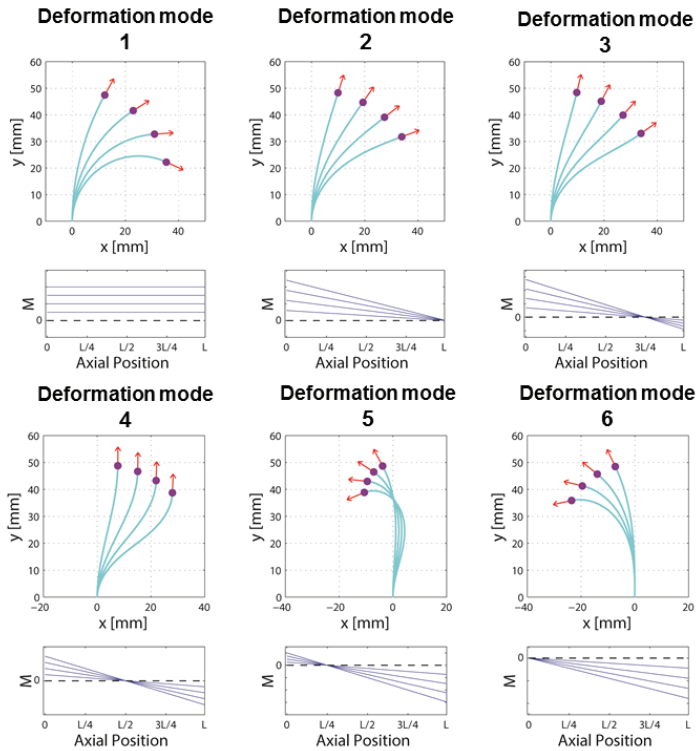


Figure 2.10: Multi-actuated steerable segment deformed in six different deformation modes, with underneath the corresponding bending moment diagrams. Deformation modes 1 and 4: deformations of a segment actuated by either a parallel cable or diagonal cable, respectively. Deformation modes 2, 3, 5 and 6: deformations resulting from the multi-actuation approach by actuations of both a parallel and diagonal placed cable.

### 2.3 MULTI-ACTUATION: FROM 2D TO 3D

To make the instrument steerable in two planes (Figure 2.12), the 2D structure of Figure 2.10 must be revolved around its central axis. This will, however, cause the diagonal cables to cross each other at the center. Something that can be avoided by replacing the diagonal cables with helical cables that twist over  $180^\circ$  around the circumference of the steerable segment, thus exploiting the same architecture of muscles in Loliginid squid's tentacle [41]. Such a helical cable will invoke a torque around the central axis of the segment. By using both CW and CCW helical cables, any undesired imbalance in torque can be avoided. A 3D multi-actuated steerable segment will thus include three groups of cables placed parallel, helically CW and CCW, wherein each group is placed in a separate concentric layer, (Figure 2.13, section view).

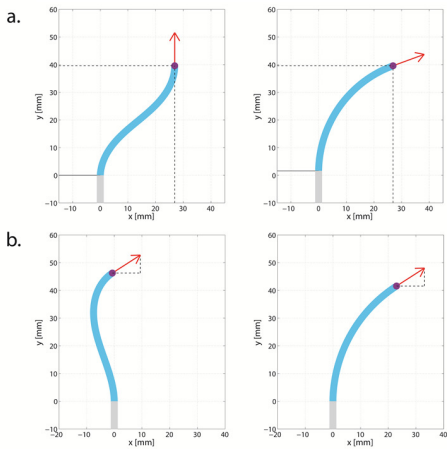


Figure 2.11: A multi-actuated segment has the ability to alter both the orientation and position of the end-effector (red arrow) independently. (a) Two deformation modes of a multi-actuated segment resulting in the same position, yet different orientation of the end-effector. Note that the shaft has to be axially translated; (b) two deformation modes of a multi-actuated segment resulting in the same orientation, yet different position of the end-effector.

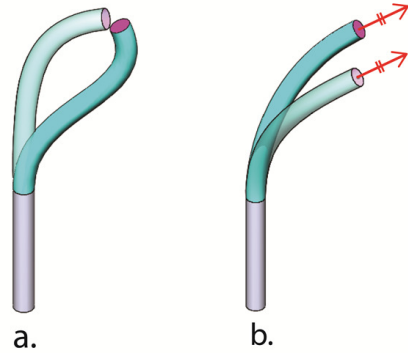


Figure 2.12: Extended workspace of a 3D multi-actuated segment, showing the possibility to maneuver the position and orientation of the end-effector independently in 3D space. (a) Capability of reaching the same position with a different angle of the end-effector; (b) capability of reaching the same orientation with a different position of the end-effector.

The additional advantage of using helical, instead of diagonal cables is the possibility of an inner free lumen at the center of the segment (Figure 2.13, section view) which can be used as a suction tube or to guide a flexible endoscope or additional cables to actuate an end-effector (i.e. graspers, cutters, and scissors).

A manual control strategy for the multi-actuated steerable segment can be realized by including a joystick that has a similar construction as the segment itself. Figure 2.13 presents a schematic representation of the resulting instrument consisting of a rigid straight shaft that connects the joystick to the tip. Using a mirrored control strategy, the tip mimics the motion of the joystick, yet in the opposite direction. Mirrored control is a commonly applied method to control steerable instruments in laparoscopy [24].

In the architecture of Figure 2.13, the parallel cables are routed in a straight line from the tip to the joystick. This ensures a mirrored relation between joystick and tip, as when the joystick, for example, moves up, the parallel cable that elongates in the joystick will pull the tip down. The helical cables will now have to change direction in the joystick, thus the helical cables that rotate CW in the tip have to rotate CCW in the joystick, and vice versa, as illustrated in Figure 2.13 (side view 1). The reason for this change in direction becomes

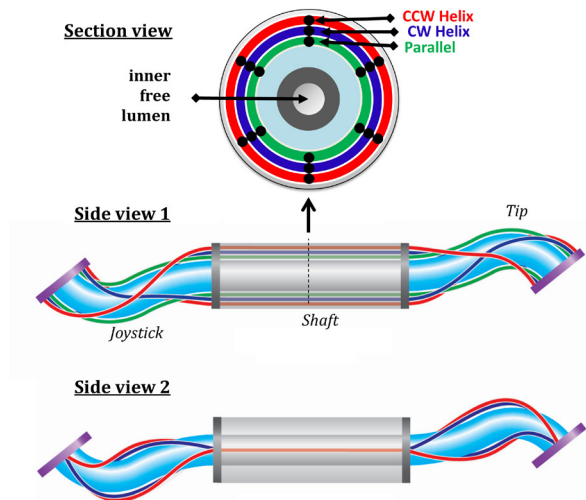


Figure 2.13: Schematic representation of a complete multi-actuated instrument that uses the mirrored control strategy. Section view: arrangement of the cables in concentric layers. Side views: the parallel cables run straight from the free ends of joystick and tip, while the helical cables have to change direction. Side view 1: the cables that run at the top and bottom of the shaft; side view 2: the helical cables that run at the middle of the shaft (other cables are not shown for simplicity).

apparent when considering the cables that run through the middle of the shaft as illustrated in Figure 2.13 (side view 2). If the direction of the helical cables is not changed, an elongated helical cable in the joystick would be coupled to a helical cable in the tip that also elongates, which is not possible and would seize the mechanism. Routing the cables through the instrument in the discussed manner ensures that the tip mimics, yet mirrors, the orientation and position of the joystick. Consequently, because the joystick and tip are placed opposite to each other, this also means that the joystick and tip extremities (purple in the figure) always stay parallel to each other.

## 2.4 HELIXFLEX PROTOTYPE

A demonstration prototype, called HelixFlex, was constructed based on the layered cable configuration, and the principles of mirrored control of Figure 2.13. This is the first prototype that incorporates the proposed multi-actuation technique. Its main function is to prove the functionality of the proposed technique and to showcase its underlying working principles. For this reason, it was chosen to not immediately design towards the required dimensions of a diameter of 3mm and a length of 30mm as specified in the

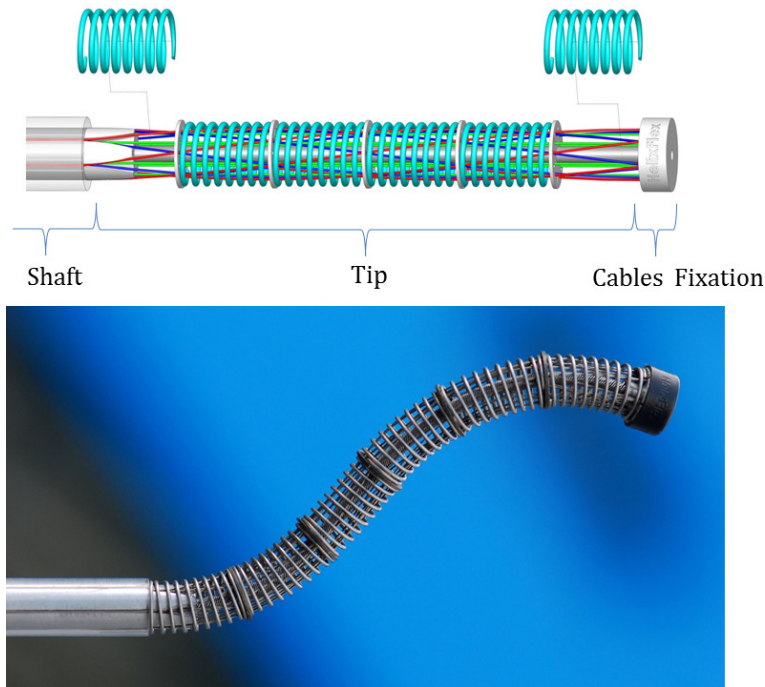


Figure 2.14: Top: CAD view of the HelixFlex's tip with two springs moved aside to show the internal cable configuration. Bottom: picture of real prototype tip bent into an S-shaped curve.

introduction. These dimensions were scaled up with a factor of two, allowing to ease the fabrication but still obtaining an instrument valid for MIS purposes.

Figure 2.14 shows a close up of the HelixFlex's steerable tip, which measures 5.8 mm in diameter ( $\varnothing$ ) and 60 mm in length, which is still smaller than the size of standard entry ports for laparoscopy which range up to 10 mm in diameter [48]. Each layer of cables counts six ( $\varnothing 0.2$  mm) stainless steel cables resulting in 18 cables that are all fixated at the free end of the tip. To correctly guide the cables along their intended route (parallel or helical), five guiding plates are placed along the length of the tip and kept in place by springs. The center contains a flexible and axially incompressible HHS<sup>®</sup> tube (Helical Hollow Strand, [49]), made from steel strings, that functions as a spline and contains an inner lumen of 1 mm.

The entire HelixFlex prototype is presented in Figure 2.15, where also the instrument's joystick is shown. The joystick incorporates the same parallel/helical cable layered structure as the tip, yet its dimensions are enlarged to a diameter of 20 mm and a length of 90 mm.



Figure 2.15: Complete HelixFlex prototype

This enlargement serves three purposes. Firstly, it eases the fixation of the cables, as they are distributed on a larger diameter. Secondly, it amplifies the movements of the joystick at the side of the tip [50]. Thirdly, it gives a magnified view of the cable structure, which is hardly visible in the tip, in line with the demonstrating nature of this prototype. Similar to the construction of the tip, the cables in the joystick are guided by guiding plates that are spaced using springs (Figure 2.16). Moreover, to prevent the cables from buckling in the enlarged space in between the guiding plates, 3D-printed spirals (shown in the exploded view of the joystick reported in Figure 2.16) are fitted in between the plates, including holes which smoothly guide the cables along their intended route. Finally, each cable is tensioned by a load of  $\pm 0.5$  N to avoid slack and fixated at the dome-shaped extremity of the joystick.

HelixFlex is equipped with a locking mechanism, positioned at the base of the joystick where the diameter of the instrument is enlarged in respect to the shaft, Figure 2.16. This locking mechanism enables the temporal fixation of all cables at once, thereby locking the shape of both joystick and tip. This would potentially allow the surgeon to release the joystick for doing other tasks during the procedure [19, 51, 52].

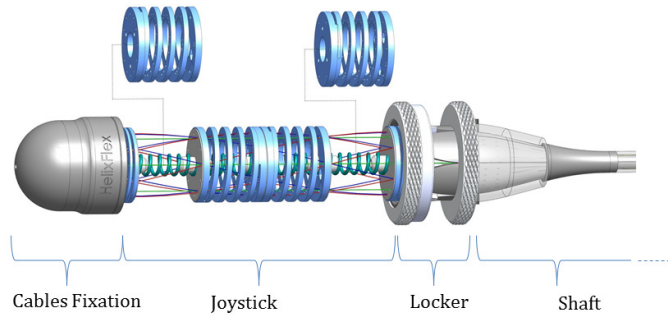


Figure 2.16: CAD view of HelixFlex's joystick with two spirals moved aside to show the internal cable configuration and components. The locker is positioned at the end of the shaft and by turning the knobs it is possible to temporarily fix all the cables at one time and therefore lock the shape of the tip of the instrument

## 2.5 PROTOTYPE EVALUATION

At first glance, the general impression of the HelixFlex while manually controlling the joystick is that the motion of the tip is very fluent. This motion is, in a sense, comparable with the smooth motion seen in the tentacle of squid.

HelixFlex is capable of creating constant radius bends and S-shaped curves, as presented in Figure 2.17 (deformation modes 1 and 4). Moreover, it can perform the deformation modes that are the result of both parallel and helical cable contraction. A number of these deformation modes (respectively modes 2, 3, 5 and 6) are also shown in Figure 2.17. Note that all the six presented deformation modes mimic the deformation modes that were predicted by the cantilever beam model and presented in Figure 2.10.

The range of the HelixFlex's workspace is evaluated on two measures: the largest angle of the tip in a constant radius bend and the largest sideway translation of the tip in an S-shaped curve. These two extreme deformations are pictured in Figure 2.18 and measured to be  $190^\circ$  for the angle of the constant radius bending and 23 mm for the largest sideway translation.

The goal of this study was to develop an actuation technique capable of controlling both the orientation and position of the end-effector relative to the shaft. To this purpose, Figure 2.19 shows two overlapping photos in which HelixFlex's tip is only translated (a) or only rotated (b), demonstrating clearly that the orientation and the position can be independently controlled. Finally, Figure 2.19 (c) shows a 3D motion of the tip, demonstrating the ability to make complex 3D curves by spatially controlling the tip in 4 DOFs.

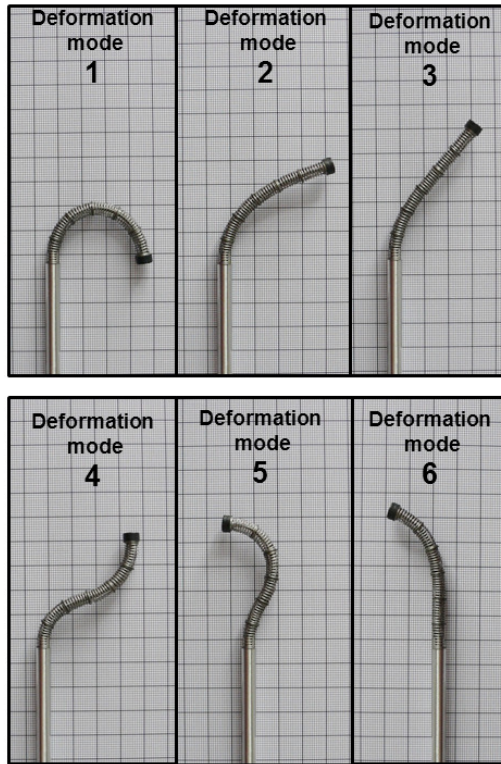


Figure 2.17: HelixFlex's tip performing the six deformation modes that were predicted by the cantilever beam model of Figure 2.1. Deformation modes 1 and 4 are generated by the exclusive use of parallel or helical cables. Deformation modes 2, 3, 5 and 6 are generated by the combined use of parallel and helix cables.

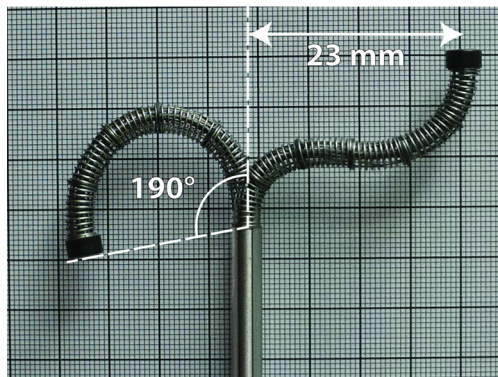


Figure 2.18: HelixFlex's tip performing two extreme deformations in a single plane, one showing the maximum curvature and the other showing the maximum sideways translation of the tip in a S-shaped curve. These two extreme positions, characterize the reachable workspace

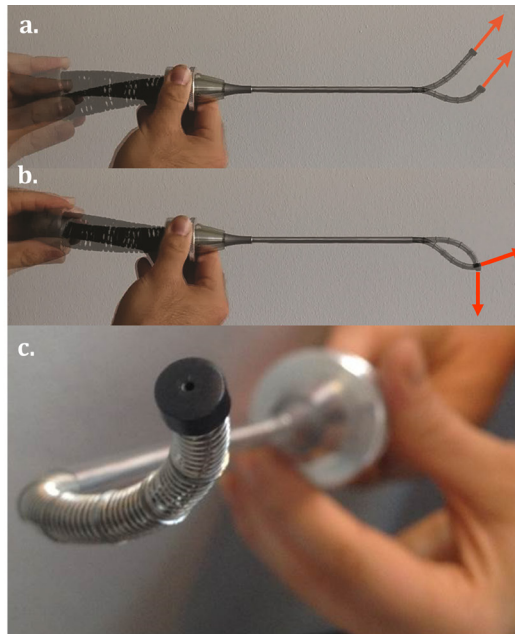


Figure 2.19: HelixFlex prototype being manually actuated by the authors: (a) showing the independent control of the tip's position, (b) showing the independent control of the tip's orientation, (c) showing the tip's capability of deforming in multiple planes at once.

## 2.6 DISCUSSION

The limited available space during EES indicates a need for a steerable instrument able to control both the orientation and position of the end-effector relative to the shaft, making sideways movements of the shaft redundant. Although a multi-steerable instrument, such as the MultiFlex of Figure 2.6, does already possess this level of maneuverability, its construction includes intermediate cable fixations along the length of its tip which make fabrication and miniaturization of such instruments challenging. The proposed multi-actuation technique was developed to exclude the need for these intermediate cable fixations. To our knowledge, HelixFlex is the first prototype that incorporates the 3D multi-actuation technique, and it shows promising results concerning the 4-DOFs maneuverability. For this reason, a patent application has been filled. Furthermore, the multi-actuation technique has interesting characteristics regarding miniaturization, control complexity and stiffening, which will now be discussed.

The diameter of HelixFlex's tip is already on the same scale as instruments used in standard laparoscopy, yet a minimum of  $\varnothing 3$  mm is preferred to cope with the limited workspace encountered during EES. Further miniaturization of HelixFlex can be realized by, for example,

2 applying the principle of the cable-ring mechanism of Figure 2.4 (right), in three concentric layers, as depicted in Figure 2.20. As the cables in a cable-ring keep each other aligned, the five guiding plates in the tip can be removed, further simplifying the mechanism to a continuous, smooth construction with a very close resemblance to biology's example in the Loliginid squid. The outside spring is still present for enclosing the cable configuration, yet it might better be replaced or enclosed by a flexible sealing to prevent entanglement of tissue between the spring coils. The decrease in diameter will affect the maximal sideways translation of the end-effector, which now measures 23 mm. If this maximal translation is linearly related to the tip's diameter, a maximum sideways translation of 12 mm for a  $\varnothing 3$  mm tip should be attainable. This would cover most of the sella turcica area which dimensions range from 6.7 to 19.8mm in height and 6.4 to 28.8mm in width.

The motion of HelixFlex's tip is very smooth, meaning that no noticeable hysteresis or 'stick-slip' events are present. The 'stick-slip' phenomenon occurs when an object is about to move and the difference between the static and dynamic friction is high, resulting in undesirable jerky movements. The smooth motion of HelixFlex's tip is most likely due to the low pre-tension ( $\pm 0.5$  N) on the cables which ensures a low initial static friction. Applying the principle of the cable-ring mechanism, as discussed above, will inevitably increase the amount of friction in the instrument. However, this does not automatically mean that it will increase the change of stick-slip, as stick-slip is due to the relation between static and dynamic friction, which will not necessarily be affected.

The control complexity of a steerable instrument can be described as how intuitive the relation between user input and its resulting tip movement is. In a multi-steerable instrument, the tip consists of multiple segments each with a set of individual steering cables. Consequently, all segments have to be controlled to achieve the desired orientation and position of the tip. In the case of MultiFlex of Figure 2.6, for example, the user must manually control each segment, resulting in a highly complex and non-intuitive manner of control. The control complexity can be simplified by including electromechanical actuators and a computerized interface [24]. The Da Vinci<sup>®</sup> System incorporates such a computerized control system which reduces the control complexity considerably [53]. A drawback of these systems is, however, the increase in overall complexity resulting in high purchase costs [42]. Moreover, these systems are less suitable for the use of handheld devices because the inclusion of electromechanical actuators will inevitably increase the size and weight of the instrument. In the case of multi-actuation, intermediate cable fixations are absent and all cables are fixated at the distal part of the tip. Consequently, the user only has to control a single point, the dome-shaped part of HelixFlex's joystick, to control the end-effector's position and orientation. Multi-actuation, therefore, reduces the control complexity compared to the multi-steerable approach.

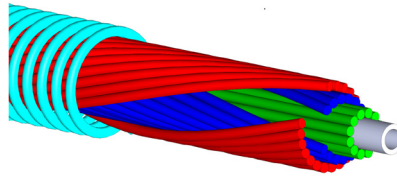


Figure 2.20: Concentric rings of parallel and helical cables.

In complex anatomical areas as the skull base, instrument navigation systems can be used to track the position and orientation of instruments and visualize them relative to pre-operative or even intra-operative CT or MRI images. These systems make use of localizers that are present near the instrument's end-effector and can be tracked using a variety of techniques based on mechanical, optical, ultrasonic or electromagnetic tracking [54]. Installing such localizers on HelixFlex will not be any different from installing them on currently used instruments, yet the flexible nature of HelixFlex's tip implies the need for additional localizers. One option would be to use two localizers, positioned at the proximal and distal part of the flexible tip. Such configuration will, however, not provide information about the shape of the tip, for which intermediate localizers would be necessary. Future work will, therefore, involve investigating the specific needs for instrument navigation concerning the HelixFlex.

Physiological tremor of the surgeon's hand will always be an issue during fine manipulation tasks using manually controlled devices. For this tremor canceling devices have been developed and some of them can also be adapted and connected to different pre-made handheld instruments [55]. However, a difference in the quantity of tremors between the current handheld instruments and HelixFlex is not expected, especially if HelixFlex is updated with a thumb joystick. The direction of the tremor does, however, change with the changing end-effector position and orientation and this might induce a learning curve for the surgeon.

The stiffness of the tip is an important requirement for a fully functional instrument suitable for clinical use [56]. The inclusion of helical cables into a single steerable segment does certainly have a positive effect on the torsion and bending stiffness of the compliant spline. The current design of HelixFlex is, however, not yet optimized for increasing the stiffness of the tip. Incorporating the cable-ring mechanism will increase the number of cables, increasing their overall resistance to stretch, thus increasing the stiffness of the tip. Furthermore, the HHS<sup>®</sup> tube, the current compliant spine, has a very low bending stiffness. Increasing the bending stiffness of the compliant spine will increase the overall stiffness of the tip. It is, however, worth noting that this increase in spine stiffness will also increase the input force required from the user to operate the joystick.

In Nature, two inherently different methods for creating a maneuverable, yet stiff, structure can be identified. One method revolves around the use of an endo- or exoskeleton consisting out of rigid bones connected by joints, as the human arm. The other method uses a hydrostatic skeleton system which consists of a flexible and elastic structure surrounded by muscles, as the muscular hydrostat of the tentacle of Loliginid squid. Both methods are inherently different as in the endo- or exoskeleton approach the amount of joints is minimized, whereas in the hydrostatic skeleton approach the amount of joints is theoretically maximized by creating a continuous structure.

2

Current steerable instruments are mainly constructed out of rigid links and hinged constructions, making them best comparable with Nature's endo- or exoskeleton approach. This approach limits the required actuation cables, yet it also requires small and difficult to fabricate hinged structures that can lead to complex designs. The multi-actuation approach, instead, is based on Nature's hydrostatic skeleton systems approach. It requires a lot more cables, yet the complicated hinged structure can now be replaced by a simple compliant structure. The added advantage is that, just as the motion of a tentacle is more fluent than the motion of a human arm, the motion of a multi-actuated tip is more fluent than the motion of conventional multi-link instruments. In terms of stiffness, both the skeleton approach and the muscular hydrostat approach can be rigidified by simultaneous contraction of all muscles [38]. Future works on the multi-actuation technique will therefore also be focused on a similar rigidifying mechanism to stiffen the tip.

Additional future works of the BITE group at the TU Delft will involve a multi-purpose instrument of which an artistic impression is given in Figure 2.21. Multi-actuation will be the cornerstone of these envisioned developments, as it shows promising features concerning its maneuverability, construction and control complexity, and potential rigidity.

## 2.7 CONCLUSION

This paper introduced a new cable-based actuation method for handheld steerable instruments for medical purposes. EES targeting complex pituitary gland tumors was taken as a reference example for situations where surgeons require higher maneuverability from the used instrumentation. It was found that a suitable instrument should allow for a stationary shaft position, while both the orientation and position or the tip could be independently controlled. Inspired by the biomechanical construction of the tentacle of squid, a new cable-based actuation method named multi-actuation was developed. The method involves multi-directional cable-configurations and was successfully incorporated

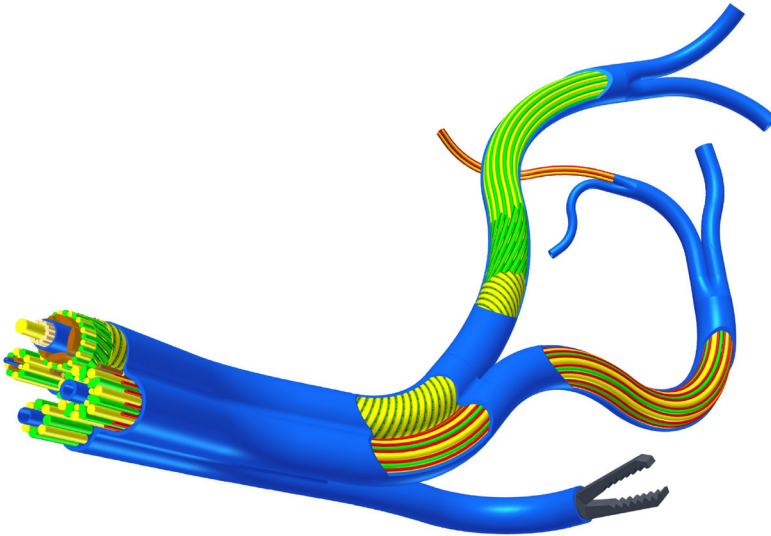


*Figure 2.21: Artistic impression of the author's vision relating to the future work concerning the multi-actuation technique to be used in a multi-purpose instrument.*

into a novel prototype called HelixFlex. This handheld instrument showed satisfactory results concerning its 4 DOFs maneuverability, as the orientation and position of the tip can be independently controlled relative to the shaft. Future research will focus on the further miniaturization of the instrument's tip, improving its rigidity, and the incorporation of the multi-actuation technique into a singlehanded manually controlled instrument.

## 2.8 REFERENCES

1. Cuschieri, A., Laparoscopic surgery: current status, issues and future developments. *The Surgeon*, 2005. 3(3): p. 125-138.
2. Rattner, D. and A. Kalloo, ASGE/SAGES working group on natural orifice transluminal endoscopic surgery. *Surgical Endoscopy and Other Interventional Techniques*, 2006. 20(2): p. 329-333.
3. Gondim, J.A., et al., Giant pituitary adenomas: surgical outcomes of 50 cases operated on by the endonasal endoscopic approach. *World neurosurgery*, 2014. 82(1): p. e281-e290.
4. Cappabianca, P., et al., Extended endoscopic endonasal approach to the midline skull base: the evolving role of transsphenoidal surgery. *Adv Tech Stand Neurosurg*, 2008. 33: p. 151-99.

5. Komotar, R.J., et al., Endoscopic endonasal compared with microscopic transsphenoidal and open transcranial resection of craniopharyngiomas. *World Neurosurg*, 2012. 77(2): p. 329-41.
6. Cappabianca, P., et al., Size does not matter. The intrigue of giant adenomas: a true surgical challenge. *Acta Neurochirurgica*, 2014. 156(12): p. 2217-2220.
7. Cusimano, M.D., et al., Outcomes of surgically treated giant pituitary tumours. *Can J Neurol Sci*, 2012. 39(4): p. 446-57.
8. Romano, A., et al., Expanding the boundaries of the transsphenoidal approach: a microanatomic study. *Clin Anat*, 2001. 14(1): p. 1-9.
9. Schwartz, T.H., et al., Endoscopic cranial base surgery: classification of operative approaches. *Neurosurgery*, 2008. 62(5): p. 991-1005.
10. de Paiva Neto, M.A., et al., Endonasal transsphenoidal surgery and multimodality treatment for giant pituitary adenomas. *Clin Endocrinol (Oxf)*, 2010. 72(4): p. 512-9.
11. Cappabianca, P., L.M. Cavallo, and E. de Divitiis, Endoscopic endonasal transsphenoidal surgery. *Neurosurgery*, 2004. 55(4): p. 933-40; discussion 940-1.
12. Cappabianca, P. and L.M. Cavallo, The evolving role of the transsphenoidal route in the management of craniopharyngiomas. *World Neurosurg*, 2012. 77(2): p. 273-4.
13. Ozcan, T., et al., Surgical limits in transnasal approach to opticocarotid region and planum sphenoidale: an anatomic cadaveric study. *World neurosurgery*, 2010. 73(4): p. 326-333.
14. Snyderman, C.H., et al., What are the limits of endoscopic sinus surgery?: the expanded endonasal approach to the skull base. *Keio J Med*, 2009. 58(3): p. 152-60.
15. Liu, J.K., et al., Surgical nuances for removal of olfactory groove meningiomas using the endoscopic endonasal transcribriform approach. *Neurosurg Focus*, 2011. 30(5): p. E3.
16. Juraschka, K., et al., Endoscopic endonasal transsphenoidal approach to large and giant pituitary adenomas: institutional experience and predictors of extent of resection. *J Neurosurg*, 2014. 121(1): p. 75-83.
17. Berguer, R., D.L. Forkey, and W.D. Smith, Ergonomic problems associated with laparoscopic surgery. *Surgical Endoscopy*, 1999. 13(5): p. 466-468.
18. Swaney, P.J., et al., Endonasal Skull Base Tumor Removal Using Concentric Tube Continuum Robots: A Phantom Study. *J Neurol Surg B*, 2015. 76(02): p. 145-149.
19. Schneider, J.S., et al., Robotic surgery for the sinuses and skull base: What are the possibilities and what are the obstacles? *Current opinion in otolaryngology & head and neck surgery*, 2013. 21(1): p. 11.
20. Jelinek, F., et al., Classification of Joints Used in Steerable Instruments for Minimally Invasive Surgery. *Journal of Medical Devices*, 2014. 8(3): p. 030914.
21. Catherine, J., C. Rotinat-Libersa, and A. Micaelli, Comparative review of endoscopic devices articulations technologies developed for minimally invasive medical procedures. *Applied Bionics and Biomechanics*, 2011. 8(2): p. 151-171.
22. Fan, C., D. Dodou, and P. Breedveld, Review of manual control methods for handheld maneuverable instruments. *Minimally Invasive Therapy & Allied Technologies*, 2013. 22(3): p. 127-135.
23. Madhani, A.J. and J.K. Salisbury, Articulated Surgical Instrument for Performing Minimally Invasive Surgery With Enhanced Dexterity and Sensitivity. US 9,510,915 B2, Applicant: Intuitive Surgical Operations Inc., Priority date 11/03/2014.

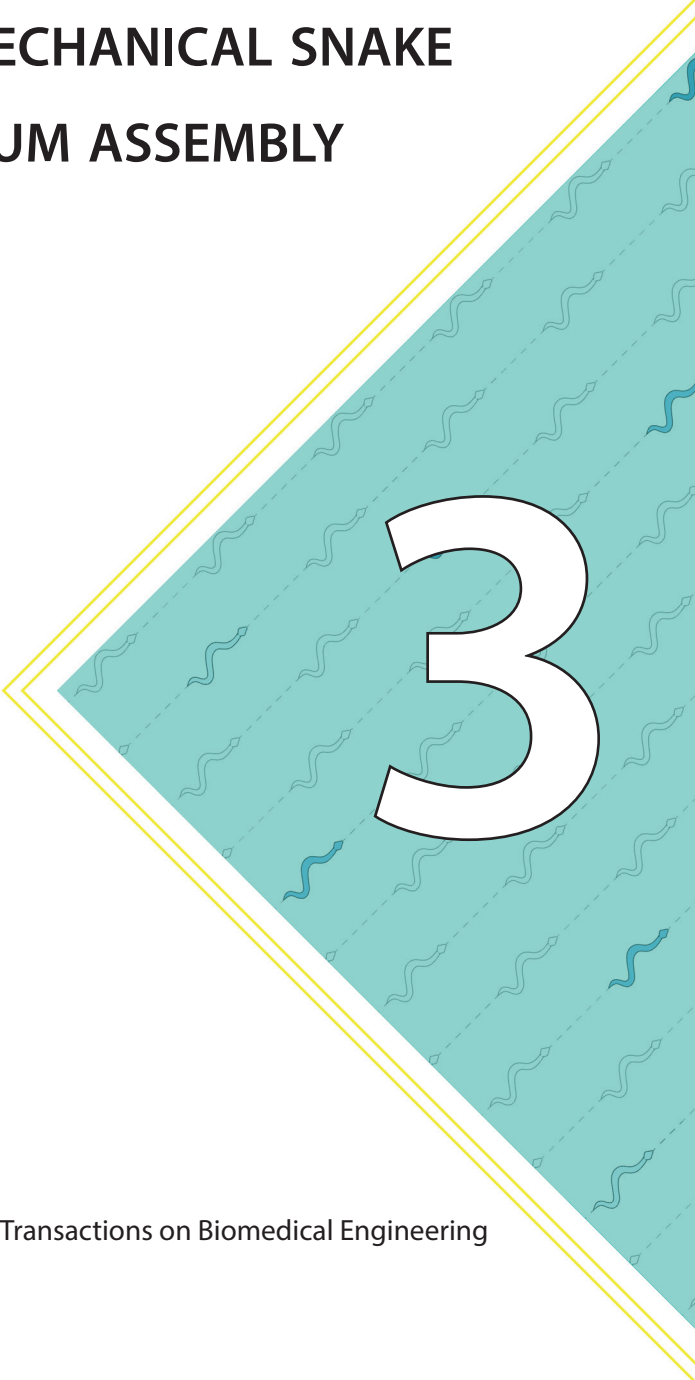
24. Cooper, T.G. and S.C. Anderson, Flexible wrist for surgical tool. US 8,337,521 B2. Applicant: Intuitive Surgical Operations Inc., Priority date 17/11/2010.
25. Robinson, G. and J.B.C. Davies. Continuum robots-a state of the art. in *Robotics and Automation*, 1999. Proceedings. 1999 IEEE International Conference on. 1999.
26. Ota, T., et al., A highly articulated robotic surgical system for minimally invasive surgery. *The Annals of thoracic surgery*, 2009. 87(4): p. 1253-1256.
27. Shammass, E., A. Wolf, and H. Choset, Three degrees-of-freedom joint for spatial hyper-redundant robots. *Mechanism and machine theory*, 2006. 41(2): p. 170-190.
28. Simaan, N., et al., Design and integration of a telerobotic system for minimally invasive surgery of the throat. *The International journal of robotics research*, 2009. 28(9): p. 1134-1153.
29. Li, C. and C.D. Rahn, Design of continuous backbone, cable-driven robots. *Journal of Mechanical Design*, 2002. 124(2): p. 265-271.
30. Webster, R.J., A.M. Okamura, and N.J. Cowan. Toward active cannulas: Miniature snake-like surgical robots. in *Intelligent Robots and Systems*, 2006 IEEE/RSJ International Conference on. 2006.
31. Burgner, J., et al., A Telerobotic System for Transnasal Surgery. *Mechatronics*, IEEE/ASME Transactions on, 2014. 19(3): p. 996-1006.
32. Webster, R.J., J.M. Romano, and N.J. Cowan, Mechanics of pre-curved-tube continuum robots. *Robotics*, IEEE Transactions on, 2009. 25(1): p. 67-78.
33. Webster, R.J. and B.A. Jones, Design and kinematic modeling of constant curvature continuum robots: A review. *The International Journal of Robotics Research*, 2010.
34. Trivedi, D., et al., Soft robotics: Biological inspiration, state of the art, and future research. *Applied Bionics and Biomechanics*, 2008. 5(3): p. 99-117.
35. Kier, W.M., The functional morphology of the musculature of squid (Loliginidae) arms and tentacles. *Journal of Morphology*, 1982. 172(2): p. 179-192.
36. Kier, W.M., The diversity of hydrostatic skeletons. *J Exp Biol*, 2012. 215(Pt 8): p. 1247-57.
37. Ranzani, T., et al., A bioinspired soft manipulator for minimally invasive surgery. *Bioinspiration & biomimetics*, 2015. 10(3): p. 035008.
38. Loeve, A., P. Breedveld, and J. Dankelman, Scopes too flexible... and too stiff. *IEEE pulse*, 2010. 1(3): p. 26-41.
39. Stefanchik, D., O.J. Vakharia, and J.T. Spivey, Braided endoscope accessories. 2008.
40. Turchetti, G., et al., Economic evaluation of da Vinci-assisted robotic surgery: a systematic review. *Surgical endoscopy*, 2012. 26(3): p. 598-606.
41. Van Leeuwen, J.L., J.H. De Groot, and W.M. Kier, Evolutionary Mechanics of Protrusible Tentacles and Tongues. *Netherlands Journal of Zoology*, 2000. 50(2): p. 113-139.
42. Breedveld, P., et al., A new, easily miniaturized steerable endoscope. *Engineering in Medicine and Biology Magazine*, IEEE, 2005. 24(6): p. 40-47.
43. Breedveld, P., Bio-Inspired Maneuverable Dendritic Devices for Minimally Invasive Surgery. [Vici proposal], Delft University of Technology, Delft, the Netherlands, 2011.
44. Zada, G., R. Du, and E.R. Laws, Defining the "edge of the envelope": patient selection in treating complex sellar-based neoplasms via transsphenoidal versus open craniotomy. *J Neurosurg*, 2011. 114(2): p. 286-300.

45. Bekeny, J.R., et al., Forces applied at the skull base during transnasal endoscopic transsphenoidal pituitary tumor excision. *Journal of neurological surgery. Part B, Skull base*, 2013. 74(6): p. 337.
46. Abu-Abeid, S., et al., Treatment of intra-gastric band migration following laparoscopic banding: safety and feasibility of simultaneous laparoscopic band removal and replacement. *Obesity surgery*, 2005. 15(6): p. 849-852.
47. FWmetals, www.fwmetals.com. [Internet], FWmetals [cited 01-02-2015]. Available from: <http://www.fwmetals.com/products/hhs-tube>.
48. Vosse, M.S., Duoflex: Development of a New Multi-Steerable Laparoscopic Instrument. [Master thesis,] Delft University of Technology, Delft, the Netherlands, 2010. Available from: <https://repository.tudelft.nl>
49. Zahraee, A.H., et al., Toward the development of a hand-held surgical robot for laparoscopy. *Mechatronics, IEEE/ASME Transactions on*, 2010. 15(6): p. 853-861.
50. Herman, B., et al., An articulated handle to improve the ergonomic performance of robotic dextrous instruments for laparoscopic surgery. *Mechanical Sciences*, 2014. 5(1): p. 21-28.
51. Freschi, C., et al., Technical review of the da Vinci surgical telemanipulator. *The International Journal of Medical Robotics and Computer Assisted Surgery*, 2013. 9(4): p. 396-406.
52. Maybody, M., C. Stevenson, and S.B. Solomon, Overview of navigation systems in image-guided interventions. *Techniques in vascular and interventional radiology*, 2013. 16(3): p. 136-143.
53. Riviere, C.N., W. Ang, and P.K. Khosla, Toward active tremor canceling in handheld microsurgical instruments. *Robotics and Automation, IEEE Transactions on*, 2003. 19(5): p. 793-800.
54. Jelinek, F., et al., Attaining high bending stiffness by full actuation in steerable minimally invasive surgical instruments. *Minimally Invasive Therapy & Allied Technologies*, 2014. 24(2): p. 77-85.





# HELICOFLEX: MECHANICAL SNAKE THROUGH MINIMUM ASSEMBLY



3

Accepted with minor revisions: IEEE Transactions on Biomedical Engineering

**ABSTRACT**

In minimally invasive surgery, maneuverability is usually limited and a large number of degrees of freedom (DOFs) is highly demanded. However, increasing the DOFs usually means increasing the complexity of the surgical instrument leading to long fabrication and assembly times. In this work, we propose a fully 3D-printed hand-held, multi-steerable device. The proposed device is mechanically actuated and possesses five serially controlled segments. We designed a new compliant segment providing high torsion and axial stiffness as well as a low bending stiffness by merging the functions of four helicoids and a continuum backbone. Compliant segments were combined to form the compliant shaft of the new device. To control this compliant shaft, a control-handle was designed that mimics the shaft structure. A prototype called the HelicoFlex was built using only three 3D-printed parts. HelicoFlex, with its 10 degrees of freedom, showed a fluid motion in performing single and multi-curved paths. The instrument was 3D-printed without any support material in the compliant shaft itself. This work contributes to enlarge the body of knowledge regarding how additive manufacturing could be used in the production of multi-steerable surgical instruments for personalized medicine.

### 3.1 INTRODUCTION

Over the last decades, one of the most significant innovations in surgery is the transition from open surgery to minimally invasive surgery (MIS). In open surgery, the area of interest is directly exposed, and depending on the specific procedure, the incision can be relatively large [1, 2]. However, increasing the size of the incision means increasing the risk of infection as well as the recovery time for the patient [3][4]. Conversely, MIS strives to reduce the incision size by using smaller instruments and indirect visualization using endoscopes. However, using conventional tools that are straight, long, and rigid while decreasing the size of the incision, has a high impact on the maneuverability of the instruments and the reachability of the area of interest. The problem is evident in Natural Orifice Transluminal Endoscopic Surgery (NOTES) which uses natural orifices such as mouth, anus, or nose as the entry port of the body [5][6]. For instance, Endoscopic Endonasal Surgery (EES) is a NOTES procedure in which the nostrils are the entry port to reach and remove tumors at the base of the skull. A common procedure is the removal of adenomas in the pituitary gland. The narrow corridor through the nostrils limits the maneuverability of the used rigid instruments.

Research groups have analyzed the problem of instrument maneuverability, and many devices have been proposed [7]. The use of the well-known da Vinci® robotic system (Intuitive Surgical Inc., Sunnyvale, Ca, USA) with integrated EndoWrist technology: a two degrees of freedom (DOFs) mechanism for steering into the distal end of the surgical instruments, increases surgeon dexterity in a laparoscopy scenario allowing procedures in which high maneuverability is required (Figure 3.1) [8]. However, steerability is still limited due to rigid instrument shafts which do not permit navigation through curves with multiple radii [9]. Moreover, miniaturized pulleys, which are at the base of the EndoWrist design, guide the cables, provoking fatigue and limiting the lifespan to a maximum of ten sterilization cycles, increasing the overall costs [10].

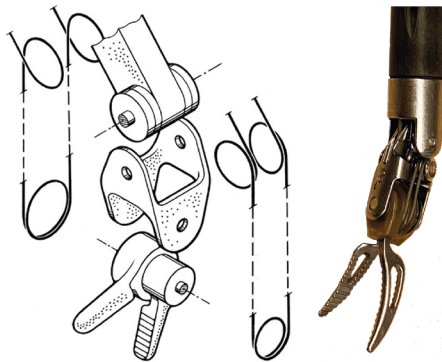


Figure 3.1: Schematic exploded view of the Endo Wrist in which the different driving cables, pulleys, and rivets are shown, adapted from Breedveld et al. [34], based on the EndoWrist patent [9], and a Ø8 mm Endo Wrist Grasper.

To overcome the rigidity of the shaft, research has been focused on the integration of an additional flexible component at the end of the rigid shaft, allowing maneuvering over more complex curvatures and expanding the motion beyond the 2 DOFs EndoWrist. The flexibility of the additional component can be obtained using continuum structures. Multi-steerable instruments based on continuum structures can be compared with “invertebrates” due to their ability to form continuous curves [11, 12]. Examples of continuum structures are concentric telescopic tube robots [13] composed of concentric pre-curved tubes placed into one another. The control of the rotation and the translation of the tubes relative to each other allows the formation of curved shapes [14, 15]. Another approach is using a single- or a multi-backbone structure. In a single-backbone structure, a single element supports the entire flexible segment. This element can be made of shape-memory alloys [16], springs [17], flexible tubes, or variable stiffness mechanisms [18, 19]. Multi-backbone structures are based on multiple elements, for example, parallel rods, that equally contribute to the motion of the flexible tip [20].

3

Regardless of the number of backbones used, multi-steerable instruments require a method of actuation. Types of actuation are based on hydraulic and pneumatic principles, as well as shape-memory alloy [7]. However, tendon-driven actuation remains most commonly used in medical applications due to the possibility of minimizing the size of the tip while at the same time controlling a large number of DOFs [21]. In an attempt to control the complex motion of such a multi-DOFs shaft, each DOFs can be individually controlled and actuated using independent electric motors. Due to their relatively large size, these motors should then be placed outside the patient at the control side of the instrument. However, the use of a large number of motors generally results in high production costs, difficulties in sterilization, and unsuitability for disposable use [22]. Moreover, a system with a large number of motors requires a large footprint, reducing the workspace for the surgeon near the patient.

In an attempt to solve these issues, manually actuated instruments such as the HelixFlex proposed by Gerboni et al. or the multi-backbone elbow device presented by Riojas et al., have been developed, presenting a completely different approach by being multi-steerable and at the same time hand-held [23, 24]. These instruments are fully mechanically actuated with no need for electric motors. Fan et al. [25] give a comprehensive overview of hand-held (multi-)steerable instruments and Anderson et al. [26] of their control methods. Although the proposed hand-held devices meet the requirements in terms of flexibility, miniaturization, and maneuverability, they are still very complex, containing numerous complex-shaped parts, impairing the assembly process, and making the device unsuited for sterilization or low-cost disposable use.

Additive manufacturing (AM), also referred to as three-dimensional (3D) printing, might provide a solution. AM enables a computer-aided design (CAD) to be directly converted into a 3D object with a layer by layer printing process. AM allows the production of structures with complex geometries that cannot be produced with conventional fabrication techniques. Moreover, this increase in geometrical complexity allows for the integration of more functionality into a single part, consequently reducing the need for assembling multiple parts. Many research groups are exploiting this technology in the field of medical instruments [27]. An example is given by the manipulator presented by Mintenbeck et al. in which AM was used in the fabrication of the steerable segments [28]. Morimoto et al. applied AM into concentric tube robots investigating different materials and 3D-printing technology [29], while at the Technical University of Munich researchers developed a 3D-printed overtube to enhance the properties of conventional flexible endoscopes [30, 31].

Although problems such as steerability and miniaturization have been addressed, design complexity is still high and the number of components is still large, hindering the reduction of assembly time. Therefore, this study explores the use of AM for the development of a manually actuated tendon-driven multi-steerable surgical device, intending to simplify its fabrication and assembly process to make it suitable for disposable use. A new device called HelicoFlex was developed as a first explorative case to combine easy manufacture with very high steering performance. HelicoFlex is the first handheld device that is printed in only three parts with five steerable segments, which enables the control of 10 DOFs. In the first part of the paper, we will explore new geometries to find a design paradigm to combine the characteristics of a compliant shaft and minimize the number of parts while using AM. In the second part of the paper, we present the entire design and study its behavior in performing complex curves.

3

## 3.2 CONCEPTUAL DESIGN

### 3.2.1 DESIGN REQUIREMENTS

The compliant shaft of our instrument should allow high steerability in terms of multiple DOFs to follow tortuous paths and complex curves with different radii. The device should, therefore, include multiple segments that are serially connected and each bendable in 2 DOFs. Each segment should have a high axial and torsional stiffness, while a relatively low bending stiffness is preferred. Axial stiffness is required for reliable control of the compliant shaft while torsional stiffness is required to endure axial torques that arise

from external loads. On the contrary, low bending stiffness is preferred as it improves the bendability of the entire shaft and limits the required tensile forces on the steering cables, reducing the forces required for actuation and resulting in lower friction forces in the system. For application in MIS, the diameter of the compliant shaft should not exceed 10 mm [32], integrating at least one lumen to allow for the insertion of additional instruments (i.e., biopsy forceps) or tools to visualize and operate on the area of interest. Guidance and fixation of cables are two of the most challenging functionalities within a tendon-driven device, and therefore often have a significant influence on the shape, fabrication, and assembly process of the device, especially in multi-steerable instruments that incorporate many cables. An effective and scalable method for integrating the functionalities of cable guidance and fixation in preferably one single component was, therefore, a key research topic in the design of our instrument. Finally, the new compliant shaft should preferably be 3D-printed without support material, which is sacrificial material needed to print specific overhangs, to reduce the post-processing time after the printing process.

## 3

### 3.2.2 DESIGN CHOICES

Conventional steerable instruments are generally based on a chain of connected rigid elements. In the specific case of EndoWrist, steering in two directions is provided by a series of miniature pulleys placed perpendicular to each other and individually controlled by driving cables looped around the pulleys (Figure 3.1). As the diameter of the pulleys is too small as compared to the thickness of the driving cables, the cables suffer from fatigue, reducing the lifespan of the EndoWrist to only ten procedures [33]. In our design, we aimed at avoiding pulleys by using a cable guidance system that does not generate fatigue. Moreover, we aimed at greatly expanding EndoWrist's motion to 10 DOFs while merging all its rigid-linked frame properties into one 3D-printed compliant component without using support, combining high axial and torsional stiffness with low bending stiffness. We strived to have at least one lumen and containing simple means to guide and fix 20 actuation cables, to facilitate fast and easy assembly.

#### COMPLIANT SEGMENT DESIGN

A compliant structure that combines high axial stiffness with low bending stiffness can be created by using a thin beam serving as a continuous backbone at the center of a steering segment (Figure 3.2a). However, a thin beam is not torsion stiff. Increasing the diameter of the beam would provide higher torsion stiffness, yet would also increase its bending stiffness, and is therefore not an option. Thus, an additional element has to be added to ensure torsion stiffness. A helicoid is a compliant element able to provide high torsion stiffness and low bending stiffness. In our design, we decided to combine these two elements: a continuous thin central backbone around which a helicoid runs (Figure 3.2b).

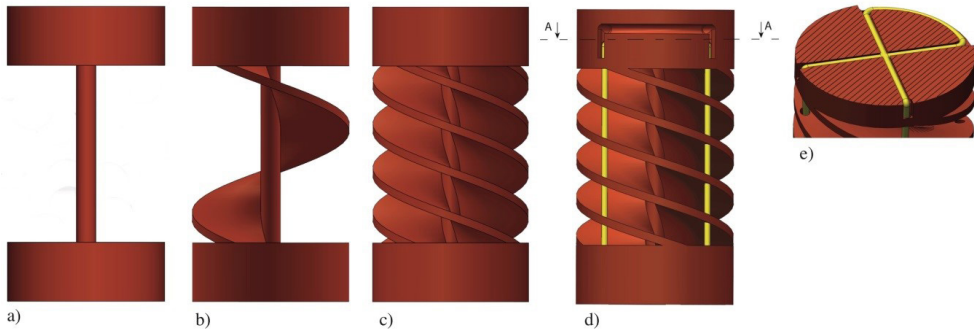


Figure 3.2: Schematic drawing of a 3D-printed compliant shaft segment with actuation cables in yellow: a) a solid backbone gives a high axial stiffness; b) a helix increases torsion stiffness; c) increasing the number of helixes makes the system more homogeneous; d) holes are added to guide four actuation cables through the helixes; and e) the segment is completed with an additional structure to loop and fasten the actuation cables.

Four helixes were evenly placed around the centerline to provide a more homogeneous torsion stiffness as compared to only one helix (Figure 3.2c). The pitch of each helix was kept equal to the length of the backbone, meaning that each helix makes one full turn within the length of the backbone.

Finally, we defined the exact shape of the four helixes. As shown in the cross-section in Figure 3.3a, we started with a thin rectangular shape for the helixes. However, at the inside of these helixes, cracks can be provoked by excessive bending. By increasing the thickness of the helixes, we can ensure that the helixes would touch each other at their outer edge, thus creating a stop for the bending (Figure 3.3b). However, increasing the thickness of the helix at the outer edge while keeping the rectangular shape would increase the bending stiffness as, in this case, more material is added to the backbone. Therefore, we decided to change the rectangular shape into a T-shape (Figure 3.3c), keeping a low bending stiffness while at the same time limiting the maximum bending angle.

### CABLE FIXATION METHOD

As previously discussed, cable fixation is an important aspect that can affect the robustness of the device, causing malfunctioning or breakages. In our compliant design, we decided on an alternative cable fixation method avoiding soldering or gluing. Exploring friction-based fixation methods led us to a solution in which the cables are looped inside the structure. As shown in Figure 3.2e, by looping a cable into a cross-shaped groove in the transversal plane of the segment and bending both its ends 90 degrees in the pulling direction, we obtain two independent actuation cables positioned at an angle

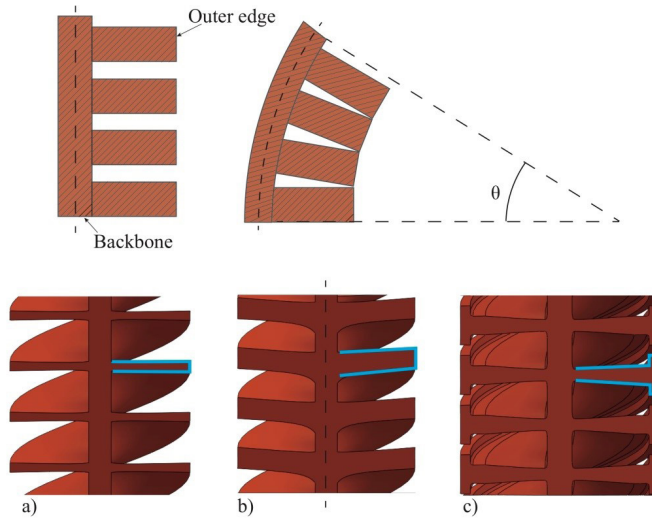


Figure 3.3: Helicoids shape design: Top: Sketch of a compliant segment in a straight and bent position. Bottom: different shapes of the helicoids cross-section: a) thin rectangular shape, b) thick rectangular shape, c) T-shape.

of 90 degrees and connected in a sturdy cable fixation point (Figure 3.2d). Fixating four actuation cables per segment was realized by adding two cable fixation points on top of each other, rotated over 180 degrees. The total height of the resulting fixation module was 3 mm, leading to a total segment length of 12 mm. For our prototype, we decided to use an outer diameter of 8 mm.

### 3.3 PROOF OF CONCEPT: HELICOFLEX

After characterizing a single 3D-printed segment of the compliant shaft, we designed the entire HelicoFlex (Figure 3.4). The instrument is composed of only three components: a compliant shaft and a compliant handle with a rigid shaft in between. We designed a handle with a compliant structure equivalent to the compliant shaft. The compliant shaft and the handle were connected using cables that actuate the device with a serial control method, described by Fan et al. [25], in which the compliant shaft mirrors the movement of the compliant handle (Figure 3.4a).

The compliant shaft of the device is composed out of compliant segments ( $\varnothing 8$  mm, length 12 mm) stacked on top of each other to create a modular shaft in which the number of segments can be changed according to the number of DOFs required. We decided for a shaft with five compliant segments, resulting in a total of 10 DOFs at a length of 60 mm

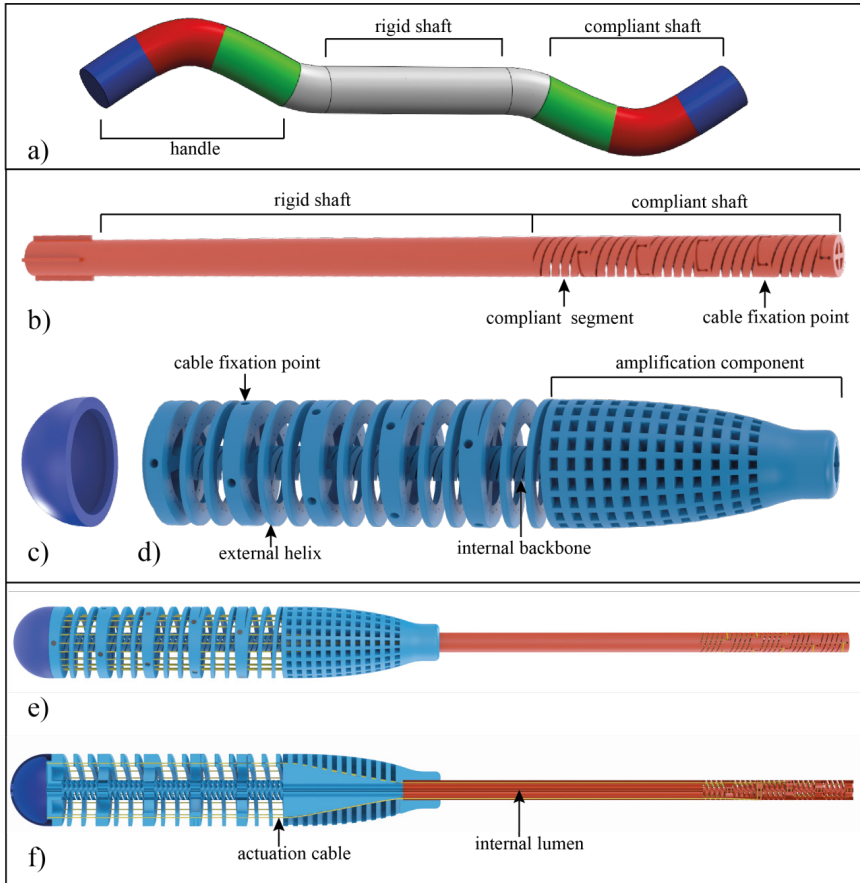


Figure 3.4: Phases in the development of the HelicoFlex: a) chosen serial control method in which each colored segment of the compliant handle controls the corresponding mirrored segment of the compliant shaft; b) compliant shaft connected to rigid shaft in which a compliant segment and a cable fixation point are highlighted; c) end cap in which the loose ends of the actuation cables are stored; d) compliant handle in which the external helix, the internal backbone, a cable fixation point at the handle side, and the amplification component are highlighted; e) assembly; and f) cross-section, showing one of the internal lumens and two actuation cables.

(Figure 3.4b). Each compliant segment has a backbone of  $\text{\O}1$  mm and is actuated by four cables that are fixed at the segment location, as shown in Figure 3.2e, and run along the compliant shaft in a cable-ring configuration. Each segment is twisted around its centerline over 18 degrees as compared to the previous segment to avoid overlapping of the 20 parallel-running cables.

The rigid shaft ( $\text{\O}8$  mm, 120 mm long) is printed in one part together with the compliant shaft and guides the cables from the compliant shaft to the handle through dedicated grooves running along its entire length (Figure 3.4b).

The compliant handle is connected to the rigid shaft using a press-fit mechanism, and its design is based on a large version of the compliant shaft (Figure 3.4d). The handle contains an inner backbone and an outer helical structure. The inner backbone has a structure similar to the compliant shaft, containing five segments with a diameter of 8 mm and a length of 22.5 mm. The outer helical structure of the handle has an outer diameter of 29 mm and contains holes through which the cables run. Running the cables through the handle at a larger diameter than in the compliant shaft creates not only additional space for precise fixation of the cables but also creates an amplification factor between the handle and the compliant shaft. Assuming that there is no friction, no play, no compression of the printed parts, and no stretching of the cables, the amplification factor can be calculated using the following equation:

$$\gamma = \beta \frac{D_{handle}}{D_{shaft}} \quad (3.1)$$

where  $\gamma$  is the desired bending angle of the tip,  $\beta$  is the corresponding bending angle of the handle,  $D_{handle}$  is the diameter of the cable ring in the compliant handle, and  $D_{shaft}$  is the diameter of the cable ring in the compliant shaft. To guide the cables smoothly from the shaft to the handle, an amplification component was designed at the base of the handle to gently amplify the cable distance from 6.4 mm to 22 mm. The amplification component guides the cables smoothly through partly covered S-shaped grooves while avoiding buckling. The amplification component is covered by a hive-inspired structure with holes. The hive structure facilitates the 3D-printing process by enabling the precise printing of cable grooves, avoiding clogging (Figure 3.4f).

In the handle, cables were fixated via dog point set screws to enable easy fine-tuning. The ends of all cables were collected and stored inside the end cap (Figure 3.4c), attached to the handle by a press-fit mechanism. Four lumens with a diameter of 1.75 mm run through the entire device to enable the insertion of thin, flexible instruments such as biopsy forceps, or thin, fiberoptic endoscopes to visualize the site of interest.

### 3.4 ADDITIVE MANUFACTURING THE HELICOFLEX

Considering the small size of some of HelicoFlex's features, we selected the AM technology taking into account the resolution achievable by the printer. A Perfactory® 4 Mini XL (EnvisionTec GmbH, Gladbeck, Germany), with a layer height in the vertical z-axis of 25  $\mu\text{m}$ , was used to fabricate all three parts of the device. The used printer is based on vat photopolymerization technology and uses the so-called Digital Light Processing (DLP) in

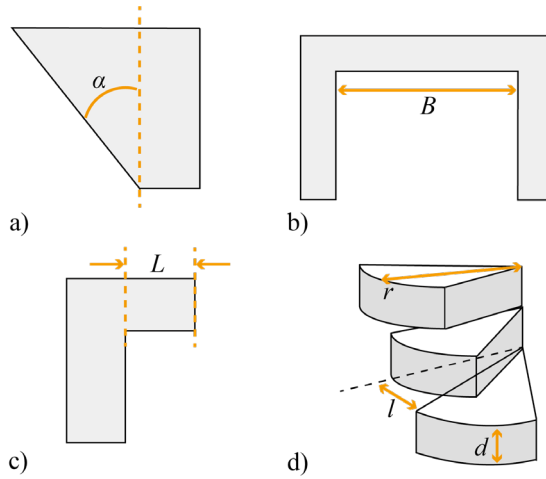


Figure 3.5: Rules to print without support: a) reducing overhang angle ( $\alpha$ ); b) limiting the length of bridges ( $B$ ); c) shortening overhanging structure ( $L$ ); d) the rules applied in our helicoid: reducing the overhang angle by increasing the pitch or reducing radius ( $r$ ) at a given layer thickness ( $d$ ) will decrease the overhang ( $l$ ) and improve the possibility of self-support.

3

which the combined work of a light source and a projector hardens the liquid resin layer by layer [35]. We printed our prototype using the R5 epoxy photopolymer resin (EnvisionTec GmbH, Gladbeck, Germany).

Both the handle and the shaft were printed vertically with the long axis parallel to the vertical z-axis of the printer. As DLP printing technology requires overhanging structures to be printed with support material, this would require a rather elaborate post-processing step in the removal of support material within the detailed helical structure. A number of studies carried out in the field of additive manufacturing for support structures show, however, that support structures are not always necessary providing that the length of overhanging layers is limited [36–40]. Following these studies, we decided to print the segments of the compliant shaft without support, using three general rules (Figure 3.5): reducing the overhang angle, limiting the length of bridges, and shortening overhanging structures.

The overhang angle is the angle between printed layers (i.e., the critical angle). Increasing the layer thickness while keeping the number of revolutions of the helicoid as well as the length of the segment equal, increases the overhang angle between two layers and thus the need for support. Therefore, by keeping the layer thickness small ( $25\ \mu\text{m}$ ) and the pitch of the helix equal to its height, the overhang angle is kept narrow, and the helicoids can support themselves. Bridges define the distance between two unconnected

points; limiting the length of the bridges avoids the use of support material. The role of the amplification component is to guide the cables through curved grooves. However, using solid material in such a long element would clog the grooves. Therefore, the hive structure was used to create short grooves, while at the same time avoiding long bridges that would have been created if rings had been used as cable guidance during the vertical 3D-printing process. Overhanging structures are shapes that stick out horizontally parallel to the building platform. In our design, combining helicoids with a central backbone allows the compliant shaft to be printed without extra support due to the constant presence of support (the backbone) in the structure [41].

Applying these rules, we printed the entire compliant shaft without any support in a single printing run. Printing without support led to a strong reduction in post-processing time with an additional advantage that eliminating support material from the printing process resulted in smooth surfaces without debris that could cause malfunctioning of the mechanism, especially in elements with a small size.

3

Printing the handle and the shaft vertically allowed the grooves for the cables to remain open along the entire length of the shaft and the handle. The handle and the shaft were printed all together in 26 hours. After the printing, all the parts were placed in an ultrasonic cleaner for a few minutes.

To control the compliant shaft, each segment must be coupled with the corresponding segment in the handle using the corresponding actuation cables. Running all 20 cables (stainless-steel  $\text{\O}0.2$  mm) through the shaft and the handle took around 5 hours. In the handle, the cables were fixated by dog point set screws to allow fine-tuning in this prototype. Although it was possible to tap directly into the 3D-printed material, this could have created points of brittleness in the resin. We, therefore, decided to place threaded inserts that allow the cable to be fine-tuned multiple times. During the assembly, the instrument was vertically placed and each cable was straightened by weights of 10 grams before fixation in the handle. The entire HelicoFlex prototype is shown in Figure 3.6.

### 3.5 HELICOFLEX PERFORMANCE

Simulating navigation through tortuous paths, the tip was moved along curves with different radii and shapes to evaluate the performance of the device, Figure 3.7. The prototype was able to perform single curved shapes with different angles (Figures 3.7a-b) and double-curved shapes with different radii (Figures 3.7c-d). Moreover, the device



Figure 3.6: The assembled HelicoFlex prototype showing a single curve.

allowed controlling each segment individually (Figures 3.7e-f). At an angle of 160 degrees, the maximum bending angle of the compliant shaft was reached because the outsides of the helicoids touched each other in the inner bend (see Figure 3.3).

Besides moving the device over different angles and shapes, we also evaluated the possibility of using the internal lumen. The device allows the insertion of a flexible fiberoptic endoscope into one of its four lumens while leaving the other three lumens free for the insertion of multiple surgical instruments, such as a biopsy forceps, as shown in Figure 3.8a. Moreover, a bendable rod can be placed inside one of the lumens of the handle and can be shaped to hold the desired position (Figure 3.8b). The fluid motion, as well as the easy maneuverability of the HelicoFlex prototype, can be seen in the video attached that is available online through the publisher of this paper.

### 3.6 DISCUSSION

In this work, we presented a 3D-printed hand-held multi-steerable instrument with five individually controlled compliant segments providing a total of 10 DOFs. One of the requirements expressed in Section 2.1 was the simplification of the assembly. In the conventional design of the EndoWrist, each part of the steerable shaft is designed for a single function as a result of which the device contains a significant number of parts that all have to be individually handled during the assembly phase, which requires a large amount of time and work. To greatly simplify the assembly, we integrated all the functionalities in the combined single shape of the helicoids, the backbone, and the cable fixation points,

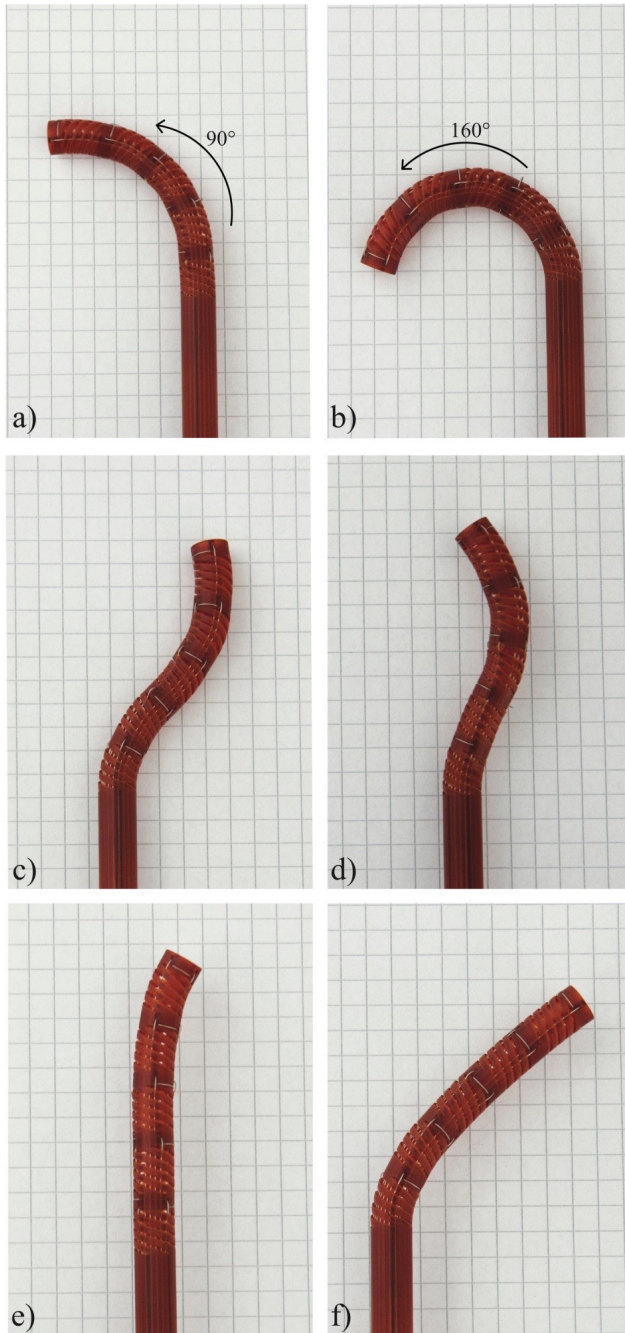


Figure 3.7: HelicoFlex compliant shaft bent in various shapes: a) 90 degrees single curved shape; b) 160 degrees single curved shape, reaching the maximum bending angle of the compliant shaft in performing a C-shape; c) double-curved with equal radii; d) double-curved with different radii; e) only the distal segment controlled; and f) only the proximal segment controlled.



Figure 3.8: Pictures of the HelicoFlex prototype; a) close-up of the compliant shaft of the HelicoFlex with a flexible biopsy forceps in one lumen and a flexible fiber optics endoscope in the second; b) bendable metal rod inserted into one of the lumens to create a certain shape in compliant shaft and keep it in position.

giving to the segment high axial and torsion stiffness and low bending stiffness with easy and reliable fixation of cables. In HelicoFlex, we integrated all these functionalities in a five-segmented compliant shaft, with a complex and unusual shape, yet 3D-printed in only one printing step. HelicoFlex shows a fluid motion and easy maneuverability during the performance of multiple shapes allowing added multifunctionality due to the presence of the four lumens. The maximum bending angle that can be obtained is 160 degrees, which is much larger than the bending angle guaranteed by commercialized instruments such as the LaparoFlex (DEAM, Amsterdam, The Netherlands) or the Autonomy Laparo-Angle (Cambridge Endoscopic Devices, Framingham, MA, USA), which usually ranges over  $\pm 60$  degrees. The 8 mm diameter of the shaft was chosen equal to the diameter of most EndoWrist instruments and as a proof of concept in this paper. However, smaller diameters seem feasible without creating essential changes in the design.

The main goal of this work was to simplify the fabrication and assembly process of a multi-steerable device by using 3D-printing technology to make it suited for disposable

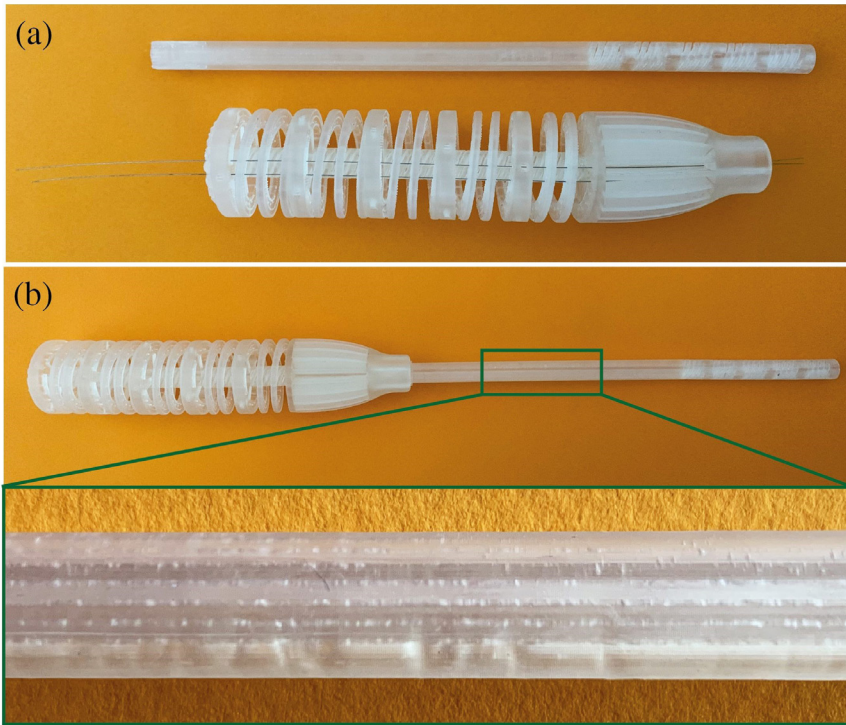


Figure 3.9: HelicoFlex printed with the E-Shell 600 biocompatible resin from (EnvisionTec GmbH, Gladbeck, Germany); (a) the shaft and the handle disassembled with two cables run through the handle; (b) the prototype assembled without cables with a close-up in which is visible how the grooves are clogged by liquid resin.

use. This led to a new type of continuous structure based on helicoids that could be printed without support. Moreover, we showed that it is possible to print an entire instrument out of one part, excluding the cables required for steering. In this prototype, we decided to use dog point set screws to fix the cables in the handle as this allows for easy finetuning in the prototype. Yet, we also experimented with glue that proved to be a fast and durable, much simpler alternative in the handle fixation (the cable fixation was tested tensioning the cable up to 1500 gr for one hour with no sign of failure). The friction-based cable-fixation in the compliant shaft required no other action than just looping the cables, which drastically decreased the assembly time. The entire device was printed in 26 hours, while threading and fixing the 20 cables took around 5 hours in this prototype. The handle and the shaft were printed with a layer thickness of  $25\ \mu\text{m}$ . Printing the same design with a layer thickness of  $50\ \mu\text{m}$  would drastically reduce the printing time to 13 hours, with only minor effects on the quality of the device. We found that the combination of helicoids with a continuum backbone limits the overhang angle between layers. In this way, we could avoid support material in the compliant shaft, which resulted in smoother surfaces without the presence of debris.

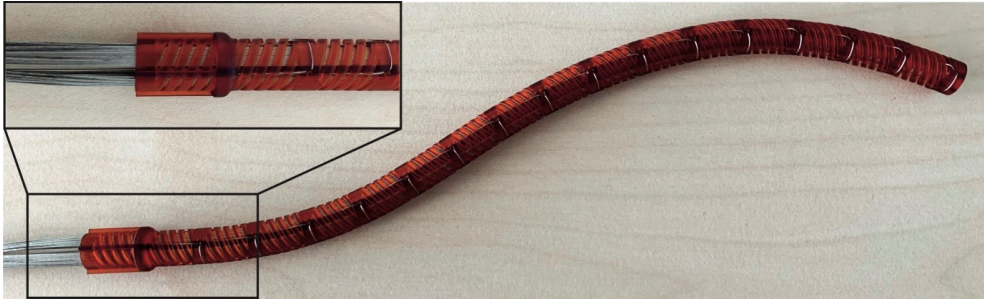


Figure 3.10: Example of 16 compliant segments combination with a close-up of the 64 actuation cables running through the Ø8 mm shaft.

In our prototype, we used a non-biocompatible acrylic resin especially developed for prototyping. The use of this resin helped in the tuning phase to analyze and improve the design quality of the prototype. Biocompatible resins, such as E-Shell600, are provided by EnvisionTec as well. However, using this resin, results are decent but not yet sufficient due to the lower viscosity of this resin, which makes the cable grooves more difficult to be printed (Figure 3.9).

Using AM, the HelicoFlex can, in future surgical applications, be customized considering the surgery, the patients, and the surgeons' needs, as well as made MRI-compatible by replacing steel cables by Dyneema. In the future, more tests to investigate the maneuverability of this new multi-steerable instrument in narrow environments will be performed as well as different materials and sizes, increasing our knowledge in this emerging new field of 3D-printed medical devices.

Using 3D-printing is often considered a cheaper method of fabrication as compared to conventional manufacturing. However, it can be accounted as such only in specific cases (i.e., the production of complex devices that cannot easily be manufactured of molded conventionally) and if the necessary fine-tuning and testing time is taken into account (i.e., high initial costs for calibrating the settings of the printer, an expert who can tune and evaluate carefully how the design can be improved considering its use, long iteration phases to reach good results). Therefore, we believe that the real strength of AM is the capability of printing structures that are impossible to produce with conventional manufacturing and being able to integrate multiple functions into a single complex-shaped part. In a further elaboration, the number of segments can be increased, even more, reaching with the used cables and dimensions, a maximum length of 16 segments in a compliant shaft with 32 DOFs (Figure 3.10). A multi-steerable structure with this complexity yet also so simple is unique.

### 3.7 CONCLUSION

In this work, we have presented the first 3D-printed multi-steerable device. We have shown that by adapting the design of a device to the fabrication capabilities of additive manufacturing, we have integrated multiple functionalities of different conventional elements into a single part, extensively decreasing the assembly time of a tendon-driven multi-steerable device for disposable medical use. The potential has been shown in a prototype: HelicoFlex. The hand-held device, made out of three components, had five tendon-driven steerable segments for a total of 10 serially controlled DOFs. HelicoFlex has shown a fluid motion and satisfactory results in performing different shapes. We have shown the high potential of additive manufacturing technology in building multi-steerable surgical instruments, limiting the number of components, and avoiding support material. HelicoFlex strives to contribute to the first generation of multi-steerable 3D-printed instruments for MIS.

3

### 3.8 REFERENCES

1. R. Bittner, The standard of laparoscopic cholecystectomy, *Langenbeck's Arch. Surg.* 389 (2004) 157–163.
2. C.W. Akins, Full sternotomy through a minimally invasive incision: a cardiac surgeon's true comfort zone, *Ann. Thorac. Surg.* 66 (1998) 1429–1430.
3. M.J. Mack, Minimally invasive and robotic surgery, *Jama.* 285 (2001) 568–572.
4. M.S.L. Liem, Y. Van Der Graaf, C.J. Van Steensel, R.U. Boelhouwer, G.-J. Clevers, W.S. Meijer, L.P.S. Stassen, J.P. Vente, W.F. Weidema, A.J.P. Schrijvers, Comparison of conventional anterior surgery and laparoscopic surgery for inguinal-hernia repair, *N. Engl. J. Med.* 336 (1997) 1541–1547.
5. E.G. Sheu, D.W. Rattner, Natural Orifice Transluminal Endoscopic Surgery (NOTESTM) BT - The SAGES Manual Operating Through the Endoscope, in: M. Kroh, K.M. Reavis (Eds.), Springer International Publishing, Cham, 2016: pp. 463–474. doi:10.1007/978-3-319-24145-6\_26.
6. C.H. Snyderman, H. Pant, R. Carrau, Classification of endonasal approaches to the ventral skull base, 2011.
7. J. Burgner-Kahrs, D.C. Rucker, H. Choset, Continuum Robots for Medical Applications: A Survey, *IEEE Trans. Robot.* 31 (2015) 1261–1280. doi:10.1109/TRO.2015.2489500.
8. G.S. Guthart, J.K. Salisbury, The Intuitive/sup TM/telesurgery system: overview and application, in: Proc. 2000 ICRA. Millenn. Conf. IEEE Int. Conf. Robot. Autom. Symp. Proc. (Cat. No. 00CH37065), IEEE, 2000: pp. 618–621.
9. A.J. Madhani, J.K. Salisbury, Wrist mechanism for surgical instrument for performing minimally invasive surgery with enhanced dexterity and sensitivity, (1998).
10. R. Prewitt, V. Bochkarev, C.L. McBride, S. Kinney, D. Oleynikov, The patterns and costs of the Da Vinci robotic surgery system in a large academic institution, *J. Robot. Surg.* 2 (2008)

- 17–20.
11. I.D. Walker, Continuous Backbone “Continuum” Robot Manipulators, *ISRN Robot.* 2013 (2013) 1–19. doi:10.5402/2013/726506.
  12. I.D. Walker, Some issues in creating “invertebrate” robots, in: *Proc. Int. Symp. Adapt. Motion Anim. Mach.*, Citeseer, 2000.
  13. H.B. Gilbert, D.C. Rucker, R.J. Webster III, Concentric tube robots: The state of the art and future directions, in: *Robot. Res.*, Springer, 2016: pp. 253–269.
  14. R.J. Webster, J.M. Romano, N.J. Cowan, Mechanics of pre-curved-tube continuum robots, *IEEE Trans. Robot.* 25 (2009) 67–78. doi:10.1109/TRO.2008.2006868.
  15. P.E. Dupont, J. Lock, B. Itkowitz, E. Butler, Design and control of concentric-tube robots, *IEEE Trans. Robot.* 26 (2010) 209–225. doi:10.1109/TRO.2009.2035740.
  16. T.D. Nguyen, J. Burgner-Kahrs, A tendon-driven continuum robot with extensible sections, *IEEE Int. Conf. Intell. Robot. Syst.* 2015-Decem (2015) 2130–2135. doi:10.1109/IROS.2015.7353661.
  17. H.-S. Yoon, J.H. Jeong, B.-J. Yi, Image-Guided Dual Master–Slave Robotic System for Maxillary Sinus Surgery, *IEEE Trans. Robot.* 34 (2018) 1098–1111. doi:10.1109/TRO.2018.2830334.
  18. I. De Falco, C. Culmone, A. Menciassi, J. Dankelman, J.J. van den Dobbelsteen, A variable stiffness mechanism for steerable percutaneous instruments: integration in a needle, *Med. Biol. Eng. Comput.* 56 (2018) 2185–2199.
  19. A. Jiang, G. Xynogalas, P. Dasgupta, K. Althoefer, T. Nanayakkara, Design of a variable stiffness flexible manipulator with composite granular jamming and membrane coupling, *IEEE Int. Conf. Intell. Robot. Syst.* (2012) 2922–2927. doi:10.1109/IROS.2012.6385696.
  20. N. Simaan, R. Taylor, P. Flint, High Dexterity Snake-Like Robotic Slaves for Minimally Invasive Telesurgery of the Upper Airway BT - Medical Image Computing and Computer-Assisted Intervention – MICCAI 2004, in: C. Barillot, D.R. Haynor, P. Hellier (Eds.), Springer Berlin Heidelberg, Berlin, Heidelberg, 2004: pp. 17–24.
  21. J. Catherine, C. Rotinat-Libersa, A. Micaelli, Comparative review of endoscopic devices articulations technologies developed for minimally invasive medical procedures, *Appl. Bionics Biomech.* 8 (2011) 151–171. doi:10.3233/ABB-2011-0018.
  22. P.W.J. Henselmans, S. Gottenbos, G. Smit, P. Breedveld, The *MemoSlide*: An explorative study into a novel mechanical follow-the-leader mechanism, 231 (2017) 1213–1223. doi:10.1177/0954411917740388.
  23. G. Gerboni, P.W.J. Henselmans, E.A. Arkenbout, W.R. van Furth, P. Breedveld, HelixFlex: bioinspired maneuverable instrument for skull base surgery, *Bioinspir. Biomim.* 10 (2015) 66013.
  24. K. Riojas, P. Anderson, R. Lathrop, S.D. Herrell, C. Ruker, R.J. Webster, A Hand-Held Non-Robotic Surgical Tool with a Wrist and an Elbow, *IEEE Trans. Biomed. Eng.* (2019).
  25. C. Fan, D. Dodou, P. Breedveld, Review of manual control methods for handheld maneuverable instruments, *Minim. Invasive Ther. Allied Technol.* 22 (2013) 127–135.
  26. P.L. Anderson, R.A. Lathrop, R.J. Webster III, Robot-like dexterity without computers and motors: a review of hand-held laparoscopic instruments with wrist-like tip articulation, *Expert Rev. Med. Devices.* 13 (2016) 661–672.
  27. C. Culmone, G. Smit, P. Breedveld, Additive manufacturing of medical instruments: A state-of-the-art review, *Addit. Manuf.* 27 (2019) 461–473. doi:https://doi.org/10.1016/j.addma.2019.03.015.

28. J. Mintenbeck, M. Siegfarth, R. Estaña, H. Wörn, Flexible instrument for minimally invasive robotic surgery using rapid prototyping technology for fabrication, *IEEE/ASME Int. Conf. Adv. Intell. Mechatronics, AIM*. (2014) 1085–1090. doi:10.1109/AIM.2014.6878225.
29. T.K. Morimoto, A.M. Okamura, Design of 3-D Printed Concentric Tube Robots, *IEEE Trans. Robot.* 32 (2016) 1419–1430. doi:10.1109/TRO.2016.2602368.
30. D.B. Roppenecker, A. Pfaff, J.A. Coy, T.C. Lueth, Multi Arm Snake - Like Robot Kinematics, *IEEE/RSJ Int. Conf. Intelligent Robot. Syst.* (2013) 5040–5045. doi:10.1109/IROS.2013.6697085.
31. Y.S. Krieger, D.B. Roppenecker, I. Kuru, T.C. Lueth, Multi-Arm Snake-Like Robot, *IEEE Int. Conf. Robot. Autom.* (2017) 2490–2495.
32. A. Schneider, H. Feussner, Chapter 7 - Operative (Surgical) Laparoscopy, in: A. Schneider, H.B.T.-B.E. in G.S. Feussner (Eds.), *Academic Press*, 2017: pp. 269–327. doi:<https://doi.org/10.1016/B978-0-12-803230-5.00007-5>.
33. F. Jelínek, R. Pessers, P. Breedveld, DragonFlex Smart Steerable Laparoscopic Instrument, *J. Med. Device.* 8 (2014) 015001-015001–9. doi:10.1115/1.4026153.
34. P. Breedveld, H.G. Stassen, D.W. Meijer, J.J. Jakimowicz, Manipulation in laparoscopic surgery: overview of impeding effects and supporting aids, *J. Laparoendosc. Adv. Surg. Tech.* 9 (1999) 469–480.
35. J. Gardan, Additive manufacturing technologies: state of the art and trends, *Int. J. Prod. Res.* 54 (2016) 3118–3132.
36. J. Jiang, X. Xu, J. Stringer, Support structures for additive manufacturing: a review, *J. Manuf. Mater. Process.* 2 (2018) 64.
37. M. Fernandez-Vicente, M. Canyada, A. Conejero, Identifying limitations for design for manufacturing with desktop FFF 3D-printers, *Int. J. Rapid Manuf.* 5 (2015) 116–128.
38. J. Kranz, D. Herzog, C. Emmelmann, Design guidelines for laser additive manufacturing of lightweight structures in TiAl6V4, *J. Laser Appl.* 27 (2015) S14001.
39. M. Cloots, A. Spierings, K. Wegener, Assessing new support minimizing strategies for the additive manufacturing technology SLM, in: *Solid Free. Fabr. Symp. (SFF)*, Austin, TX, Aug, 2013: pp. 12–14.
40. M. Langelaar, Topology optimization of 3D self-supporting structures for additive manufacturing, *Addit. Manuf.* 12 (2016) 60–70.
41. D. Chakravorty, 3D Printing Support Structures – All You Need To Know in 2019, *All3DP*. (2019). <https://all3dp.com/1/3d-printing-support-structures/> (accessed July 22, 2019).





# MEMOFLEX I: PATH-FOLLOWING USING A SINGLE SPATIAL TRACK



4

**Paul W.J. Henselmans, Gerwin Smit, Paul Breedveld**

Published as:

*Mechanical Follow-the-Leader motion of a hyper-redundant surgical instrument: Proof-of-concept prototype and first tests. Proceedings of the Institution of Mechanical Engineers, Part H: Journal of Engineering in Medicine, 2019. 233(11): p. 1141-1150.*

**ABSTRACT**

One of the most prominent drivers in the development of surgical procedures is the will to reduce their invasiveness, attested by Minimally Invasive Surgery (MIS) being the gold standard in many surgical procedures and Natural Orifices Transluminal Endoscopic Surgery (NOTES) gaining acceptance. A logical next step in this pursuit is the introduction of hyper-redundant instruments that can insert themselves along multi-curved paths referred to as Follow-the-Leader (FTL) motion. In the current state of the art, two different types of FTL-instruments can be distinguished. One type of instrument is robotized; the movements of the shaft are controlled from outside the patient by actuators, e.g. electric motors, and a controller storing a virtual track of the desired path. The other type of instrument is more mechanical; the movements of the shaft are controlled from inside the patient by a physical track that guides the shaft along the desired path. While in the robotized approach all DOFs of the shaft require an individual actuator, the mechanical approach makes the number of DOFs independent from the number of actuators. A desirable feature as an increasing number of actuators will inevitably drive up costs and increase the footprint of an instrument. Building the physical track inside the body does, however, impede the miniaturization of the shaft's diameter. This paper introduces a new fully mechanical approach for FTL-motion using a predetermined physical track that is placed outside the body. This new approach was validated with a prototype called MemoFlex I, which supports a  $\varnothing 5$  mm shaft (standard size in MIS) that contains 28 DOFs and utilizes a simple steel rod as its physical track. Even though the performance of the MemoFlex I leaves room for improvement, especially when following multiple curves, it does validate that the proposed concept for Follow-the-Leader motion in 3D space.

## 4.1 INTRODUCTION

Minimally Invasive Surgery (MIS) strives to reduce the invasiveness of surgical procedures by limiting the size of the required incisions. With its obvious benefits of less scar tissue, faster recovery time and fewer complications, MIS has gained broad acceptance. The currently used instruments for MIS are slender (max  $\varnothing$ 5 mm) and predominantly straight and rigid. Due to their rigidity, the path from incision to the operative area must be a straight line. This can pose a problem as the human anatomy consists of organic shapes and a tortuous network of nerves and vessels, through which a straight path is not always an option. Workarounds exist, for example, the abdomen can be inflated to increase the amount of workspace. However, such methods are not applicable in more dense areas in the human body, e.g. the skull base, reducing the possibilities for easy reach of the operative area. Therefore, MIS instruments are ideally not rigid but flexible, allowing them to curve along with the anatomy of the human body. Passive flexible instruments, such as for example catheters or colonoscopes, can only be used to move along existing anatomic pathways such as blood vessels or intestines. Reaching less accessible locations within the human body implies a need for active flexible instruments with an actively controllable shape, allowing steering along multi-curved paths along vulnerable anatomy (Figure 4.1a) [1, 2].

Instruments that contain such active flexibility are referred to as hyper redundant, a term first coined by the field of robotics [3]. The term hyper redundant reflects the fact that this type of devices contain more degrees of freedom (DOFs) than is strictly necessary for maneuvering their end effector. These additional DOFs allow a hyper redundant instrument to actively reshape its shaft, a useful feature for maneuvering within a spatially restricted environment.

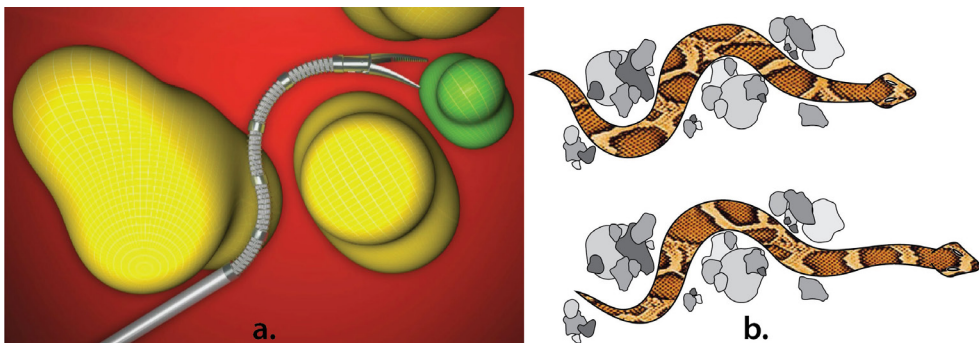


Figure 4.1: Follow-the-Leader motion. a) Artistic representation of a Follow-the-Leader instrument used to avoid obstacles. b) Snake navigating through cluttered environment by steering its head and maneuvering its body along the created path using Follow-the-Leader motion. jpg

A hyper redundant instrument enables so-called Follow-the-Leader (FTL) motion, which is comparable to a type of forward locomotion of a snake (Figure 4.1b) [4]. In this comparison, the head of the snake is regarded as the leader, which is steered, for example, to maneuverer along the stones of Figure 4.1b. As the snake moves forward, the body follows the curved path initiated by the head. In this way, FTL-motion allows motion along multi-curved pathways, while reducing the required access (= the width of the path) to a minimum. These characteristics make FTL-motion especially suitable for Natural Orifice Transluminal Endoscopic Surgery (NOTES) wherein natural orifices such as the nose, mouth or anus are used as the surgical entry point [5, 6]. A good example being Endoscopic Endonasal Surgery (EES) wherein the instrument enters through the nose to reach the skull base [7, 8]. The skull base contains a network of blood vessels, nerves, and other delicate structures and the surgical workspace is limited (105.1 x 76.2 x 51,9 mm) [9]. As a result, some areas remain inaccessible by straight instruments and FLT instrumentation could extend the reach of the procedure.

## 4.2 STATE OF THE ART

Several approaches to FTL-motion of medical instruments have been proposed in literature. They will be discussed based on how these approaches affect the diameter of the shaft and its level of redundancy. A division is made between robotized instruments that use a virtual track and more mechanical instruments that build a physical track.

### 4.2.1 INSTRUMENTS USING A VIRTUAL TRACK

Literature contains several robotized systems that store a virtual track of the desired path on a computer [2]. The computer controls every DOFs of the hyper redundant shaft via individual actuators, which are either embedded in the shaft or placed at the instrument's base outside the patient [10-15]. Instruments with actuators at their base are easiest to miniaturize, the thinnest one currently existing having a diameter of Ø8 mm [14]. A drawback of using a computerized virtual track is that every DOFs of the hyper redundant shaft must be controlled by an individual actuator, with ten being the maximum found number of DOFs in literature of medical instruments [13]. As the level of redundancy within the shaft directly relates to the complexity of the path, i.e. more DOFs allow a more tortuous path, the allowed complexity of the path becomes directly dependent on the number of actuators in the system. This is an undesirable feature as increasing the number of actuators will inevitably drive up costs and require more space near the patient in the workspace of the surgeon.

#### 4.2.2 INSTRUMENTS USING A PHYSICAL TRACK

Some FTL-instruments contain fewer actuators than the number of DOFs in their hyper redundant shafts, reducing the overall complexity of the system (16-20). The thinnest ones being the concentric tube robots or active cannulas, first developed by Webster et al. at Vanderbilt University and since then extensively researched by others [21-24]. Their shafts consist of a telescoping mechanism of pre-curved, compliant, thin-walled tubes, with diameters ranging from 0.8 to 2.4 mm depending on the application [25]. Translating and rotating these compliant tubes relative to one another causes them to interact and deform, changing the overall shape of the shaft. FTL-motion can be achieved by modeling the interaction between the pre-curved tubes, and planning the required control sequence for shaft motion [26, 27]. The predefined curves of these tubes, however, limit the FTL-motion to a restricted set of highly specific pre-planned paths. There are instruments that are capable of FTL-motion along a wider array of nonspecific paths, the most promising being the Highly Articulated Robotic Probe (HARP, and also known as CardioArm), developed by Ota et al., and commercialized as the Flex Robotic System by Medrobotics [17-19, 28]. Its shaft consists of two arms that are placed concentrically within each other. Both arms can independently advance and switch between a flexible and locked state. FTL-motion is achieved by letting the arms alternate between flexible and locked, while the locked arm memorizes the current shape of the system and serves as a guide for the flexible arm that advances and is steered in a new direction. The shaft has an impressive 105 DOFs, while the HARP only needs 6 actuators for steering, locking, and advancing its arms [17, 29]. In this way, the level of redundancy of its shaft becomes independent of the number of actuators.

The HARP showcases an interesting approach to FTL-motion: where normally a computer stores a virtual track of the path and drives a set of actuators, one for each DOFs, the HARP builds a physical track inside its body that guides the motion. Consequently, the level of redundancy within the shaft, and thus the complexity of the paths that can be followed, becomes independent from the number of actuators. Nevertheless, building the physical track inside the shaft impedes miniaturization of the diameter of the HARP, which is currently  $\varnothing 10$  mm [17, 18].

This paper introduces a new approach for an FTL-instrument that uses a physical track placed outside of the shaft, i.e. at the user side of the instrument that does not enter the patient and for this reason, is less bound to the severe diameter restrictions for minimally invasive shafts. In this way, the DOFs of its hyper-redundant shaft become independent from the number of actuators, while the shaft's diameter can be miniaturized to an MIS standard of  $\varnothing 5$  mm.

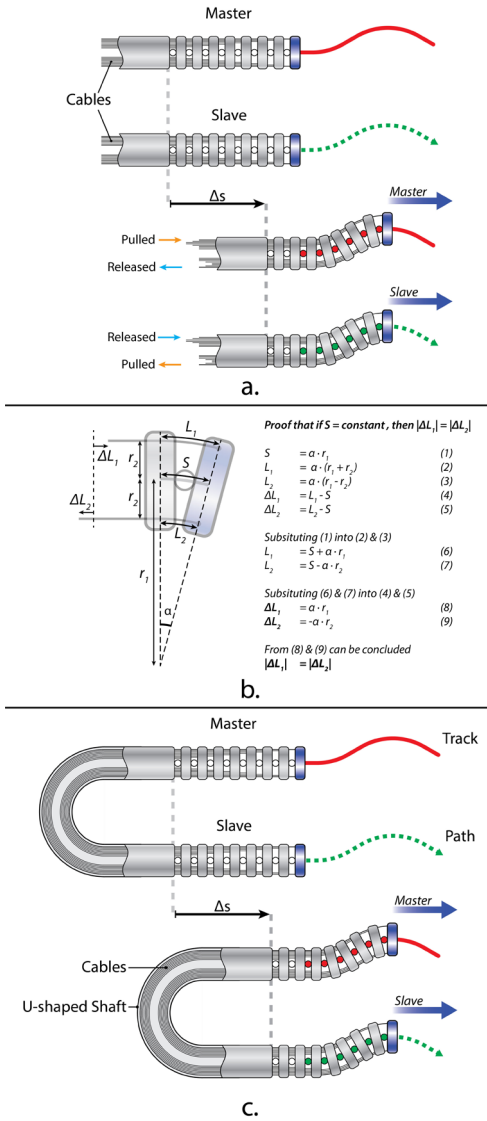


Figure 4.2: Schematic representation of a new approach for a Follow-the-Leader instrument. a) The instrument containing a master that follows a physical track located outside the patient's body, and a slave that copies the movement of the master and propagates along the path inside the patient's body. The "Released" and "Pulled" arrows indicate the tension in the cables of the first segment. b) Length behaviour of antagonist cables  $L_1$  &  $L_2$ . If the length of the segment  $S$  is fixed and the cables are presumed to bend with a constant radius, the absolute length changes  $|\Delta L_1|$  &  $|\Delta L_2|$  of antagonistic cables are equal. c) Hypothetical instrument. The cables in the master are coupled to their antagonists in the slave. A U shaped shaft connects the master to the slave, and guides the cables.

### 4.3 A NEW APPROACH

The basic principle of the proposed approach is illustrated in Figure 4.2a. The general setup contains two similar structures, the master and the slave, each consisting of jointed segments stacked in series to form a flexible structure. All segments are connected to a pair of cables. The function of the master is to follow a physical track located outside the patient's body. The function of the slave is to copy the movements of the master, and in this way propagate along the desired path inside the patient's body.

For the slave to copy the movements of the master, its cables need to be coupled to those of the master. The function of the cables is to transfer the forces that are generated in the master to the slave. Directly coupling a cable in the master to its equivalent cable in the slave is, however, not possible. This has to do with the fact that the master is forced into the desired shape by the track, while the slave is forced into that same shape by the cables. Consequently, equivalent cables in the master and slave will travel the same distance, yet the tensions in the cables should be reversed, i.e. a cable that is pulled in the master should be released in the slave and vice versa, as indicated in Figure 4.2a. There is however a simple workaround. As proven in Figure 4.2b, if a cable is assumed to bend with a constant radius within a segment, the absolute length changes of its antagonist cable are equal to each other. This means that a cable in the master and its antagonist in the slave travel the same distance with tension in the same direction. It is, therefore, possible to connect a cable of the master to its antagonist in the slave. The result is something like the hypothetical configuration illustrated in Figure 4.2c, were a rigid U shaped shaft was added to connect the master to the slave and to guide the cables.

Even though the U shaped configuration of Figure 4.2c could function in theory, there are two downsides of using a U shaped shaft as compared to a more conventional straight shaft. First of all, the cables will experience additional friction as they change direction through the bend. Secondly, a U shaped instrument is rather inconvenient during a surgical procedure as it blocks the workspace in front of the patient. For these reasons, a straight shaft is preferred.

In Figure 4.3a, the direction of the master is rotated over  $180^\circ$  to enable the inclusion of a straight shaft. The track is in this configuration also rotated over  $180^\circ$  in a mirrored direction opposite to the path. As a result, the shaft must telescopically extend so that the master can move backward along the mirrored track while the slave moves forward along the path. An extending shaft is, however, an impractical solution as the cables running through the shaft then need to extend as well.

The extending shaft in Figure 4.3a was necessary because both the track and path were considered stationary. However, while the path, for obvious reasons, has to remain stationary, the track does not. Therefore, the track can be moved relative to the instrument, avoiding the need for an extending shaft. This principle is visualized in Figure 4.3b, where the shaft is straight and has a fixed length. The movement is now considered from the slave. For the slave to travel a distance  $\Delta s$  over the path, the master must travel the same distance over the track. Because the master is now rigidly connected to the slave, it moves along with the slave away from the track with distance  $\Delta s$ . As a consequence, the track must travel twice the distance  $\Delta s$  relative to the stationary path, i.e. the speed of the track

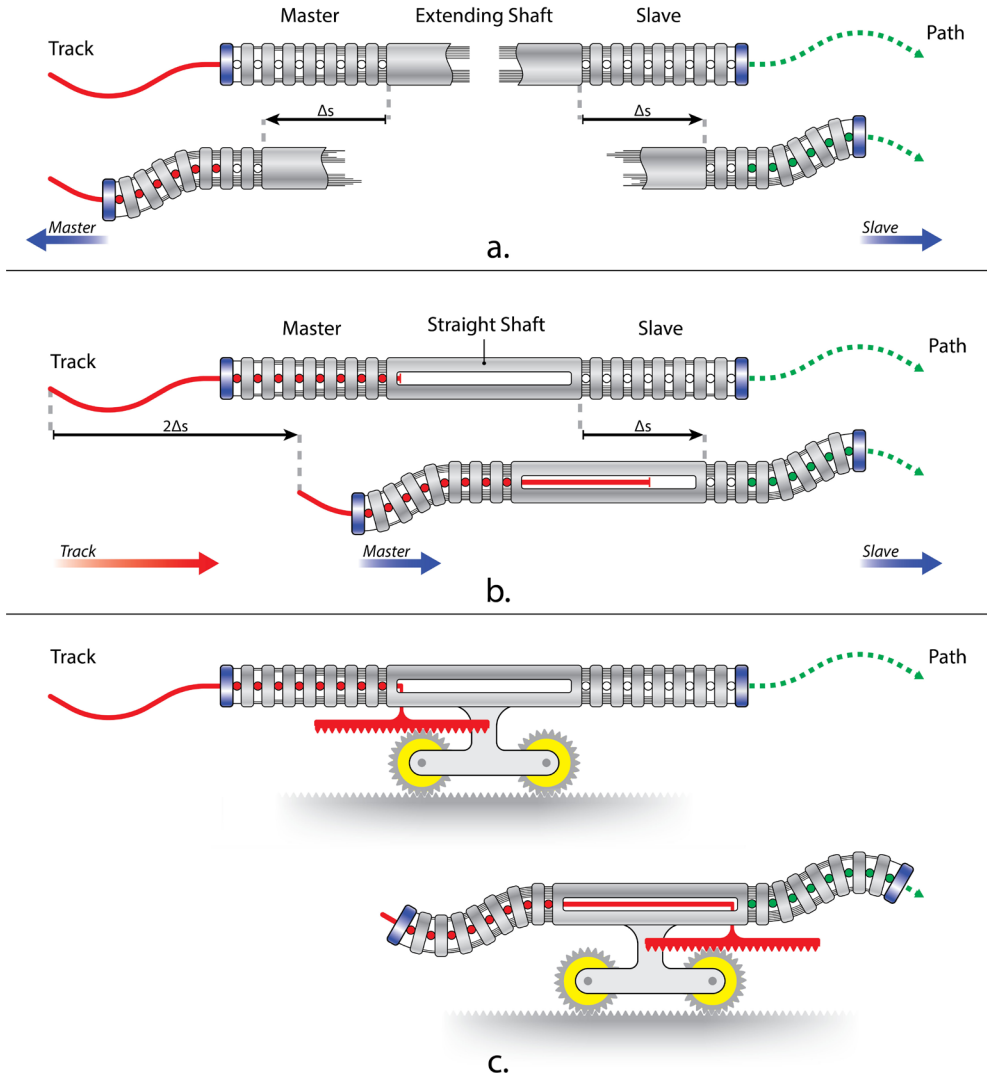


Figure 4.3: Straight configuration a) Improved configuration of Figure 2c. With a straight shaft, the track and path face in the opposite direction. To allow the master to move forward over the track while the slave moves forward over the path, the shaft and cables need to extend. b) Improved configuration of Figure 3a avoiding the extension of the shaft. Master and slave rigidly connected by the shaft. The track is given double the speed of the instrument to compensate for the opposite direction between track and path. c) A mechanism of gears and gear racks pulls the track through the master at double the speed of the instrument.

must be double the speed of the instrument. Thus, the opposite direction between track and path can be compensated by pulling the track through the master at double the speed of the instrument.

Figure 4.3c shows a schematic mechanism of gears and gear racks that doubles the speed of the track compared to the instrument. The instrument is connected to the center of the gears, which run forward over a stationary gear rack. The track is connected to a gear rack (red) that connects to the top of the gears. In this way, the speed of the track will always be double the speed of the instrument.

## 4.4 PROOF OF CONCEPT

To validate the concept of Figure 4.3c, a Proof of Concept (PoC) prototype was developed based on the following requirements. The prototype should be steerable in two planes to allow movement in 3D space. Both the master and slave should be axially and torsion stiff while having a low bending stiffness. The slave should support an inner channel to provide functionality, e.g. a tube for suction, a fiber for vision, or cable for actuation of an end effector. The diameter of the slave should stay within  $\text{\O}5$  mm, a typical dimension for MIS instruments. Our PoC prototype was developed for validating the functionality of the proposed concept, and not for direct use in a medical setting. Requirements as biocompatibility, sterilizability, and integration into current medical protocols and procedures were therefore not yet addressed.

# 4

### 4.4.1 MASTER DESIGN

For the track, a bendable stainless steel rod with a diameter of  $\text{\O}3$  mm was chosen. For the master to capture the shape of the sliding track, a flexible “track follower” structure in the master is required. A possible track follower structure is illustrated in Figure 4.4a, wherein a set of rings are slid over the track. Each ring sits perpendicular to the centerline of the track, and thus copies the angle of the track at that specific position. By placing multiple rings at fixed intervals along the length of the track, the shape of the track is captured.

The track follower structure in Figure 4.4a has a few downsides. First, it is difficult to guarantee that the rings remain perpendicular to the centerline of the track, especially if the rings are thin. A ring that sits oblique to the track’s centerline, i.e. not perfectly perpendicular, will lead to an inaccurate copy of the shape of the track and can result in jamming, resulting in blockage of the track when it is pulled through the rings. Making the rings thick as to avoid jamming is not an option, as steep curves in the track would then no longer fit through the holes in the rings. In a search for a better alternative, we started considering using a helical structure (Figure 4.4b). A helical structure has a single point of contact at any cross-section along the track, making it impossible to grip onto the track,

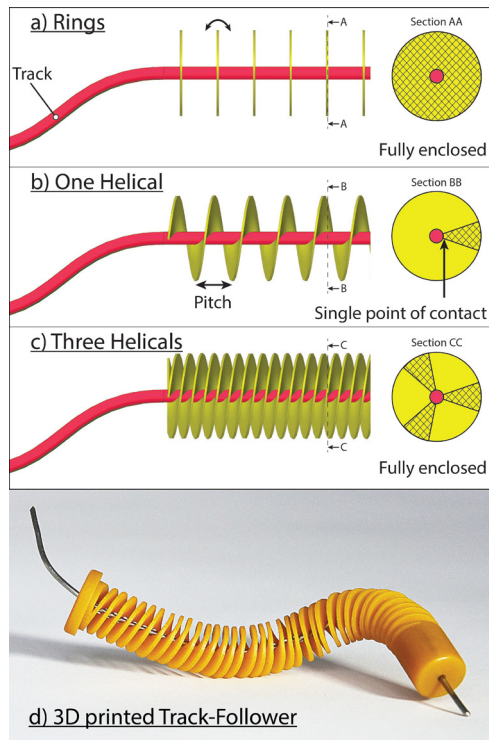


Figure 4.4: Three track follower. a) Structures to capture the shape of a track. For further explanation, see text. d) Track follower based on three helices conforming to the shape of a  $\varnothing 3$  mm track represented by a bent steel rod. 3D Printed from the flexible material ABFlex on an Envisiontec Perfactory 4.

thus avoiding any possibility of jamming. Moreover, similar to a compression spring, a helical will be able to bend along with the curvature of the track, and in this way capture the shape of the track continuously. However, one helical alone does not encircle the track at every cross-section, reducing the resolution of the captured shape. We, therefore, decided to use three helices placed at  $120^\circ$  intervals along the circumference of the track, Figure 4.4c. This structure was 3D-printed and shown in Figure 4.4d together with the  $\varnothing 3$  mm bent steel rod that forms the track.

Next to the ability to capture the shape of the track, the master needs to be axially stiff, torsion stiff, have a low bending stiffness, and guide the cables. As the helical track follower of Figure 4.4d is not axially stiff, it was enclosed by an exoskeleton as illustrated in Figure 4.5a. The exoskeleton is composed out of a series of rings that enclose the track follower and are connected in a way that they form a sequence of universal joints. The cables are guided through holes in the rings and fixed by screws at the desired spot. By using an exoskeleton with a universal joint construction, axial and torsion stiffness is provided without adding additional bending stiffness to the master.

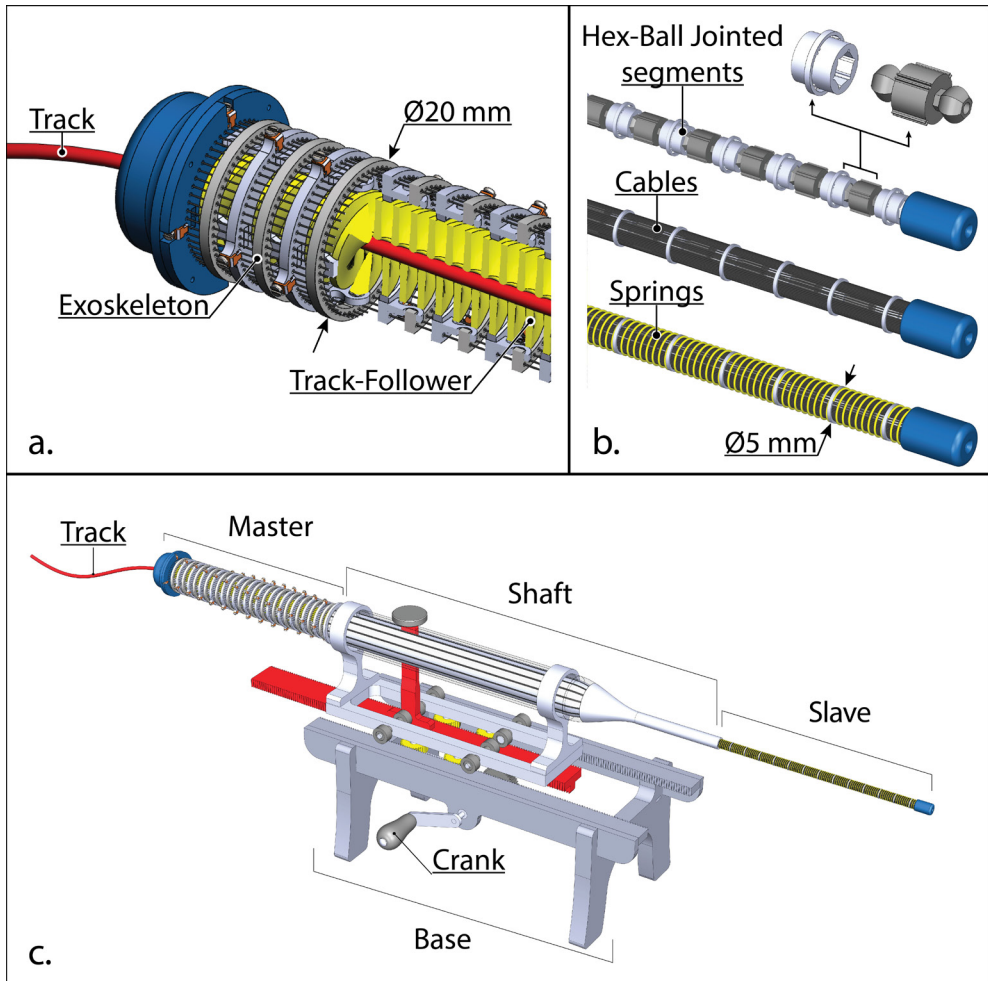


Figure 4.5: CAD drawings of PoC instrument. a) The master consisting of the helical track follower and an axial and torsion stiff exoskeleton that fixates and guides the cables. b) The construction of the  $\text{Ø}5 \text{ mm}$ , 112 mm long slave containing 14 segments providing a total of 28 degrees of freedom. c) CAD drawing of the completed MemoFlex prototype. The cable ring diameter in the master ( $\text{Ø}18 \text{ mm}$ ) is four times larger than the cable ring diameter in the slave ( $\text{Ø}4.5 \text{ mm}$ ). This results in an amplification factor four between the motion of master and slave, e.g. a  $5^\circ$  bend in the master will result into a  $20^\circ$  bend in the slave.

#### 4.4.2 SLAVE DESIGN

The slave was constructed following the principle of the squid inspired cable ring mechanism applied in a range of surgical instrument prototypes developed at the BITE group at TU Delft [30, 31]. Stranded stainless steel cables with a diameter of  $\text{Ø}0.2 \text{ mm}$  were arranged in a  $\text{Ø}4.5 \text{ mm}$  cable ring, allowing space for a total of 56 cables. Each segment is controlled in 2 DOFs by 4 cables, enabling a total of  $56/4=14$  segments and motion in 28

DOFs. The outside diameter of the slave ( $ds$ ) is  $\varnothing 5$  mm, and the length of each segment was chosen to be 8 mm, resulting in a total slave length of 112 mm. Figure 4.5b shows the construction of the slave. The segments are connected via a series of hex ball joints. These joints allow for bending with zero stiffness while providing the necessary axial and torsion stiffness. Every segment contains two hex ball joints allowing a maximum bend of  $60^\circ$ . The cables were glued into the grooves at the circumference of the segments, and springs enclose the cable ring and provide guidance to the cables.

#### 4.4.3 PROOF OF CONCEPT PROTOTYPE: MEMOFLEX I

Figure 4.5c shows the entire PoC prototype named MemoFlex I. The master and slave are connected to each other via a rigid shaft. The shaft accommodates the increase in diameter of the cable ring from slave ( $\varnothing 4.5$  mm) to master ( $\varnothing 18$  mm) by guiding the cables through grooves at its surface. The increase in diameter spreads the cables outward, creating space to reach the track within the shaft, as proposed in Figure 4.3c. The master and slave both have a length of 112 mm, and the entire length of the instrument is 500 mm. The supporting base contains a gearing mechanism to ensure that, upon manually turning a crank, the instrument moves forward while the track is pulled through the master at double the speed.

# 4

## 4.5 PERFORMANCE TEST

The MemoFlex I was successfully fabricated as illustrated in Figure 4.6. Its performance was evaluated using two different tracks: a single curve (S-curve) and a double curve (S-curve). The results of these tests are illustrated in Figure 4.7a, which shows the slave at three positions (insertion, halfway and final position), and an overlay of intervals of approximately 10 mm during forward motion. The blue cap on the tip of the slave is not an actively driven segment, but is solely used for storing the cable endings and is expected to sway along with the motion. Accurate FTL performance would result in the total width of the slave's footprint to be as close as possible to the diameter of the slave.

From Figure 4.7a it is clear that MemoFlex I can follow a S-curve reasonably well, with the maximum width of the slave's footprint being approximately three times the diameter of the slave ( $3 \cdot ds$ ), including the blue cap. Figure 4.7a also shows the performance in following an S-curve, which is considerably worse. In its end position, the slave does mimic the desired S shape, yet during the motion, the slave strays away from the path. The maximum footprint of the slave is approximately  $8 \cdot ds$ .

## MEMOFLEX I: PATH-FOLLOWING USING A SINGLE SPATIAL TRACK



4

Figure 4.6: Proof of concept prototype; the MemoFlex I. All parts were fabricated out of aluminum, except for the wheels (nylon), gear rack (stainless steel) and gears (brass). The outside of the shaft is transparent to allow visual feedback of the cables during their assembly.

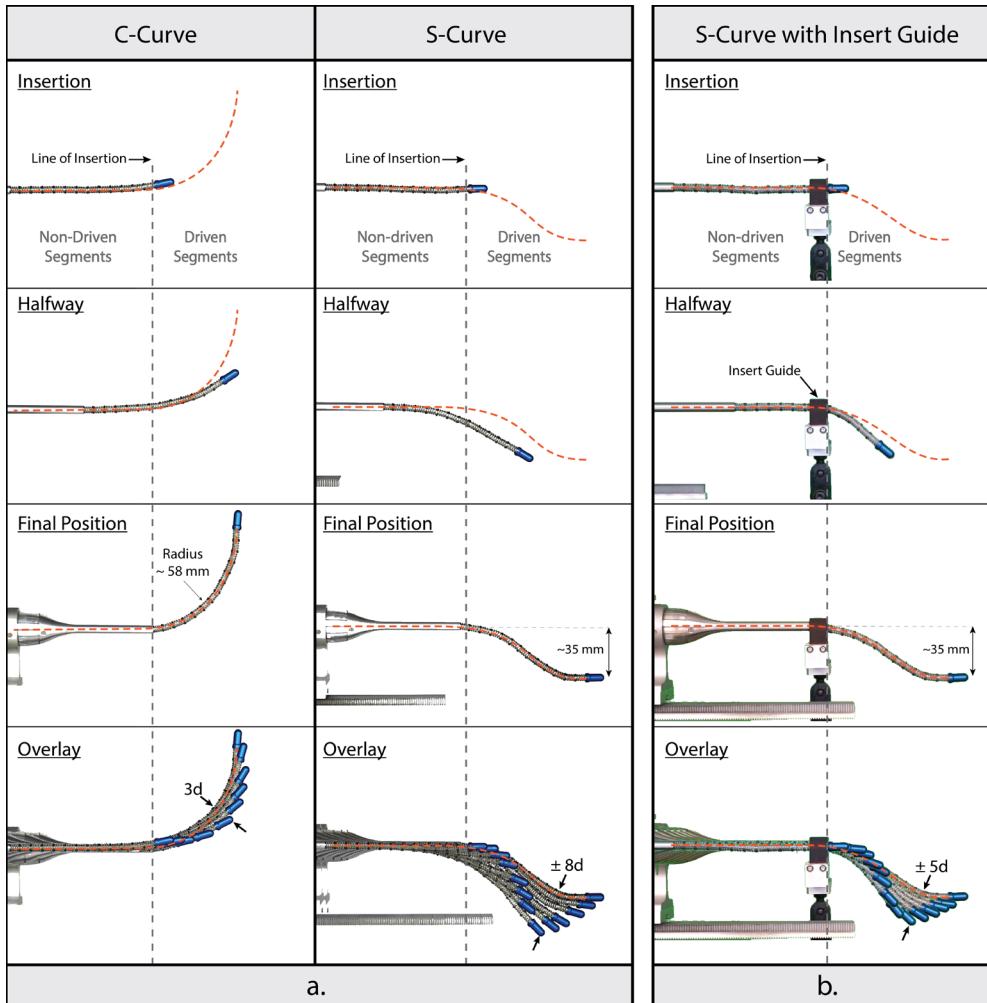


Figure 4.7: Evaluation of the MemoFlex showing the movement of the slave. a) From left to right, the slave following a C-curve with a radius of  $\pm 58$  mm and a footprint of  $\pm 3d$ , and S curve with a step of  $\pm 35$  mm and a footprint of  $\pm 8d$ . The orange striped line indicates the path. b) The slave following a S-curve while supported by the insert guide with a step of  $\pm 35$  mm and a footprint of  $\pm 5d$ .

The line of insertion in Figure 4.7a represents the point after which the segments become actively driven towards the desired shape. The segments after this line are referred to as driven segments, while the segments before this line are referred to as non-driven segments. The non-driven segments should remain in a straight position. Especially at the halfway position of the S-curve, it is clear that this is not the case, as the non-driven segments bend along in the direction of the driven segments. This is avoidable by supporting the slave at the line of insertion. In Figure 4.7b, the slave is again following the S-curve, but now a part referred to as the insert guided is added to the setup. The insert

guide is a ring fixed to the ground that encloses and supports the slave. By comparing the halfway position of the S-curve in Figure 4.7b to the halfway position of the S-curve of Figure 4.7a, it is clear that adding the insert guide improved performance. The non-driven segments are no longer able to move along with the driven-segments, and the maximum footprint of the slave has decreased from  $8 \cdot ds$  to approximately  $5 \cdot ds$ .

Stiffness is an important measure for the functionality of a surgical instrument, as it determines the forces an instrument can apply. The stiffness of the slave was measured at its tip by pulling the slave upward using an analog force gauge. This measurement was done with the slave in two different positions; the initial straight position and the end-position of the S-curve. The stiffness at the initial position was measured to be 0,01 N/mm (0,2 N over a distance of 18 mm), and the stiffness at the end-position was measured to be 0,06 N/mm (0,6 N over a distance of 10 mm). Due to hysteresis as a result of friction and play within the system, the slave did not return to its initial position after completing the measurement. In the straight position, this resulted in a deviation of 7 mm from the initial position. In the end position of the S-curve, this resulted in a deviation of 1 mm from the initial position. The differences between the measurements on the straight position and the end-position can be explained by the fact that in the straight position the cables are not yet used for actuation. As a result, the tension in the cables will be lower and the cables can even be slack, which directly effects the stiffness of the slave and the amount of hysteresis in the system.

## 4.6 DISCUSSION

The MemoFlex I shows that the proposed concept of using a physical track placed outside the shaft is viable, and allows the diameter of the shaft to be miniaturized to  $\varnothing 5$  mm. However, improvements are necessary to generate satisfying results. The main cause of the error was identified to be the non-driven segments diverting from their straight path. A solution was found in supporting the slave at the line of insertion. Although this enhanced its performance significantly, there is still room for improvement.

The performance of the MemoFlex I is considerably effected by mechanical losses in the system. These losses were especially noticeable in the form of hysteresis during the stiffness measurement on the straight position of the slave. The loses can mainly be described to friction in the joints of the slave and master, and friction and play between the cables and their guiding components. Although the fully mechanical nature of the MemoFlex I makes it impossible to completely prevent or compensate for such losses,

they can be minimized. An interesting approach would be to use a continuous instead of a rigid-linked construction in the master and slave. In this way, the joints are replaced by a compliant backbone, eliminating the friction in the joints. Moreover, a continuous approach will allow the cables to be guided more fluently, which can have a positive effect on the play and friction between the cables and their guiding components.

#### 4.6.1 NOTES

The technique of the MemoFlex I could have various applications in NOTES, though its current dimensions especially suite the surgical workspace of EES. The presented C-curve could, for example, reach the anterior cranial fossa via the endonasal approach, an area that can be problematic with straight instruments [32]. The S-curve could, for example, be used to approach the pituitary at a different angle or possibly even reach behind it. The MemoFlex I will, however, not be able to perform all tasks due to its limited stiffness. The applied forces during tasks as soft tissue interaction or bony interaction at the skull base were measured to be 0.13 N and 0.82 N, respectively [33]. In its current form, the MemoFlex I is not stiff enough to exert such forces without considerable deflection. Moreover, a brake should be installed on the gearing mechanism, as the entire instrument can now be pushed back due to external loading. The MemoFlex I will be able to perform tasks that do not require high forces at the tip such as visualization and suction.

#### 4.6.2 FUTURE DEVELOPMENTS

The MemoFlex I prototype is the first step in the development of fully mechanical instruments capable of Follow-the-Leader motion. Even though the results were not fully satisfactory, the prototype's behavior does show the viability of the proposed concept and it can be concluded that the flaws arise from the implementation rather than from the concept itself. In general, a fully mechanical approach has some advantages for medical applications compared to robotized systems. For one, eliminating the need for a computer reduces the instrument's footprint in the already crowded operation room. Moreover, eliminating the need for actuators decreases the size of the master, taking up less space in the surgeon's working area close to the patient. Furthermore, the absence of electric components could considerably drive down the costs of production. That said, the higher level of control offered by robotized systems can produce more accurate results. Future research will have to show if a sufficient level of accuracy is attainable by a fully mechanical approach.

A next step in the development of the MemoFlex I will be focused on adapting a continuous approach to the design of the master and slave. The compliant track-follower

could, for example, be expanded to also serve as a guide for the cables in the master. Moreover, this structure could then be extended towards the slave, paving the way to an all in one piece 3D-printed instrument. 3D Printing can also prove to be useful for the fabrication of patient-specific tracks. The shape of the track would be based on a path planned prior to the surgery by a physician based on CT or MIR images. This 3D track could then be printed from a stiff material, e.g. stainless steel. Future developments will thus be focused on the use of 3D-printing, and we envision that, combined with the absence of electrical components, this could considerably drive down the costs of production and potentially lead to a fully disposable Follow-the-Leader solution.

## 4.7 CONCLUSION

This paper introduces a novel fully mechanical approach for Follow-the-Leader motion of a hyper redundant surgical instrument. To eliminate the need for a single actuator per degree of freedom of a hyper redundant instrument, the approach includes the use of a physical track. This track was placed outside of the patient to allow for the miniaturization of the diameter of the instrument. The proposed technique was implemented in a prototype called MemoFlex I supporting a hyper redundant shaft with a diameter of 5 mm and 28 degrees of freedom. MemoFlex I showed the validity of the proposed technique, and its evaluation showed higher accuracy for following S-curves (footprint of the path  $\sim 3$  times the instrument's diameter ( $3\text{-}ds$ )) than for S-curves ( $\sim 8\text{-}ds$ ). The performance for s-curves was improved by supporting the shaft at the point of insertion ( $\sim 5\text{-}ds$ ).

## 4.8 REFERENCES

1. Burgner-Kahrs J, Rucker DC, Choset H. Continuum robots for medical applications: a survey. *IEEE Transactions on Robotics*. 2015;31(6):1261-80.
2. Loeve A, Breedveld P, Dankelman J. Scopes too flexible and too stiff. *IEEE Pulse*. 2010;1(3):26-41.
3. Chirikjian GS. Theory and applications of hyper-redundant robotic manipulators [Dissertation]. California: California Institute of Technology; 1992.
4. Choset H, Henning W. A follow-the-leader approach to serpentine robot motion planning. *Journal of Aerospace Engineering*. 1999;12(2):65-73.
5. Atallah S, Martin-Perez B, Keller D, Burke J, Hunter L. Natural-orifice transluminal endoscopic surgery. *The British journal of surgery*. 2015;102(2): 73-92.
6. Arkenbout E, Henselmans PJ, Jelínek F, Breedveld P. A state of the art review and categorization of multi-branched instruments for NOTES and SILS. *Surg Endosc*.

- 2015;29(6):1281-96.
7. Cappabianca P, Cavallo LM, de Divitiis E. Endoscopic endonasal transsphenoidal surgery. *Neurosurgery*. 2004;55(4):933-940.
  8. Cappabianca P, Cavallo LM, Esposito F, De Divitiis O, Messina A, De Divitiis E. Extended endoscopic endonasal approach to the midline skull base: the evolving role of transsphenoidal surgery. *Advances and technical standards in neurosurgery*. 2008;33:151-99.
  9. Burgner J, Swaney PJ, Rucker DC, Gilbert HB, Nill ST, Russell PT, et al., editors. A bimanual teleoperated system for endonasal skull base surgery. 2011 IEEE/RSJ International Conference on Intelligent Robots and Systems; 2011 25-30 Sept; San Francisco; CA; 2011: p.2517-2523.
  10. Wayne JD. Quo Vadis: Another new colonoscope. *American Journal of Gastroenterology*. 2007;102(2):267-8.
  11. Shang J, Noonan DP, Payne C, Clark J, Sodergren MH, Darzi A, et al., editors. An articulated universal joint based flexible access robot for minimally invasive surgery. *Robotics and Automation (ICRA)*, 2011 IEEE International Conference on on Robotics and Automation. Shanghai; 2011: p.1147-1152.
  12. Tappe S, Pohlmann J, Kotlarski J, Ortmaier T, editors. Towards a follow-the-leader control for a binary actuated hyper-redundant manipulator. *IEEE International Conference on Intelligent Robots and Systems*; Hamburg; 2015: p.3195-3201.
  13. Son J, Cho CN, Kim KG, Chang TY, Jung H, Kim SC, et al. A novel semi-automatic snake robot for natural orifice transluminal endoscopic surgery: preclinical tests in animal and human cadaver models (with video). *Surg Endosc*. 2015;29(6):1643-7.
  14. Neumann M, Burgner-Kahrs J. Considerations for follow-the-leader motion of extensible tendon-driven continuum robots. 2016 IEEE International Conference on Robotics and Automation (ICRA); 2016 16-21 May; Stockholm; 2016: p. 917-923.
  15. Palmer D, Cobos-Guzman S, Axinte D. Real-time method for tip following navigation of continuum snake arm robots. *Robotics and Autonomous Systems*; 2014;62(10):1478-85.
  16. Kang B, Kojcev R, Sinibaldi E. The first interlaced continuum robot, devised to intrinsically Follow-the-Leader. *PLoS ONE*. 2016;11(2).
  17. Ota T, Degani A, Schwartzman D, Zubiato B, McGarvey J, Choset H, et al. A highly articulated robotic surgical system for minimally invasive surgery. *The Annals of Thoracic Surgery*. 2009;87(4):1253-6.
  18. Rivera-Serrano CM, Johnson P, Zubiato B, Kuenzler R, Choset H, Zenati M, et al. A transoral highly flexible robot. *The Laryngoscope*. 2012;122(5):1067-71.
  19. Johnson PJ, Rivera Serrano CM, Castro M, Kuenzler R, Choset H, Tully S, et al. Demonstration of transoral surgery in cadaveric specimens with the medrobotics flex system. *Laryngoscope*. 2013;123(5):1168-72.
  20. Amanov E, Granna J, Burgner-Kahrs J, editors. Toward improving path following motion: Hybrid continuum robot design. 2017 IEEE International Conference on Robotics and Automation (ICRA); 2017 29 May-3; Singapore; 2017: p. 4666-4672
  21. Dupont PE, Lock J, Itkowitz B, Butler E. Design and control of concentric-tube robots. *Robotics*, IEEE Transactions on. 2010;26(2):209-25.
  22. Gilbert HB, Rucker DC, Webster RJ, III. Concentric tube robots: The state of the art and future directions. *Springer Tracts in Advanced Robotics*. 2016; p. 253-69.

23. Burgner J, Rucker DC, Gilbert HB, Swaney PJ, Russell PT, Weaver KD, et al. A telerobotic system for transnasal surgery. *Mechatronics, IEEE/ASME Transactions on*. 2014;19(3):996-1006.
24. Mahoney AW, Gilbert HB, III RJW. A review of concentric tube robots: modeling, control, design, planning, and sensing. *The Encyclopedia of Medical Robotics*. 2018; p. 181-202.
25. Webster RJ, Okamura AM, Cowan NJ, editors. Toward active cannulas: miniature snake-Like surgical robots. 2006 IEEE/RSJ International Conference on Intelligent Robots and Systems; 2006 9-15 Oct.; Beijing; 2006: p. 2857-2863.
26. Gilbert HB, Webster RJ, editors. Can concentric tube robots Follow-the-Leader? Proceedings - IEEE International Conference on Robotics and Automation; 2013; Karlsruhe; 2013: p. 4881-4887.
27. Gilbert HB, Neimat J, Webster RJ. Concentric tube robots as steerable needles: achieving follow-the-leader deployment. *IEEE Transactions on Robotics*. 2015;31(2):246-58.
28. Corporation M. [internet] Flex Robotic System, Raynham, Massachusetts: Medrobotics; 2019 Available from: <https://medrobotics.com>
29. Henselmans PWJ, Gottenbos S, Smit G, Breedveld P. The *memoslide*: an explorative study into a novel mechanical follow-the-leader mechanism. *Proceedings of the Institution of Mechanical Engineers, Part H: Journal of Engineering in Medicine*. 2017;231(12):1213-23.
30. Breedveld P, Sheltes JS, Blom EM, Verheij JEI. A new, easily miniaturized steerable endoscope. *Engineering in Medicine and Biology Magazine, IEEE*. 2005;24(6):40-7.
31. Breedveld P, Scheltes JS. Instrument for fine-mechanical or surgical applications. *Google Patents*; 2005.
32. Liu JK, Christiano LD, Patel SK, Tubbs RS, Eloy JA. Surgical nuances for removal of olfactory groove meningiomas using the endoscopic endonasal transcribriform approach. *Neurosurgical Focus*. 2011;30(5):E3.
33. Bekeny JR, Swaney PJ, Webster RJ, 3rd, Russell PT, Weaver KD. Forces applied at the skull base during transnasal endoscopic transsphenoidal pituitary tumor excision. *Journal of Neurological Surgery Part B, Skull Base*. 2013;74(6):337-41.



# MEMOFLEX II: PATH-FOLLOWING USING MULTIPLE PLANAR TRACKS



5

Submitted

**ABSTRACT**

The fields of Minimally Invasive Surgery (MIS) and Natural Orifices Transluminal Endoscopic Surgery (NOTES) strive to reduce the level of invasiveness by entering the body through smaller incisions and natural orifices. Hyper-redundant snake-like instruments can help in this pursuit of reducing invasiveness. Such instruments can pass along multi-curved pathway through the body without any support or guidance from its anatomical environment. In this way, the width of the surgical pathway and thus the invasiveness of the procedure can be reduced significantly. This is referred to as Follow-the-Leader (FTL) motion.

Generally, surgical instruments intended for FTL-motion are robotic systems that require medical-grade actuators, sensors, and controllers, driving up costs and increasing their footprint in the operation room. Our goal was to discard the need for actuators, sensors, and controllers, and develop a new non-robotic instrument capable of FTL-motion. A proof of concept prototype called MemoFlex II was developed, consisting of a cable-driven hyper-redundant shaft that is controlled via physical tracks. The MemoFlex II was able to perform FTL-motion along predetermined paths. Among other things, this study reports on a  $\varnothing 8$  mm shaft containing seven segments and 14 degrees of freedom (DOFs) following several multi-curved paths with an average maximal footprint between 11,0 and 17,1 mm.

## 5.1 INTRODUCTION

The field of Natural Orifice Transluminal Endoscopic Surgery (NOTES) strives to reduce the invasiveness of surgery by using the body's natural orifices as the surgical entry-point [1], for example by entering the mouth to reach the stomach through the esophagus, or by entering the nose to reach the skull base through the nasal cavity [2-4]. In such cases, a straight pathway from entry-point to operation area is not always an option, and the instrumentation has to be flexible to conform to the tortuous lumens and cavities of the human body. Instruments with some form of flexibility are available, for example, catheters or flexible endoscopes. Although some of these instruments are steerable at the tip, they rely on the surrounding anatomy to support and guide their motion. Such guided motion can be very effective, a prime example being catheters guided through blood vessels. In other areas in the body, however, the anatomy can be too soft, e.g. in the colon, or too delicate, e.g. in the skull base, to deliver sufficient support and guidance [5]. Self-guided instruments that can travel along multi-curved pathways while supporting their own weight and guiding their own motion, can navigate through such soft or delicate areas, and have the potential to expand the reach of surgical procedures.

A special type of motion along multi-curved pathways is called Follow-the-Leader (FTL) motion, a term first coined in the field of snake-like robotics [6]. This motion is comparable with the videogame "Snake", wherein the player steers the direction of the snake's head (the leader) while the snake's body automatically follows the created trajectory. A key characteristic of this motion is that it minimizes the required access, i.e. in an ideal situation, the width of the curved pathway is equal to the width of the snake. FTL-motion is very beneficial for surgical practice as it enables motion along complex pathways while minimizing the required access and in that way the invasiveness of the procedure [7].

### 5.1.1 STATE OF THE ART

FTL-instruments found in literature developed for surgical purposes can be divided into two groups: shape-shifting instruments and telescoping instruments. Shape-shifting instruments contain a flexible shaft consisting of multiple steerable segments placed in series. FTL-motion is achieved by re-shaping the entire shaft to the shape of the path as the instrument moves forward, i.e. the shape of the shaft is shifted backward along its body as the instrument as a whole moves forward. In telescoping instruments, the shaft consists of telescoping segments placed parallel to each other. Instead of moving the instrument forward as a whole, FTL-motion is now achieved by extending the tip of the shaft, while the rest of the shaft holds its position and shape.

Shape-shifting requires a serially segmented hyper-redundant shaft. These shafts are referred to as hyper-redundant as they contain (much) more degrees of freedom (DOFs) than strictly necessary for positioning their end-effector. FTL-motion is realized when each segment takes over the position and shape of the segment in front of it as the shaft moves forward. To achieve this, all segments have to be simultaneously actuated. In the literature, several experimental hyper-redundant shafts aimed for medical applications are described [7-29], a few of them employing FTL-motion with the group of Shigeo Hirose from Tokyo Institute of Technology already demonstrating it in 1988 [8-12]. The actuators that are needed to realize the motion are either embedded in the shaft, referred to as intrinsic actuation, [11-20] or placed at the base of the instrument outside the shaft, referred to as extrinsic actuation [21-28]. The common denominator for shape-shifting instruments is that all DOFs of the shaft must be simultaneously actuated to realize shape-shifting. As a consequence, shape-shifting instruments include at least one actuator for every DOFs in their hyper-redundant shafts.

Telescoping instruments were also found in literature [30-38]. The concentric tube robots pioneered by the group of Robert Webster III at Vanderbilt University are the thinnest existing telescoping instruments, with outer diameters found in literature down to 2.39 mm [30]. Concentric tube robots are based on a telescoping mechanism of concentric pre-curved tubes. By twisting and sliding the tubes relative to one another, the overall shape can be adjusted. As the movement of one tube affects the entire shape of the device, these instruments can only achieve FTL-motion over a limited set of specific paths [31, 39]. As a solution, Nguyen et al. proposed a hybrid steerable version wherein the tubes are cable-driven instead of pre-curved [36]. This resulted in more control over the shape of the shaft, at the cost of a larger diameter ( $\varnothing 6$  mm). A more dexterous telescoping mechanism is the HARP (also called CardioArm,  $\varnothing 10$  mm) developed by Chose et al. and commercialized by Medrobotics into the Flex Robotic System [35, 40, 41]. This system uses a telescoping mechanism of two concentric tubes that alternate between flexible and rigid states [42]. The tube that is made flexible is moved forward while guided by the tube that is made rigid in its curved shape. By alternating between the tubes, the instrument as a whole moves forward. The common denominator for telescoping instruments is that their parallel segments create a physical track that guides the next segment along the desired path.

## 5

### 5.1.2 ADVANTAGES AND DISADVANTAGES

The current shape-shifting instruments incorporate an independent actuator for every individual DOFs in their hyper-redundant shafts, providing independent control over every individual segment. However, FTL-motion in principle only requires a segment to

copy the shape and position of its predecessor, making independent control over every segment not a necessity. As a result, the current shape-shifting instruments require a level of control that is much higher than is strictly necessary for FTL-motion, leading to over-complex, expensive robotic systems.

Telescoping instruments use parallel segments to create a physical track that guides the next segment. The advantage as compared to shape-shifting instruments is that they require fewer actuators, and in this perspective a lower level of control. However, a disadvantage is that telescoping instruments rely on the relative change in stiffness between their parallel segments [5]. Consequently, it must be possible to alternate the segments between a flexible and rigid state, as in the HARP, otherwise, the segments can influence each other, resulting in distortion of the original shape and thus a diversion from the required path; a phenomenon that is most apparent in concentric tube robots.

### 5.1.3 GOAL

This paper explores a new concept for an FTL-instrument that aims to combine the characteristics of shape-shifting and telescoping instruments. It is based on a cable-driven hyper redundant shaft (adapted from shape-shifting instruments) that is extrinsically controlled via a physical track (adapted from telescoping instruments). In this way, the shaft does not require an independent actuator for each DOFs, thus drastically reducing the required level of control and eliminating the need for computer-controlled actuation, while at the same time being suitable for a large variety of pathways not limited by the drawbacks of a telescopic device.

## 5.2 MECHANISM DESIGN

### 5.2.1 MECHANICAL FOLLOW-THE-LEADER CONCEPT IN 2D

Figure 5.1a shows the 2D concept of our FTL-instrument. The instrument contains a hyper-redundant shaft consisting of a series of jointed segments, each connected to a pair of cables. On the other side of the instrument, each pair of cables connect to one control-point. The vertical movement of a control point pulls one cable while releasing its antagonist. In this way, the vertical positions of the control points translate to the angles of the segments and thus to the shape of the shaft.

FTL-motion is characterized by the first segment of the shaft (the leader segment, red in Figure 5.1a) tracing a path that is followed by the rest of the segments (the follower

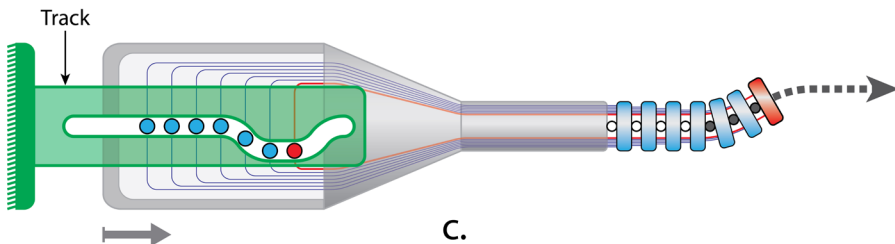
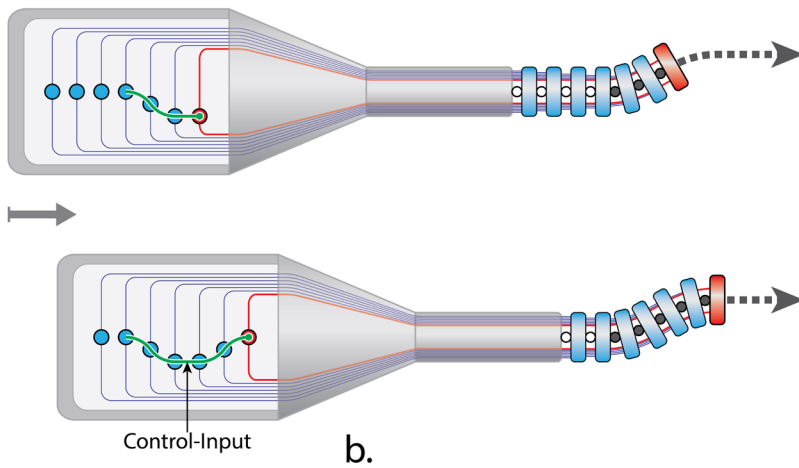
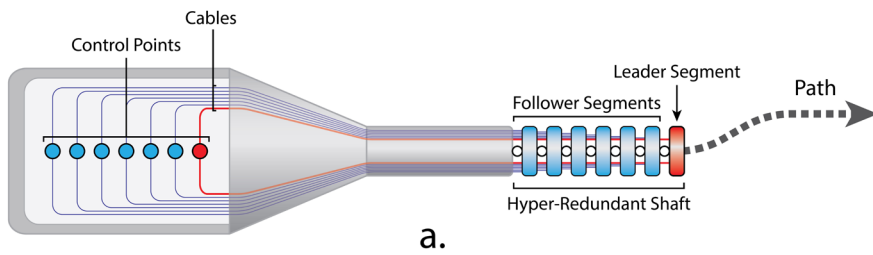


Figure 5.1: 2D Concept of a Follow-the-Leader instrument. a) Instrument consisting of a cable-driven shaft. The vertical positions of the control-points determine the angles of the segments and thus the shape of the shaft. b) As the leader-segment follows the path, the path of leading control-point (red) is outlined to visualize the control-input. Follow-the-Leader motion is achieved when the neighboring control-points follow the same control-input. c) A stationary track based on the control-input physically guides the control-points as the instrument moves forward, steering the shaft of the desired path.

segments, blue in Figure 5.1a). The leader segment is controlled over the desired path by moving its “leading” control point (red in Figure 5.1a) vertically while the instrument as a whole moves forward, as illustrated in the two steps of Figure 5.1b. As the motion continuous, the movement of the leading control point can be represented by a continuous line (green). This line is referred to as the control-input and represents all the vertical positions of the leading control-point as it travels along the desired path. Because

the follower segments are physically identical to the leader segment, they will behave identically to the same control input. Passing the control input of the leader segment to the follower segments should, therefore, result in the follower-segments traveling along the same path as the leader segment. FTL-motion can thus be achieved by passing the control-input of the leader-segment to the control points of the follower segments.

In mechanical terms, the control-input can be represented by a physical track, as visualized in Figure 5.1c, where the track contains a groove that encloses the control-points and is shaped conform to the control-input. In this configuration, the track remains stationary while the instrument moves forward. The track will guide the vertical movements of all control-points simultaneously, and in this way, FTL-motion can be achieved. The complex problem of controlling every cable of the hyper redundant shaft individually is in this way reduced to a relatively simple cam-follower mechanism wherein all cables are controlled by a single physical track.

### 5.2.2 MECHANICAL FOLLOW-THE-LEADER CONCEPT IN 3D

In the 2D concept of Figure 5.1c all cables are controlled by a single track. As a result, antagonistic cables are connected to the same control-point, and these control-points are placed at the centerline of the instrument. As a consequence, the cables have to be redirected along a 90 degree bend before being connected to the control-points. From a mechanical perspective, redirecting the cables, e.g. by pulleys or Bowden cables, will introduce friction within the system and/or increase its complexity. Redirecting cables can be avoided by rotating the track over 90-degrees as illustrated in Figure 5.2. With this solution, the track can no longer remain stationary while the instrument moves forward, but has to move downward along the now vertically placed set of control-points. Moreover, this configuration requires two tracks per plane instead of only one: one track controlling the upward motion and another track controlling the downward motion. The two tracks should be mirrored versions of each other so that one track pulls at a cable while the other track releases the antagonist cable over the same length. A 3D instrument should have a total of four such tracks to control the motion in the horizontal and vertical plane: two tracks for the motion in the horizontal plane and two tracks for the motion in the vertical plane.

### 5.2.3 CABLE-CONFIGURATION IN THE 3D SHAFT

The hypothetical 2D shaft of Figure 5.1 should be converted to function in three dimensions. This results in a 3D shaft composed out of a bendable backbone that is divided into segments by solid disks. Four cables attach to each disk at 90 degrees intervals,

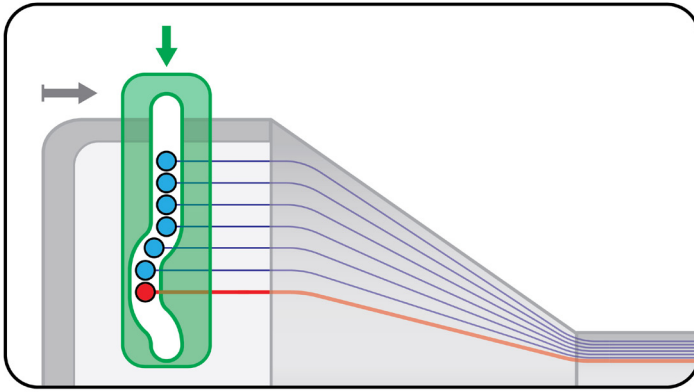


Figure 5.2: Partial view showing a variant of the 2D concept of Figure 1c with the track rotated over 90 degrees

providing independent control of the bending motion in the horizontal and vertical planes. Figure 5.3a shows such a hypothetical shaft in which the cables are placed in a circle and routed in a straight line along the circumference of the shaft. A drawback of this simple configuration is that it will not function in the concept of Figure 5.1c, because it is vital in this concept that the follower segments behave identically to the leader-segment. The segments of Figure 5.3a do not behave identically to one another as their cables are not attached in the same horizontal and vertical plane. As a result, each segment will bend in a plane that is slightly rotated as compared to the bending plane of its predecessor. Figure 5.3b shows a solution in which all cables are attached in the horizontal and vertical planes. This configuration requires the cables to be stacked, which will increase the shaft's diameter, making its miniaturization challenging. Figure 5.3c shows another solution in which the cables are routed along a helical path with a large pitch along the circumference of the shaft. All segments behave identically in this configuration as the cables are all attached in the same horizontal and vertical plane, with the advantage that the shaft can be easily miniaturized as all cables are routed along its circumference.

5

#### 5.2.4 FULL 3D CONCEPT

The entire 3D instrument is schematically visualized in three stages in Figures 4a-c. Figure 5.4a shows the shaft and the cables, which are routed towards a larger diameter in the control-side of the instrument that contains a grooved cylinder, referred to as the revolver. Bars are positioned in the grooves of the revolver, allowing them to slide forward and backward. A cable connects to each bar so that the sliding of the bar pulls or releases the cable. The control-points are represented by blue ball bearings that are fixed to each bar.

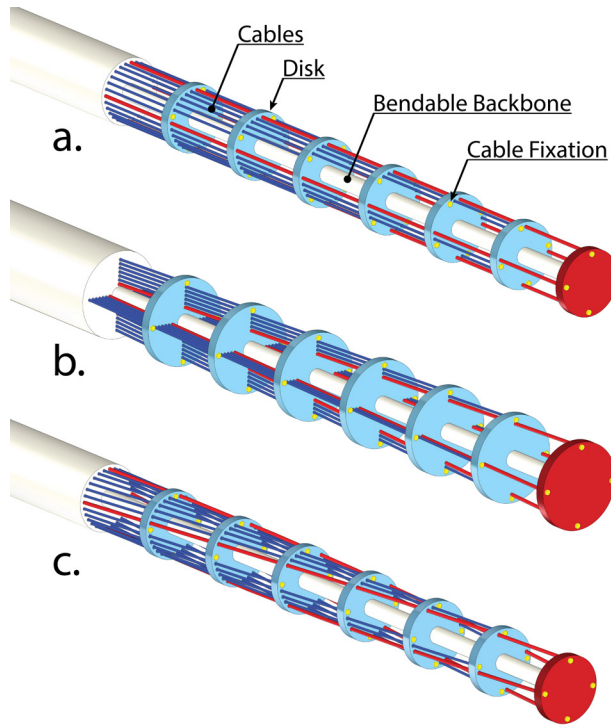


Figure 5.3: Hypothetical shaft composed of a bendable backbone that is segmented by solid disks. a) Conventional cable-configuration. b) Cables fixated in the horizontal and vertical plane and stacked towards the centerline. c) Cables fixated in the horizontal and vertical plane and routed in a helical around the circumference of the shaft.

The integration of the four tracks in the system is illustrated in Figure 5.4b. The tracks are held by a light green track-ring that can rotate around the revolver. The track-ring is fitted with straight grooves enclosing the ball-bearings in their initial configuration, holding them in a straight line so that the shaft is initially straight. The tracks, visualized in the dark green inserts, are fitted in line with these straight initial grooves. The mechanism works by rotating the track-ring as the instrument moves forward, resulting in the ball bearings passing, one by one, from the straight initial groove to the curved groove of the track. During their rotation, the tracks will force the bars to move forward or backward, pulling or releasing the cables and causing the shaft to follow the preprogrammed track. Finally, Figure 5.4c shows how the rotation of the track-ring can be coupled to the forward and backward motion of the instrument. The instrument is suspended in a stationary exoskeleton containing four straight grooves and two helical grooves (only two straight grooves and one helical groove are visible in the figure). The straight grooves facilitate the forward and backward motion of the instruments while the track-ring is guided by the helical grooves, facilitating its rotation as the instrument moves forward or backward.

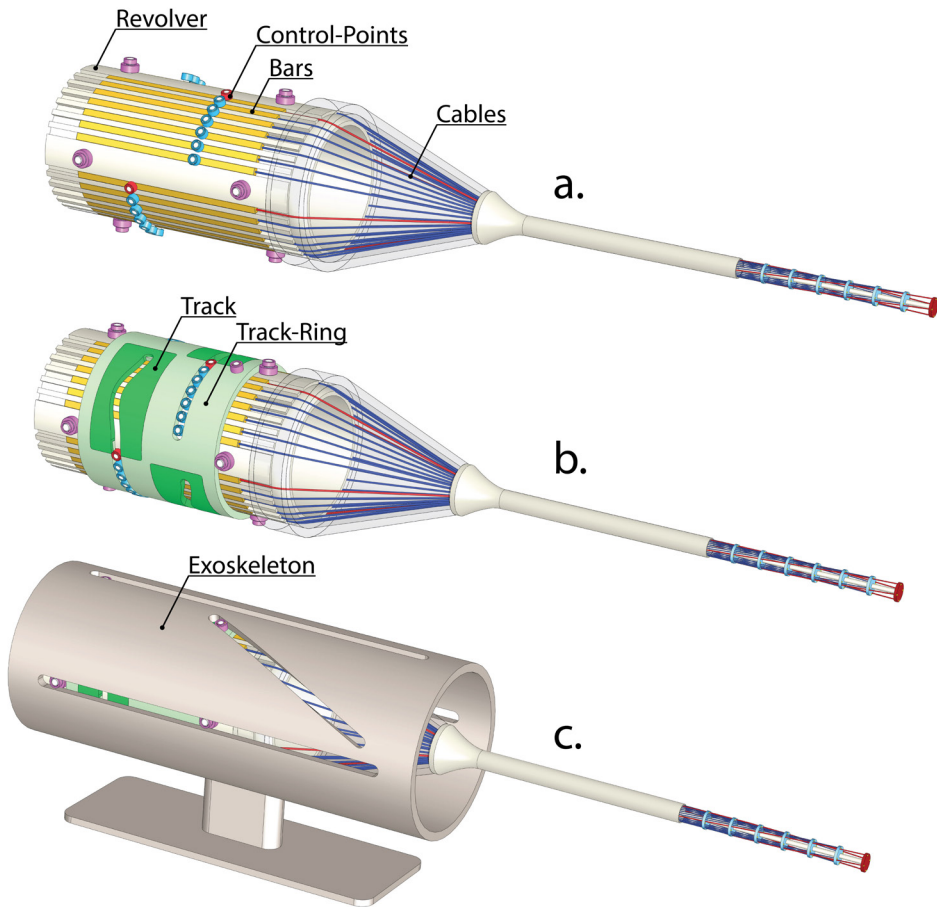


Figure 5.4: Full 3D instrument. For explanation, see text.

### 5.3 EXPERIMENTAL SETUP

A Proof of Concept (PoC) prototype called MemoFlex II was developed (Figure 5.5). Most of its components were machined out of aluminum. The bars were fabricated out of brass, creating low sliding friction with the aluminum revolver, and fitted with  $\varnothing 4$  mm ball bearings to serve as control-points. A cone from acrylic material connects the shaft to the revolver, its transparency allowing for visual feedback during the assembly phase. The exoskeleton was fabricated out of aluminum, and as much material as possible was removed to visualize the internal mechanism. The tracks were 3D-printed to make them easy to replace. The shaft is a novel continuous compliant structure that was 3D-printed out of one single part from R5 photopolymer on an Envisiontec Perfactory 4 3D-print

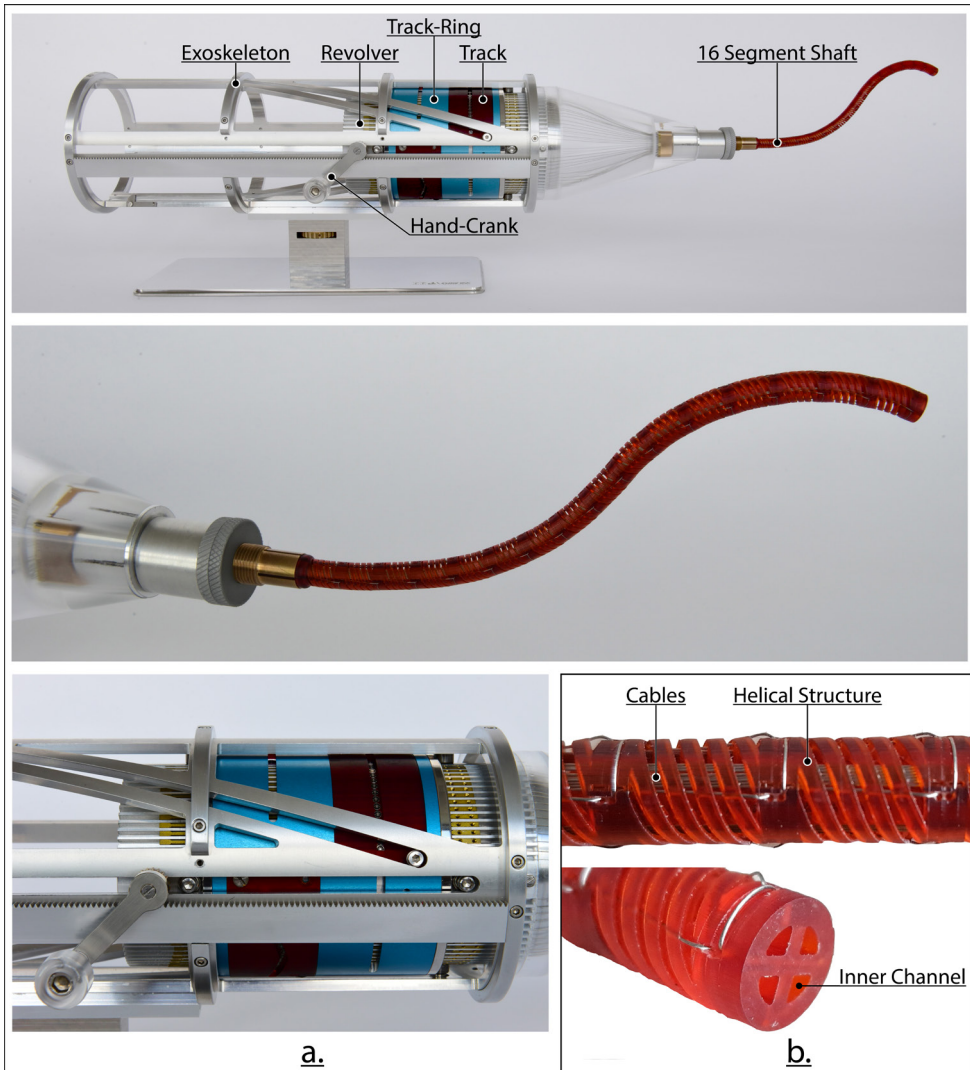


Figure 5.5: Proof of Concept prototype MemoFlex II. a) From top to bottom, the MemoFlex II with a 16 segment shaft mounted, a close-up of the shaft, and a close-up of the revolver and track-ring within the exoskeleton. b) Close-up of the 3D-printed shaft.

machine, a close-up is given in Figure 5.5b. The shaft consists of a solid central backbone surrounded by segments built up from 3D-printed helical structures. The backbone gives the shaft high axial stiffness, while the helical structure provides high torsion stiffness combined with low bending stiffness for easy bending of the segments. The cables are routed helically around the centerline at an angle of 8 degrees and run through 3D-printed holes at the circumference of the helical structures. In this way, the helical structures also serve as a guiding mechanism for guiding the cables smoothly along the bends. The shaft

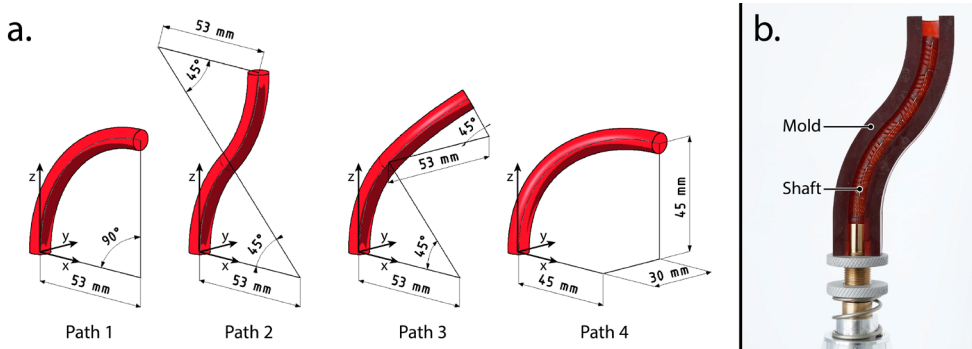


Figure 5.6: Reverse engineering tracks based on molds of the path a) Paths 1 to 4. b) 7 Segment shaft inserted in the mold of Path 2.

has a diameter of  $\varnothing 8$  mm, and each segment has a length of 12 mm. Four inner  $\varnothing 1.2$  mm channels run through the entire length of the shaft for use as lumens for insertion of additional instruments such as a gripper or suction tube. In our prototype, one of the channels was reserved for a  $\varnothing 1.2$  mm steel rod that is fixed to the stationary exoskeleton. This rod ensures that the segments that are not yet actively controlled are held in their initial straight position. The MemoFlex II is manually actuated via a rotating hand-crank. This pushes the revolver forward, while the helical grooves in the exoskeleton generate the appropriate rotation of the track-ring. The MemoFlex II can support a total of 64 cables for controlling 16 individual segments.

## 5

### 5.3.1 REVERSE ENGINEERING THE TRACKS

To determine their required shape, the tracks were reverse-engineered by shaping the shaft to a pre-described path and measuring the accompanying position of the cables. Four paths were chosen that were based on a shaft with seven segments and a total length of 84 mm (Figure 5.6a). A mold for each path was 3D-printed, providing a precisely fitting channel in which the shaft could be inserted (Figure 5.6b). Once the shaft was placed inside the mold, the accompanying elongation and shortening of the steering cables was registered by measuring the movement of the corresponding bars and ball-bearings inside the MemoFlex II. These measurements were used to configure the tracks.

### 5.3.2 EXPERIMENTAL MEASUREMENTS

The performance of the MemoFlex II was analyzed based on videos. As the shaft moved forward in the Z-direction, it was simultaneously filmed in both the horizontal X-plane and vertical Y-plane. Twelve consecutive video-frames were taken from each video, and superimposed upon each other to form a single figure. This resulted in two figures per

path, one showing the route of the shaft in the X-plane and the other showing the route of the shaft in the Y-plane. This way of presenting visualizes the footprint of the shaft, i.e. it shows how much space the shaft required during the entire motion. Next, for each of the paths of Figure 5.6, the projections in the horizontal X- and vertical Y-planes were determined, representing the intended path in the ideal situation without position errors. The resulting ideal shaft contours were added to the figures as a reference to the intended paths. This helped visualize how well the shaft follows the intended path and reaches the desired end-position.

Two measurements were taken from these figures. As a first measurement, the maximum width of the footprint ( $\Delta W_{xz}$  and  $\Delta W_{yz}$ ) was derived. For perfect FTL-motion, the maximum width of the shaft's footprint is equal to its diameter. The maximum width of the footprint therefore provides a measure of how well the shaft can conform to the path traced by its tip, i.e. how well the MemoFlex II performs FTL-motion. Note that this measurement shows how well the shaft followed the route that was traced by its tip but provides no information on how well this route matches the intended path.

As a second measurement, the position error of the end-point of the shaft in its final position compared to the end-point of the reference contours was derived. This error was measured in 3D in each of the directions X, Y and Z ( $\Delta x$ ,  $\Delta y$ , and  $\Delta z$ ). The spatial position error ( $\Delta xyz$ ) was then calculated using:

$$\Delta xyz = \sqrt{\Delta x^2 + \Delta y^2 + \Delta z^2}. \quad (5.1)$$

The spatial position error is a measure for the accuracy with which the MemoFlex II reached the desired end-position as specified by the pre-described paths of Figure 5.6.

## 5.4 RESULTS

The MemoFlex II functions well, being capable of following a path in a fluent motion. Moreover, due to the continuous motion of its mechanism, there is no significant limitations on its forward velocity. Figure 5.7 shows the results of the reverse engineering method for all four paths. The footprint of the shaft can be seen through the superimposed consecutive video frames. The green dashed lines represent the reference contours of the pre-described paths. The maximum footprints in the horizontal and vertical plane ( $\Delta W_{xz}$  and  $\Delta W_{yz}$ ) are denoted by arrows. The values for  $\Delta y$  and  $\Delta z$  were measured in the horizontal X-plane and the value of  $\Delta x$  was measured in the vertical Y-plane. Table 5.1

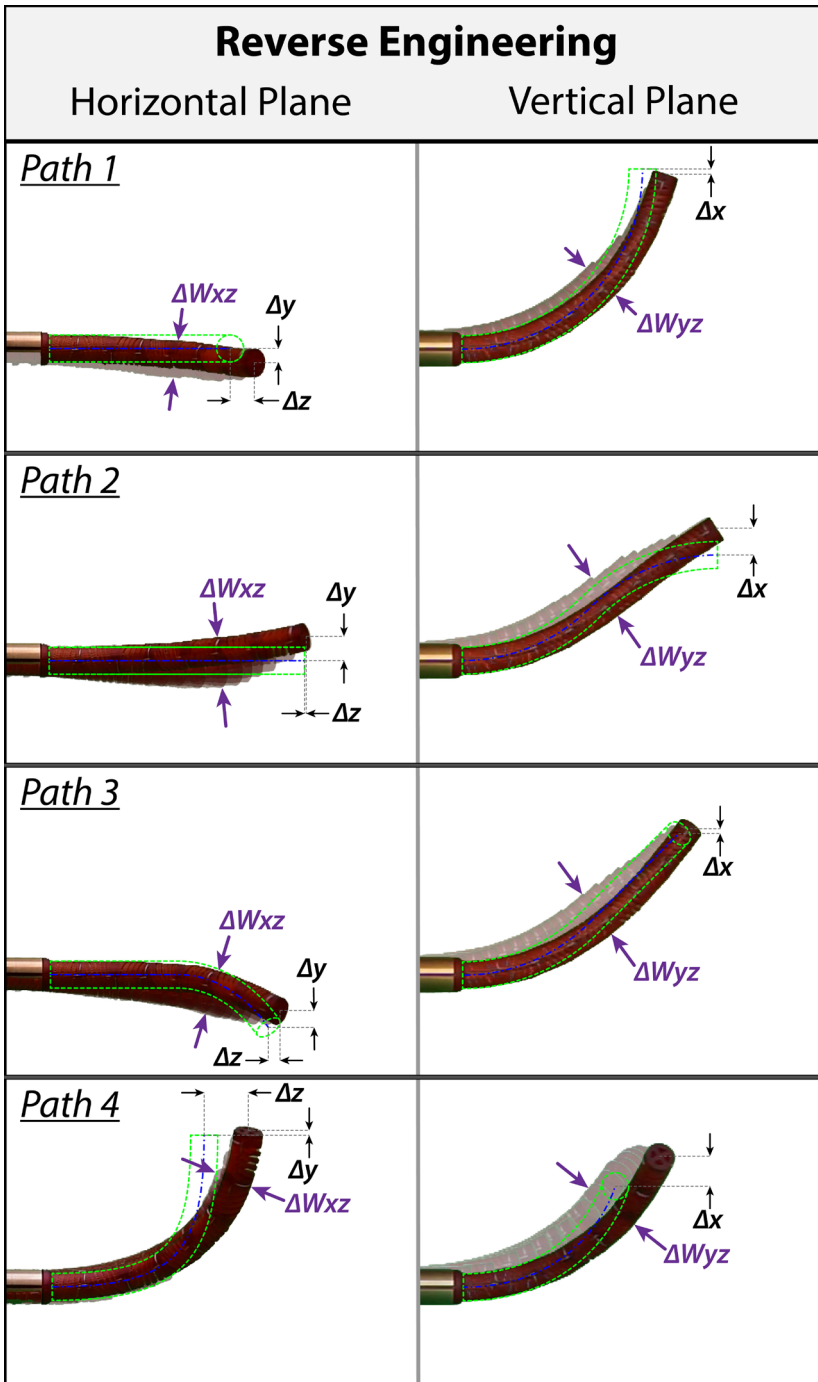


Figure 5.7: Results for the reverse engineering method for a shaft with seven segments. For measurements see Table 5.1. For further explanation see text.

Table 5.1: Measurements from Figure 7 in mm.  $\Delta W_{xz}$  and  $\Delta W_{yz}$  represent the average footprint in the horizontal and vertical plane for the four followed tracks in Figure 5.7.  $\Delta xyz$  is the root square of  $\Delta x$ ,  $\Delta y$  and  $\Delta z$ , and represents the position error of the shaft compared to the intended path.

	$\Delta W_{xz}$	$\Delta W_{yz}$	$\Delta x$	$\Delta y$	$\Delta z$	$\Delta xyz$
<b>Path 1</b>	11,0	11,8	1,6	3,9	7,0	8,2
<b>Path 2</b>	15,0	13,8	8,1	7,1	0,5	10,7
<b>Path 3</b>	13,1	14,4	1,4	4,9	3,4	6,2
<b>Path 4</b>	11,3	17,1	8,8	1,4	12,8	15,6
<b>average</b>	12,6	14,3				10,2

shows the average values of the footprint and spatial position errors of all four paths together.

The results show that the MemoFlex II is capable of FTL-motion and that the reverse engineering method for configuring the tracks worked reasonably well. The average footprint of the Ø8 mm shaft in the horizontal and vertical planes was 12,6 mm and 14,3 mm, respectively. The average spatial position error was 10,2 mm.

## 5.5 FURTHER OPTIMIZATION OF THE SYSTEM

In general, the MemoFlex II appears to have the most difficulties when following double-curved paths representing S-curves. Considering Path 2 in Figure 5.7, for example, the first curve of the path is followed reasonably well, while the second curve is damped and has almost no curvature. Another set of tracks was therefore constructed following a trial-and-error approach with the specific goal to improve on the performance of a double-curved path.

The trial and error approach started with a track-configuration that was similar to the reverse-engineered tracks of Path 2. This track configuration was then fine-tuned based on the reasoning that since the second curve appeared damped, the cables responsible for actuating that curve require more pulling. The part of the grooves in the tracks responsible for that pulling action was therefore made steeper, exaggerating the required motion. The performance of the resulting tracks was then tested in the MemoFlex II, and another round of fine-tuning was performed to further optimize the behavior. This process of trial-and-error continued until the MemoFlex II followed a double-curved path of which the second curve matched the curvature of the first curve.

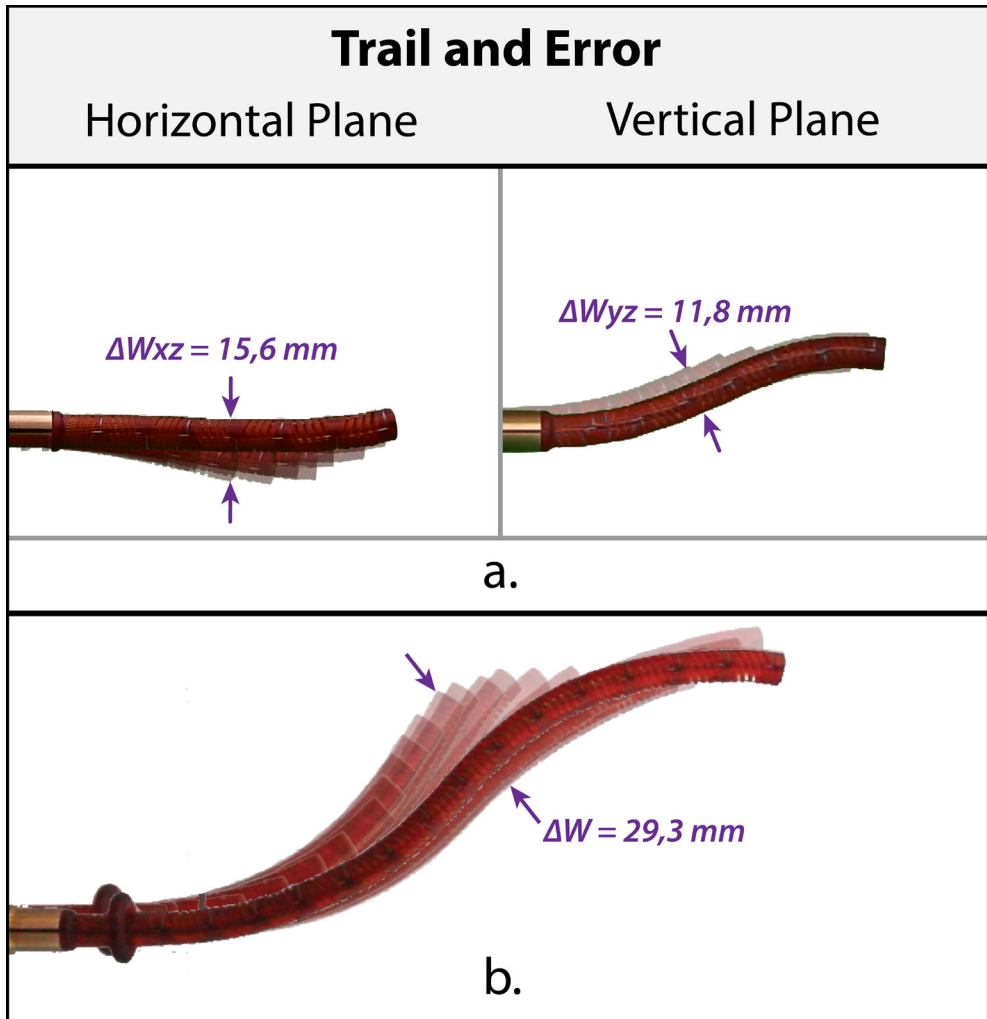


Figure 5.8: Results from the tracks based on the trial and error approach. a) Shaft with seven segments. b) Shaft with 16 segments.

Figure 5.8a presents the results of the trial-and-error approach. The maximum width of the footprint ( $\Delta W_{xz}$  and  $\Delta W_{yz}$ ) was determined again, and the values are now given in the figure itself. In contrast with Figure 5.7, the results of Figure 5.8 do not include a green reference contour, the reason being that the tracks were based on a trial-and-error approach and thus no specific pre-described path was used. Consequently, no spatial position error was calculated. Figure 5.8a shows that the first and second curves of the shaft do now approximately have an equal curvature in their final position.

## 5.6 DISCUSSION

In this paper, we developed a fully mechanical Follow-the-Leader instrument based on a cable-driven hyper-redundant shaft that is extrinsically actuated by a physical track. This resulted in a prototype called MemoFlex II. By adopting a fully mechanical approach, no actuators were required.

### 5.6.1 PERFORMANCE

Table 5.1 shows that the MemoFlex II performed better when following Path 1 that only contains a single curve, as compared to following Paths 2, 3 and 4 that contain multiple 2D or 3D curves. This is especially visible for Path 2 in Figure 5.7, of which the second curvature of the double-curved path is almost nonexistent. At first, one is tempted to explain this behavior through the play between the cables and its guiding components. Such play makes it possible for a cable to take the shortest route through the shaft, which reduces its effectivity for actuation. Yet, during the reverse engineering method, the cables run along the same routes and encounter the same play, meaning that this play was already incorporated in the design of the tracks. Another explanation can be found when considering the difference in cable tension during the reverse engineering method and the motion of the shaft. Due to the bending stiffness of the central backbone of the shaft, some force is required to bend it into shape. When applying the reverse engineering method, the shaft is forced into shape externally by the mold. During the motion itself, however, the shaft is forced into shape internally by the cables, leading to a higher tension in the cables. This additional cable tension will result in elastic stretching of the cables, shorten the central backbone, and increase the friction on the cables in shaft bends as they slide through their 3D-printed guiding holes. All of these effects work against the “preprogrammed” bending motion, resulting in flattened shaft curvatures. This effect is visible in the vertical plane of Path 1 of Figure 5.7, where the curvature of the shaft is lower than the curvature of the green reference contour. The effect is amplified when following a multi-curved path, like in the case of Path 2 where the two curves are in opposite direction. The reason is that the cables that actuate the second curve are routed along the outside of the first curve. Because this first curve has a flattened curvature, the route is shorter than intended during the reverse engineering of the tracks, thus significantly reducing the effectiveness of the cables in actuating the second curve.

Another effect that influences the performance of the MemoFlex II is the cross-coupling between segments. A cable that is connected to segment  $n$  will tend to bend the intermediate segments as well, i.e. the bending moment of one segment influences the behavior of the segments that lay between it and the shaft. This cross-coupling is amplified due to the central backbone which passes the bending moment along segments. This

effect is especially visible for the shaft with 16 segments in Figure 5.8b. When the tip of the shaft (Segment 1) changes direction to enter the second curve of the path, not only Segment 1, but the entire shaft moves a little bit in that direction. In theory, the cables of the other segments should resist this movement assuming that they are infinitely stiff in axial direction. In reality, however, this is not the case, resulting in the entire shaft swaying along a bit whenever the path changes direction.

### 5.6.2 AN INDIVIDUAL TRACK PER CABLE

Throughout this paper, FTL-motion was approached via a linear model, i.e. when all segments are identical, FTL-motion can be achieved by providing each segment with the same control-input. This led to the assumption that multiple cables could be controlled by a single groove. In reality, however, effects like cable stretching, cable friction and cross-coupling between segments, introduce non-linear effects into the system. A way to compensate for these effects is to create a separate control input for each individual cable instead of using a shared control input for all cables simultaneously, i.e. by controlling every cable by its own optimized groove. These grooves could, for example, be placed in series beside each other in the Track-Ring. For a shaft with seven segments and thus 14 DOFs, this would require 28 individual grooves. Although this sounds like a massive extension to the current system, in reality, this should not be that hard to incorporate, the reason being that, even though every groove will be individually optimized, the basic shape of the individual grooves will still be quite similar. This allows the grooves to be stacked close to one another, allowing for one track to support multiple grooves as shown in Figure 5.9. Such a configuration will only marginally extend the length of the revolver, while considerably increasing the level of control over the cables and enhancing the overall performance.

5

### 5.6.3 MODEL-BASED ENGINEERING OF THE TRACKS

Our experiments have shown that the reverse engineering approach works, although it does not produce highly accurate results. The trial-and-error approach increased the performance but is not a viable end solution as the iterative process is highly labor-intensive. A better solution could be found by using a model-based approach for engineering the tracks. This would require a kinematic simulation model that computes the required tension in the cables based on the bending behavior of the shaft due to its geometrical and material properties. From these computed cable tensions the required positional changes of the cables can be calculated, producing the required control input for each cable, and complementing the use of an individual track per cable.

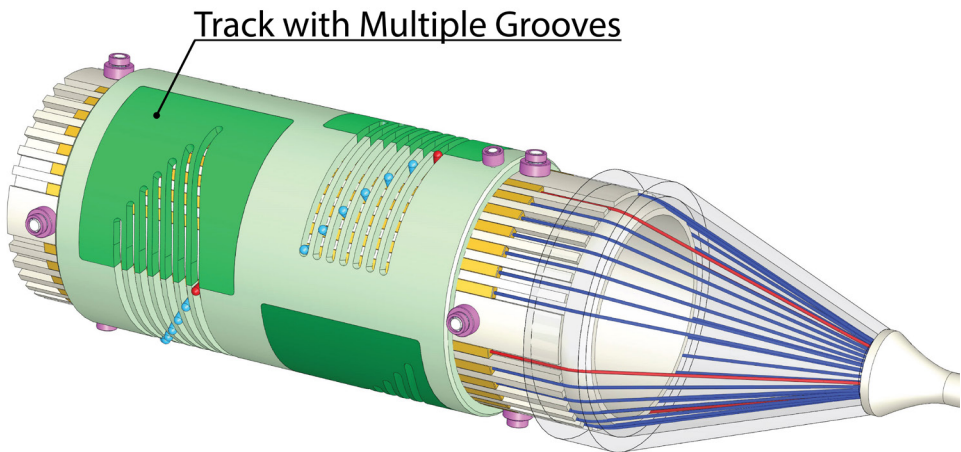


Figure 5.9: Alteration of Figure 4b, now including a track with an individual groove per cable.

#### 5.6.4 THE MEMOFLEX II IN A MEDICAL SETTING

In a medical setting, we envision a future, optimized version of our instrument to function partly as a re-usable and partly as a disposable device – similar to the successful Da Vinci master-slave system of the US company Intuitive Surgical, which consists of reusable robotic arms and cable-driven instruments capable of 2 DOFs steering that is disposed of after a number of surgical procedures. For our MemoFlex II, the control section would be re-usable, while the shaft would be disposed of after one single use. Efficiently connecting the great number of steering cables of the disposable shaft to the re-usable control section will be one of the most prominent technical challenges, and will be part of future research [43].

In this study, 3D-printing was used for fast and relatively cheap fabrication of singular parts, e.g. the tracks, and the fabrication of parts that are impossible to manufacture using conventional techniques, e.g. the spiral structure in the shaft. In a medical setting, 3D-printing would be very useful for the fabrication of patient-specific parts. The tracks could, for example, be printed based on patient-specific MRI or CT images. Even the shaft itself could become patient-specific, for example by changing its length, diameter, the number of channels and other structural and material properties to suit the needs of a specific type of operation. For these reasons, we foresee that 3D-printing will become an integral part of integrating the MemoFlex II in a medical setting.

## 5.7 CONCLUSION

This paper introduced a novel concept for achieving multi-curved Follow-the-Leader motion of a surgical instrument. The concept involves a cable-driven hyper-redundant shaft that is extrinsically controlled using a cam-follower mechanism based on physical tracks. By adopting this fully mechanical approach, no actuators were required. A prototype called MemoFlex II was developed to validate the proposed concept. It supports a Ø8 mm 3D-printed shaft with a modular setup to support a maximum of 32 DOFs. A Ø8 mm shaft with seven segments was able to follow predetermined multi-curved paths with a maximum footprint between 11,0 and 17,1 mm. In a future medical setting, we envision the MemoFlex II to function as a partly re-usable and partly disposable device, wherein 3D-printing would allow for patient-specific tracks based on MRI or CT imaging and patient-specific shafts that are structurally optimized to suit the specific needs of individual MIS or NOTES procedures.

## 5.8 REFERENCES

1. Atallah S, Martin-Perez B, Keller D, Burke J, Hunter L. Natural-orifice transluminal endoscopic surgery. *The British journal of surgery*. 2015;102(2):e73-92.
2. McLaughlin N, Eisenberg AA, Cohan P, Chaloner CB, Kelly DF. Value of endoscopy for maximizing tumor removal in endonasal transsphenoidal pituitary adenoma surgery. *J Neurosurg*. 2013;118(3):613-20.
3. Cavallo LM, Prevedello DM, Solari D, Gardner PA, Esposito F, Snyderman CH, et al. Extended endoscopic endonasal transsphenoidal approach for residual or recurrent craniopharyngiomas. *J Neurosurg*. 2009;111(3):578-89.
4. Cappabianca P, Cavallo LM, de Divitiis E. Endoscopic endonasal transsphenoidal surgery. *Neurosurgery*. 2004;55(4):933-40; discussion 40-1.
5. Loeve A, Breedveld P, Dankelman J. Scopes too flexible and too stiff. *IEEE Pulse*. 2010;1(3):26-41.
6. Choset H, Henning W. A Follow-the-Leader Approach to Serpentine Robot Motion Planning. *Journal of Aerospace Engineering*. 1999;12(2):65-73.
7. Burgner-Kahrs J, Rucker DC, Choset H. Continuum robots for medical applications: a survey. *Ieee Transactions on Robotics*. 2015;31(6):1261-80.
8. Ikuta K, Tsukamoto M, Hirose S, editors. Shape memory alloy servo actuator system with electric resistance feedback and application for active endoscope. *Proceedings 1988 IEEE International Conference on Robotics and Automation*; 1988 24-29 April 1988.
9. Buckingham R. Snake arm robots. *Industrial Robot: the international journal of robotics research and application*. 2002;29(3):242-5.
10. Palmer D, Cobos-Guzman S, Axinte D. Real-time method for tip following navigation of continuum snake arm robots. *Robot Auton Syst*. 2014;62(10):1478-85.
11. Son J, Cho CN, Kim KG, Chang TY, Jung H, Kim SC, et al. A novel semi-automatic snake

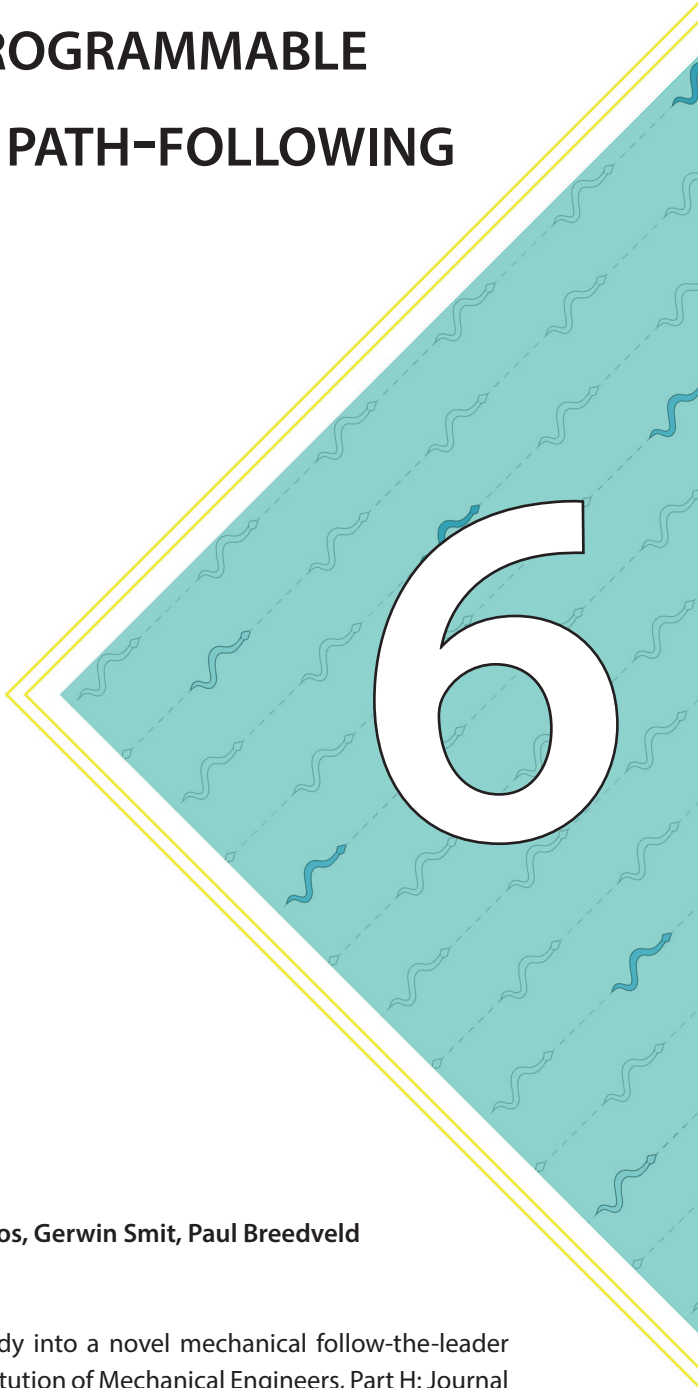
- robot for natural orifice transluminal endoscopic surgery: preclinical tests in animal and human cadaver models (with video). *Surg Endosc.* 2015;29(6):1643-7.
12. Tappe S, Yu D, Kotlarski J, Ortmaier T. Model reduction methods for optimal follow-the-leader movements of binary actuated, hyper-redundant robots. *Mechanisms and Machine Science* 2018. p. 35-43.
  13. Sars VD, Haliyo S, Szewczyk J. A practical approach to the design and control of active endoscopes. *Mechatronics.* 2010;20(2):251-64.
  14. Tortora G, Dimitracopoulos A, Valdastrì P, Menciasì A, Dario P, editors. Design of miniature modular in vivo robots for dedicated tasks in Minimally Invasive Surgery. 2011 IEEE/ASME International Conference on Advanced Intelligent Mechatronics (AIM); 2011 3-7 July 2011.
  15. Rivas-Blanco I, Saz-Orozco Pd, García-Morales I, Muñoz V, editors. Robotic system for single incision laparoscopic surgery. *IECON 2012 - 38th Annual Conference on IEEE Industrial Electronics Society*; 2012 25-28 Oct. 2012.
  16. Cepolina FE, Zoppi M. Design of multi-degrees-of-freedom dexterous modular arm instruments for minimally invasive surgery. *Proceedings of the Institution of Mechanical Engineers, Part H: Journal of Engineering in Medicine.* 2012;226(11):827-37.
  17. Ho M, McMillan AB, Simard JM, Gullapalli R, Desai JP. Toward a Meso-Scale SMA-Actuated MRI-Compatible Neurosurgical Robot. *IEEE Transactions on Robotics.* 2012;28(1):213-22.
  18. Clark J, Noonan DP, Vitiello V, Sodergren MH, Shang J, Payne CJ, et al. A novel flexible hyper-redundant surgical robot: prototype evaluation using a single incision flexible access pelvic application as a clinical exemplar. *Surg Endosc.* 2015;29(3):658-67.
  19. Tzorakoleftherakis E, Mavrommati A, Tzes A. Design and Implementation of a Binary Redundant Manipulator With Cascaded Modules. *Journal of Mechanisms and Robotics.* 2015;8(1):011002--10.
  20. Berthet-Rayne P, Gras G, Leibrandt K, Wisanuvej P, Schmitz A, Seneci CA, et al. The i 2 Snake Robotic Platform for Endoscopic Surgery. *Annals of Biomedical Engineering.* 2018;46(10):1663-75.
  21. Simaan N, editor Snake-Like Units Using Flexible Backbones and Actuation Redundancy for Enhanced Miniaturization. *Proceedings of the 2005 IEEE International Conference on Robotics and Automation*; 2005 18-22 April 2005.
  22. Shang J, Noonan DP, Payne C, Clark J, Sodergren MH, Darzi A, et al. An articulated universal joint based flexible access robot for minimally invasive surgery. *Robotics and Automation (ICRA), 2011 IEEE International Conference on*; 2011 9-13 May 2011.
  23. He J, Liu R, Wang K, Shen H, editors. The mechanical design of snake-arm robot. *IEEE 10th International Conference on Industrial Informatics*; 2012 25-27 July 2012.
  24. Reiter A, Bajo A, Iliopoulos K, Simaan N, Allen PK, editors. Learning-based configuration estimation of a multi-segment continuum robot. 2012 4th IEEE RAS & EMBS International Conference on Biomedical Robotics and Biomechanics (BioRob); 2012 24-27 June 2012.
  25. Li Z, Du R. Design and Analysis of a Bio-Inspired Wire-Driven Multi-Section Flexible Robot. *International Journal of Advanced Robotic Systems.* 2013;10(4):209.
  26. Krieger YS, Roppenecker DB, Stolzenburg J, Lueth TC, editors. First step towards an automated designed Multi-Arm Snake-Like Robot for minimally invasive surgery. 2016 6th IEEE International Conference on Biomedical Robotics and Biomechanics (BioRob); 2016 26-29 June 2016.
  27. Evangelio N, Tzes A, editors. A human-in-the-loop controlled shape memory alloy actuated robotic probe for minimally invasive surgical procedures. 2016 *ELEKTRO*; 2016

- 16-18 May 2016.
28. Ouyang B, Liu Y, Sun D, editors. Design and shape control of a three-section continuum robot. 2016 IEEE International Conference on Advanced Intelligent Mechatronics (AIM); 2016 12-15 July 2016.
  29. Cianchetti M, Ranzani T, Gerboni G, Nanayakkara T, Althoefer K, Dasgupta P. Soft Robotics Technologies to Address Shortcomings in Today's Minimally Invasive Surgery: The STIFF-FLOP Approach 2014. 122-31 p.
  30. Webster III RJ, Romano JM, Cowan NJ. Mechanics of pre-curved-tube continuum robots. IEEE Transactions on Robotics. 2009;25(1):67-78.
  31. Mahoney AW, Gilbert HB, III RJW. A REVIEW OF CONCENTRIC TUBE ROBOTS: MODELING, CONTROL, DESIGN, PLANNING, AND SENSING. The Encyclopedia of Medical Robotics. p. 181-202.
  32. Gilbert HB, Rucker DC, Webster RJ, III. Concentric tube robots: The state of the art and future directions. Springer Tracts in Advanced Robotics 2016. p. 253-69.
  33. Kang B, Kojcev R, Sinibaldi E. The first interlaced continuum robot, devised to intrinsically Follow-the-Leader. PLoS ONE. 2016;11(2).
  34. Amanov E, Granna J, Burgner-Kahrs J, editors. Toward improving path following motion: Hybrid continuum robot design. 2017 IEEE International Conference on Robotics and Automation (ICRA); 2017 29 May-3 June 2017.
  35. Ota T, Degani A, Schwartzman D, Zubiate B, McGarvey J, Choset H, et al. A Highly Articulated Robotic Surgical System for Minimally Invasive Surgery. The Annals of Thoracic Surgery. 2009;87(4):1253-6.
  36. Nguyen TD, Burgner-Kahrs J, editors. A tendon-driven continuum robot with extensible sections. Intelligent Robots and Systems (IROS), 2015 IEEE/RSJ International Conference on; 2015 Sept. 28 2015-Oct. 2 2015.
  37. Conrad BL, Zinn MR. Interleaved Continuum-Rigid Manipulation: An Approach to Increase the Capability of Minimally Invasive Surgical Systems. IEEE/ASME Transactions on Mechatronics. 2017;22(1):29-40.
  38. Li Z, Chengzhi S, Hongmin W, editors. Design and prototyping of a concentric wire-driven manipulator. 2016 6th IEEE International Conference on Biomedical Robotics and Biomechatronics (BioRob); 2016 26-29 June 2016.
  39. Gilbert HB, Neimat J, Webster RJ. Concentric Tube Robots as Steerable Needles: Achieving Follow-the-Leader Deployment. IEEE Transactions on Robotics. 2015;31(2):246-58.
  40. Johnson PJ, Rivera Serrano CM, Castro M, Kuenzler R, Choset H, Tully S, et al. Demonstration of transoral surgery in cadaveric specimens with the medrobotics flex system. Laryngoscope. 2013;123(5):1168-72.
  41. Corporation M. website Flex Robotic System Raynham, Massachusetts: Medrobotics; 2019 [Available from: <https://medrobotics.com>].
  42. Henselmans PW, Gottenbos S, Smit G, Breedveld P. The MemoSlide: An explorative study into a novel mechanical follow-the-leader mechanism. Proceedings of the Institution of Mechanical Engineers, Part H: Journal of Engineering in Medicine. 2017;231(12):1213-23.
  43. Velsink F. Sterile barriers: Exploring possible design directions for barriers between the sterile and the nonsterile part of a cable-driven surgical instrument [Master]. Delft: Delft University of Technology; 2017.





# MEMO*SLIDE*: PROGRAMMABLE MECHANISM FOR PATH-FOLLOWING



6

**Paul W.J. Henselmans, Stefan Gottenbos, Gerwin Smit, Paul Breedveld**

Published as:

The *MemoSlide*: An explorative study into a novel mechanical follow-the-leader mechanism. Proceedings of the Institution of Mechanical Engineers, Part H: Journal of Engineering in Medicine, 2017. 231(12): p. 1213-1223.

**ABSTRACT**

Follow-the-Leader (FTL) propagation allows for the insertion of flexible surgical instruments along curved paths, reducing the access required for natural orifice transluminal endoscopic surgery. Currently, the most promising FTL-instruments use the Alternating Memory (AM) method containing two mechanical memory-banks for controlling the motion of the flexible shaft, which reduces the number of actuators to a minimum. These instruments do however require concentric structures inside the shaft, limiting its miniaturization. The goal of this research was, therefore, to develop a mechanism conform the principles of the AM method that could be located at the controller-side instead of inside the shaft of the instrument, which is positioned outside the patient and is therefore less restricted in size. First, the three dimensional (3D) motion of the shaft was decoupled into movement in a horizontal and vertical plane, which allowed for a relatively simple planar AM mechanism design for controlling planar FTL-motion. Next, the planar movement of the AM mechanism was discretized, increasing its resilience to errors. The resulting AM-mechanism was incorporated and tested in a proof of concept prototype called the *MemoSlide*. This prototype does not include a flexible shaft but was fully focused on proving the function of the AM-mechanism. Evaluation of the *MemoSlide* shows the mechanism to work very well, being able to transfer any planar path that lays within its physical boundaries along the body of the mechanism without accumulating errors.

## 6.1 INTRODUCTION

Advancements in Minimally Invasive Surgery (MIS) has led to a reduction of the invasiveness of surgical procedures, leading to less scar tissue, a lower risk of infection, and shorter hospital stays [1-3]. The field of Natural Orifices Transluminal Endoscopic Surgery (NOTES) strives to further reduce the negative effects of surgery by using natural orifices such as the mouth, nose, and anus as the surgical entry-point [4, 5] This approach does introduce technical challenges as the currently used rigid  $\varnothing 5$  mm instruments designed for MIS are not able to confine to the curved nature of the human anatomy but dictate a straight path from entry-point to the lesion. Making the  $\varnothing 5$  mm instruments flexible, as for example the MultiFlex of Figure 6.1a, could therefore extend the reach of NOTES procedures in compact anatomical areas [6, 7].

To maneuver a flexible instrument through compact anatomical areas, its movements must be controlled in such a manner that the instrument propagates along a curved path, comparable to the motion of a biological snake. A snake steers its head while the remainder of its body follows the created path. In this way, the snake can navigate through cluttered environments while avoiding obstacles like the stones in Figure 6.1b. Chose et al. introduced the term Follow-the-Leader (FTL) for this type of movement as the snake's body follows the head that functions as the leader.

In the following section, the state of the art in FTL-instruments will be discussed based on the used technique and its potential for miniaturization to  $\varnothing 5$  mm. Techniques that require interaction with the environments to propagate along a curved path, e.g. a catheter that



Figure 6.1: Flexible surgical instrument and Follow-the-Leader propagation. (a) The MultiFlex, an  $\varnothing 5$  mm flexible instrument with 10 degrees of freedom [28]. The instrument is controlled by manually adjusting the shape of the handle, which is mimicked by the flexible part of the shaft. (b) Snake moving through a cluttered environment by transferring a curved path initiated by its head along its body. This motion is referred to as a Follow-the-Leader propagation.

is guided through a lumen, are not considered. Only techniques that can move in free space without guidance from the environment are regarded as FTL-instruments and will be discussed.

### 6.1.1 STATE OF THE ART

Concentric tube robots are currently the thinnest existing instruments mentioned in research towards FTL-propagation [8-11]. These instruments contain a telescoping mechanism of pre-curved compliant tubes placed concentrically within one another. Rotating or translating the tubes relative to each other causes them to interact and deform, with the result that the instrument changes shape. Based on a model of the interaction between the tubes, a control sequence can be planned to achieve FTL-propagation [12, 13]. However, the predefined curvature and compliancy of the tubes restrict the propagation to only specific and relatively simple paths, like a single bend or a constant curvature helix, that have to be planned prior to the surgical procedure.

Several FTL-instruments that can follow non-specific paths without planning were also found in literature. Typically, their shafts contain multiple Degrees of Freedom (DOFs) that are independently controlled by an individual actuator [14-22]. These actuators can be embedded in the shaft near the DOFs they actuate. Embedding the actuators within a  $\varnothing 5$  mm shaft is highly challenging while maintaining sufficient power output at safe temperatures. With the addition of a transmission system, the actuators can also be placed outside of the shaft at the controller-side of the instrument, e.g. by using cables that connect the actuator placed outside the shaft to the DOFs in the shaft [19-21]. Actuators placed at the instrument's controller-side, and therefore outside the patient, are less restricted in size. The thinnest instrument found in literature using this approach is  $\varnothing 8$  mm. Its shaft consists of three telescoping segments that each can be bend in two DOFs by using cables. In principle, these instruments could be miniaturized down to  $\varnothing 5$  mm [19, 20]. Moreover, by connecting each DOFs to an individual actuator, the DOFs can be independently controlled which allows for propagation along non-specific paths without the need for planning.

A downside of using an individual actuator for every DOFs in the shaft is that it requires a large number of actuators. Moreover, as a complex 3D path requires more DOFs in the shaft than a path with a single curve, the complexity of the path that can be followed becomes dependent on the number of actuators in the system. As medical-grade actuators (conforming to ISO 13485) are not cheap, e.g. a DC motor with gearhead can easily cost over € 200,-, it is preferable to use a minimal number of actuators [23].

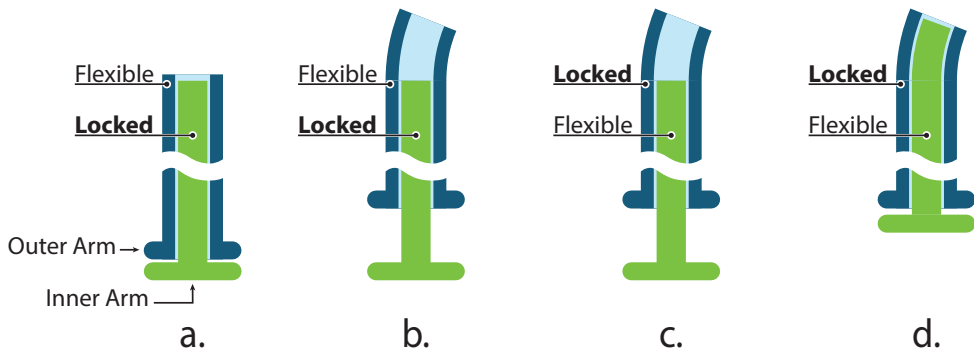


Figure 6.2: Schematic 2D drawing showing the functioning of the HARP consisting of two concentrically placed flexible arms which can both be independently locked [25, 26]. For explanation: see text.

There are instruments capable of propagating along tortuous paths with less than one actuator for each DOFs.<sup>24-26</sup> The most promising instrument is the Highly Articulated Robotic Probe (HARP), which consists of two concentrically placed arms that contain friction-based locking systems to switch between rigid and flexible states (Figure 6.2a) [25, 26]. FTL-propagation is achieved by a series of alternating steps. First, the inner arm is rigidified, while the outer arm is made flexible. The outer arm is then advanced while using cables to steer its tip in the desired direction (Figure 6.2b). Next, the outer arm is rigidified, while the inner arm is made flexible (Figure 6.2c). The inner arm is now advanced while being guided by the rigid outer arm (Figure 6.2d). Once the inner arm catches up with the outer arm, the sequence is repeated. The HARP therefore only needs actuators for steering, rigidifying and advancing its arms, with the result that the complexity of the path becomes independent from the number of actuators.

The HARP's outer diameter is 12 mm and is difficult to miniaturize down to the desired  $\varnothing 5$  mm due to its concentrically placed friction-based locking systems. The locking systems are constructed out of a series of ball-joints, which can be pressed together via cables to induce friction creating a friction torque around the joints and therefore rigidifying the shaft. Miniaturization of the shaft's diameter with a scaling factor of  $s$  reduces the moment arm of the friction torque with factor  $s$ , therefore increasing the required friction force by the same factor  $s$ . Moreover, the surface area of the friction force will decrease with factor  $s^2$ . The increase in friction force and a decrease in surface area will cause the material stress to increase with factor  $s^3$ , making it very difficult to avoid plastic deformation. The HARP's method of FTL-propagation is, however, very interesting: where normally the path information is measured and memorized by a computer that drives a set of actuators, one for each DOFs, the HARP is based on two mechanical memory-banks (the two concentric arms) that alternate between copying, memorizing and shifting the path information.

The result is that the complexity of the path becomes independent from the number of actuators. In this paper, this method for FTL-propagation will be referred to as the “Alternating Memory method” or AM method.

### 6.1.2 PROBLEM STATEMENT AND GOAL

An instrument using the Alternating Memory (AM) method for Follow-the-Leader (FTL) propagation alternates the path information between two mechanical memory-banks. The advantage is that the instrument does not require an actuator for every Degree of Freedom (DOFs) in its flexible shaft, with the result that the number of actuators is fixed and becomes independent of the complexity of the path. Placing the memory-banks inside the instrument’s flexible shaft does, however, impede miniaturization of the shaft, as seen in the HARP. In this paper, we introduce a novel concept using the AM-method for FTL-propagation while focusing on the development of a control mechanism that can be located at the controller-side of the instrument, which is outside of the patient and therefore less restricted in size.

## 6.2 MECHANISM DESIGN

### 6.2.1 MINIATURIZATION OF THE SHAFT WITH THE CABLE-RING MECHANISM

If the memory-banks are placed at the controller-side of the instrument, then the motions of its memory-banks have to be transported towards the flexible shaft. This can be realized by the cable-ring mechanism in which a set of steering cables is enclosed in a ring between two springs as illustrated in Figure 6.3 [27]

By fixing cables at intermediate points along the length of the shaft, the maneuverability of the shaft is enhanced. The MultiFlex of Figure 6.1a is an example of a cable-ring controlling five segments with a total of ten DOFs within a Ø5 mm shaft.<sup>28</sup> The elegance of this mechanism is that the cables keep each other aligned, which eliminates the need for additional guiding components while maximizing the number of cables. The number of cables in a cable-ring can be calculated by:

$$n_{cables} = \frac{2 \cdot \pi \cdot r_c}{d_{cable}}, \quad (6.1)$$

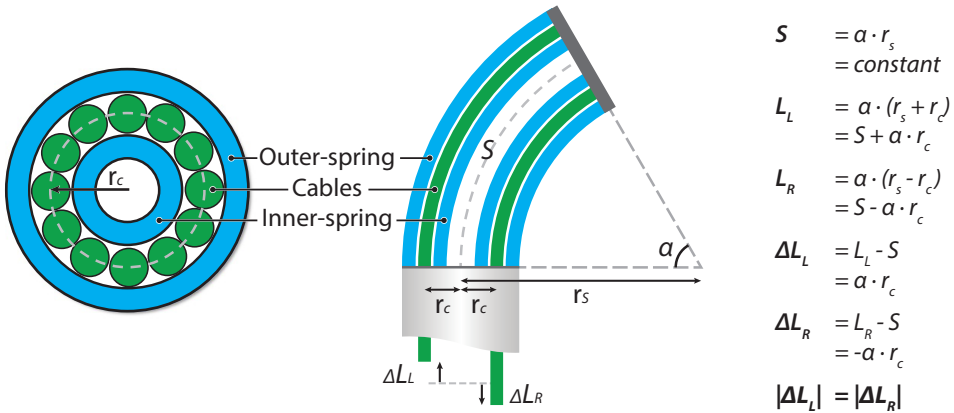


Figure 6.3: Cable-ring mechanism. Left: schematic cross-sectional view of a cable-ring mechanism. Cables are enclosed in a ring by an inner-spring and an outer-spring. Right: schematic side view of a cable-ring segment in bent position. Assuming that the centerline ( $S$ ) does not change length, the absolute length change ( $|\Delta L|$ ) of antagonist cables is equal.

where  $r_c$  [mm] is the radius of the cable-ring, and  $d_{cable}$  [mm] the diameter of the cables. For a  $\varnothing 5$  mm shaft design including  $\varnothing 0.2$  mm stranded steel cables and an outer-spring with  $\varnothing 0.2$  mm wire, the maximum radius of the cable-ring will be 2.3 mm. This allows for approximately 72 cables. By using four cables to control each segment in two DOFs, this shaft design allows for a maximum of 18 segments with a total of 36 DOFs at a diameter of only  $\varnothing 5$  mm. The cable-ring mechanism thus offers a convenient solution to transport the motions of the memory-banks from the controller-side to shaft, while enabling miniaturization of the shaft to the desired dimensions.

The cables can be guided from the proximal side of the shaft towards the memory-banks by using e.g. pulleys, tubes, guiding slots or Bowden cables. Such guiding methods are commonly applied in steerable instrumentation [29-31].

The function of the memory-banks is to control the distance over which a cable is pulled or released. Assuming that segment bends with a constant curvature as illustrated on the right of Figure 6.3, the distance over which a cable travels ( $\Delta L_C$  [mm]) relates to the radius of the cable-ring ( $r_c$  [mm]) and the bending angle of the segment ( $\alpha$  [rad]) as:

$$|\Delta L_C| = r_c \cdot \alpha. \quad (6.2)$$

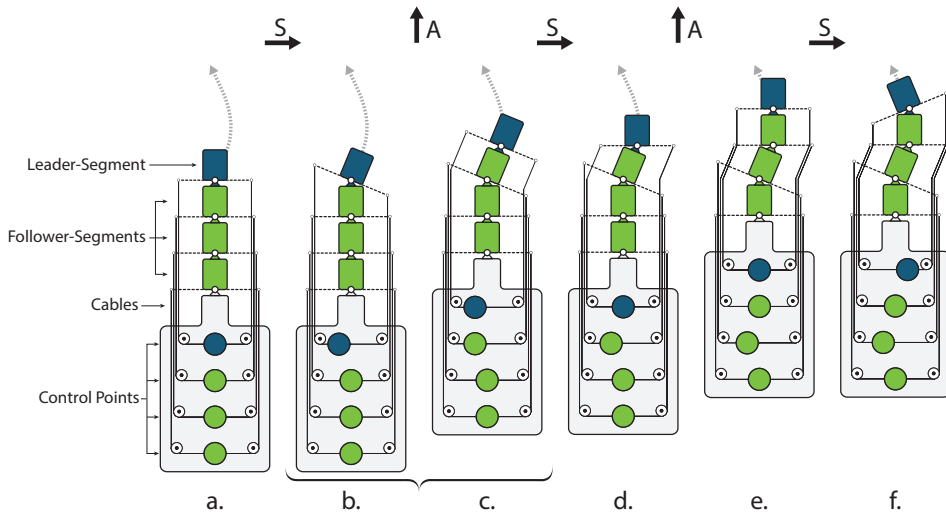


Figure 6.4: Two dimensional schematic representation of cable control for Follow-The-Leader (FTL) propagation. Arrows with an 'S' stand for a steering action. Arrows with an 'A' stand for an advancing action. For explanation: see text. The brace is used in Figure 6.5.

Equation (6.2), shows that to reach a bending angle of 100 degrees with the proposed cable ring dimensions, a cable needs to be shifted over  $\pm 4$  mm. Equation (6.2) holds for both a cable that is pulled and its antagonist that is released.

## 6.2.2 CABLE CONTROL FOR FOLLOW-THE-LEADER MOTION

A two-dimensional representation of a shaft connected to the cables of a cable-ring is shown in Figure 6.4a. The shaft consists of  $N = 4$  segments, the first segment being the leader-segment, and the other three segments being the follower-segments. At the controller-side of the instrument, the cables controlling the four segments in the shaft are connected to components referred to as control-points. From equation (6.2) it is clear that the absolute length changes between antagonist cables are equal, consequently, antagonist cables can be connected at opposite sides of the same control-point. A sideways translation of a control point results in a rotation of the connected segment. The configuration of all control points together determines the overall shape of the shaft.

FTL-propagation can be realized by repeating the following two actions as indicated by the arrows in Figure 6.4. Starting with steering, the direction of the leader-segment is changed by translating the first control-point (the leader control-point) sideways (Figure 6.4b). Following with advancing, the instrument is pushed one segment-length forward while the steering action given to the first segment is transported along its adjacent segment. This shifting of information also occurs between the other segments, i.e. the position of

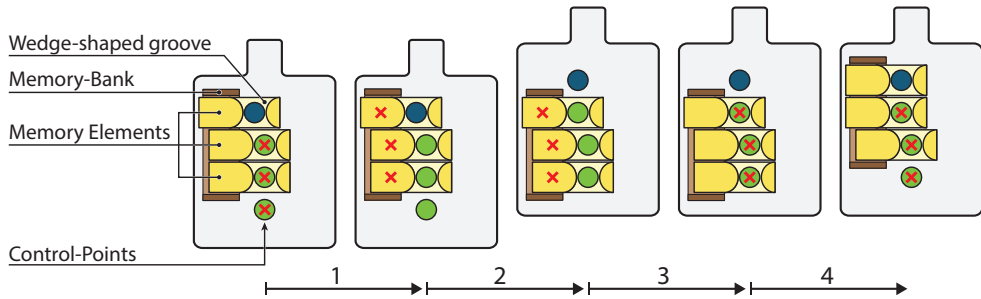


Figure 6.5: The instrument of Figure 6.4 drawn without the shaft with the addition of an Alternating Memory (AM) mechanism. The figure zooms in on the advancing action above the brace of Figure 6.4. For explanation: see text.

control-point 1 is moved to control-point 2, the position of control-point 2 is moved to control-point 3 etc. (Figure 6.4c). Next, the leader-element is steered to another direction (Figure 6.4d), after which another advancing step is made (Figure 6.4e-f). During FTL-propagation, the steering and advancing actions are repeated multiple times.

### 6.2.3 THE ALTERNATING MEMORY MECHANISM

For updating the positions of the control-points during the advancing action, a mechanism needs to be added at the controller-side of the instrument in Figure 6.4. This mechanism must interact with the control-points so that their positions are moved to the adjacent control-points as the instrument moves forward. A mechanism with this functionality is shown in Figure 6.5, and will be referred to as the Alternating Memory (AM) mechanism. The basic components of the AM-mechanism are a memory-bank and a set of memory elements. The memory-bank encloses the memory-elements and can slide vertically over a distance of one segment. The memory elements can slide individually from left to right within the memory-bank. They contain wedge-shaped grooves enclosing the control-points that control the segments. These wedge-shape grooves enable the memory-elements to copy the position of a control-point.

The configuration of the memory elements and the control-points can be memorized by locking them in position. This locking occurs in an alternating fashion, i.e. when the control-points are locked, the memory elements are released, and vice versa. A locked component is visualized in Figure 6.5 by a cross inside the component, e.g. in the left part of Figure 6.5 the control-points are locked while the memory elements are released.

Looking at the advancing action for FTL-propagation, highlighted by the brace in Figure 6.4, the functioning of the AM-mechanism is based on the following four steps (see arrows in Figure 6.5).

- *The positions of the memory-elements are locked, after which the control-points are released.*
- *The instrument with the control-points is slid one step upwards while the memory-bank holds its position. The wedge-shaped grooves in the memory elements force the control-points to align with the locked memory elements.*
- *The positions of the control-points are locked, after which the memory-elements are released.*
- *The memory-bank is slid one step upwards to its initial position relative to the instrument. The wedge-shaped grooves of the memory-elements now force the memory elements to align with the locked control-points, reading out the new position of the control-points.*

The mechanism thus alternates between copying, memorizing and shifting path information by copying and sliding the position of the control-points.

### 6.3 PROOF OF CONCEPT PROTOTYPE: MEMOSLIDE

To test the AM-mechanism of Figure 6.5, the mechanism was translated into a Proof-of-Concept (PoC) prototype called *MemoSlide* (Figure 6.6). The *MemoSlide* was designed to control a shaft with  $N=11$  segments, i.e. one leader-element and ten follower-elements. The PoC prototype does not yet include a flexible shaft; its design was purely focused on testing the novel concept of the AM-mechanism.

The control-points of the mechanism that were previously unsupported, are now supported to leader and follower-elements as shown in Figure 6.6a. In the *MemoSlide*, the motion of these elements is constrained so that they can only translate sideways. Above the memory elements and follower-elements, two locking-bars were added that lock the memory- and follower-elements. Two sets of cams, a left set and a right set (Figure 6.6 c-e), regulate the locking motion as well as the sliding motion of the memory-bank. Operating the mechanism is realized by a steering wheel and crank. With the steering wheel, the user can control the steering action of the leader-element. Rotating the crank drives the cam mechanism that sets the advancing action for FTL-propagation in motion.

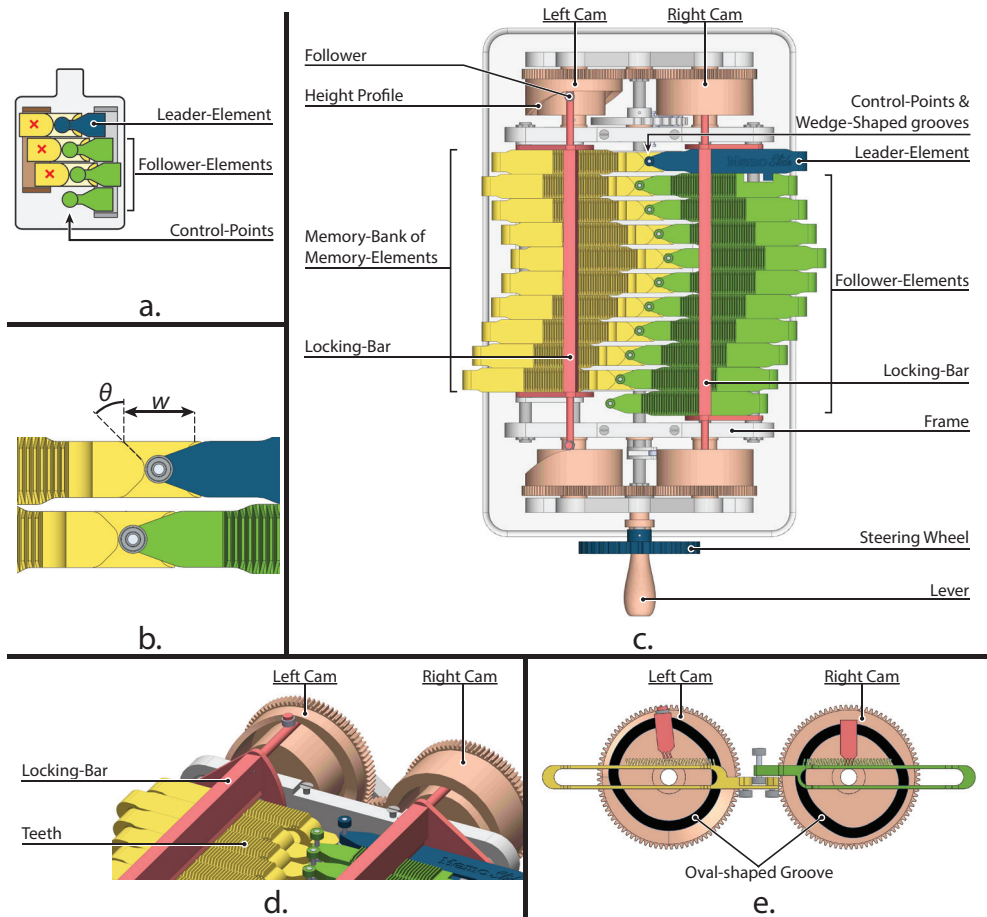


Figure 6.6: The proof of concept prototype MemoSlide. (a) Schematic representation with the control-point now supported by the leader & follower-elements. (b) Close-up of the control-points and wedge-shaped grooves in the MemoSlide. (c) Top view of the MemoSlide showing all its components. The steering wheel is used for the steering action of Figure 6.4, moving the leader-element to the left or right. The crank is used for the advancing action of Figure 6.4, rotating the cams that regulate the locking of the elements and the sliding motion of the memory-bank. The sliding motion of the memory-bank is initiated by the height profile on the circumference of the left cam pushes the left locking bar downward. (d) 3D View of the cam driven discrete locking system. (e) The oval-shaped grooves in the cams regulate the lowering and raising of the locking bars, respectively resulting in the locking and releasing of the corresponding elements.

A detailed view of the locking-bars and the cams is given in Figure 6.6d-e. The bottom part of the two locking-bars is fitted with a row of three teeth, and each of the memory- and follower-elements are fitted with an array of similar teeth. Controlled by the cams, the locking bars are raised or dropped, interlocking their teeth with those of the memory- or follower-elements, respectively resulting in releasing and locking of the corresponding elements.

The cams regulate the four steps of the AM-mechanism, represented by the up/down motion of the locking bars and the forward/backward sliding motion of the memory-bank. Locking and releasing the locking bars is realized by connecting the bars to horizontal rods that slide in oval-shaped grooves within the cams (Figure 6.6e). Rotating the two cams results in the required up/down motion of the bars, in a way that the two bars are out of phase, so that a simultaneous rotation of both cams will result in the alternative locking and releasing of the follower and memory-elements as shown in Steps 1 and 3 of Figure 6.5.

The range and discrete step-size of the steering action, and the range of motion of the entire shaft, are determined by the dimensions of the wedge-shaped groove, the distance between the teeth and the number of teeth, respectively. The dimensions of the wedge-shaped groove are based on its width ( $w$ ) and angle ( $\theta$ ) (Figure 6.6b). The maximum travel distance of a cable was calculated to be 4 mm. To accommodate left and right steering, the width of the wedge-shaped grooves need to be at least twice as long and was set at 8 mm. Various wedge-angles are possible, for this design an angle of  $45^\circ$  was chosen based on initial tests to find a good balance between the sliding distance and operation force. In future designs, this angle can be further optimized. The distance between the teeth was chosen to be 1 mm. Using equation (6.2) each interval translates to a  $25^\circ$  bend of a shaft segment. The number of teeth was set on 31, which means the shaft would be able to bend  $375^\circ$  in both directions starting from its initial straight position.

The *MemoSlide* was fabricated and is shown in Figure 6.7. The device has a footprint of 129 mm by 143 mm, about the size of an A5 piece of paper, and a height of 102 mm. The control-points of the mechanism were embodied by a set of ball-bearings attached to the bottom of the follower-elements to realize a smooth interaction with the wedge-shaped grooves of the memory-elements (Figure 6.7a). Another set of ball-bearings, attached to the top of the follower-elements, run through slots in a bronze plate shown at the top of the mechanism in Figure 6.7b. This plate was added to smoothly guide the sideways motion of the elements. Most components were made out of aluminum, whereas bronze bushings was used for parts involved in sliding contact. The axes that support the cams and steering mechanism were made of stainless steel due to its strength and low friction coefficient with the bronze. The result is that *MemoSlide* operates smoothly with a very low required operating force on the crank.

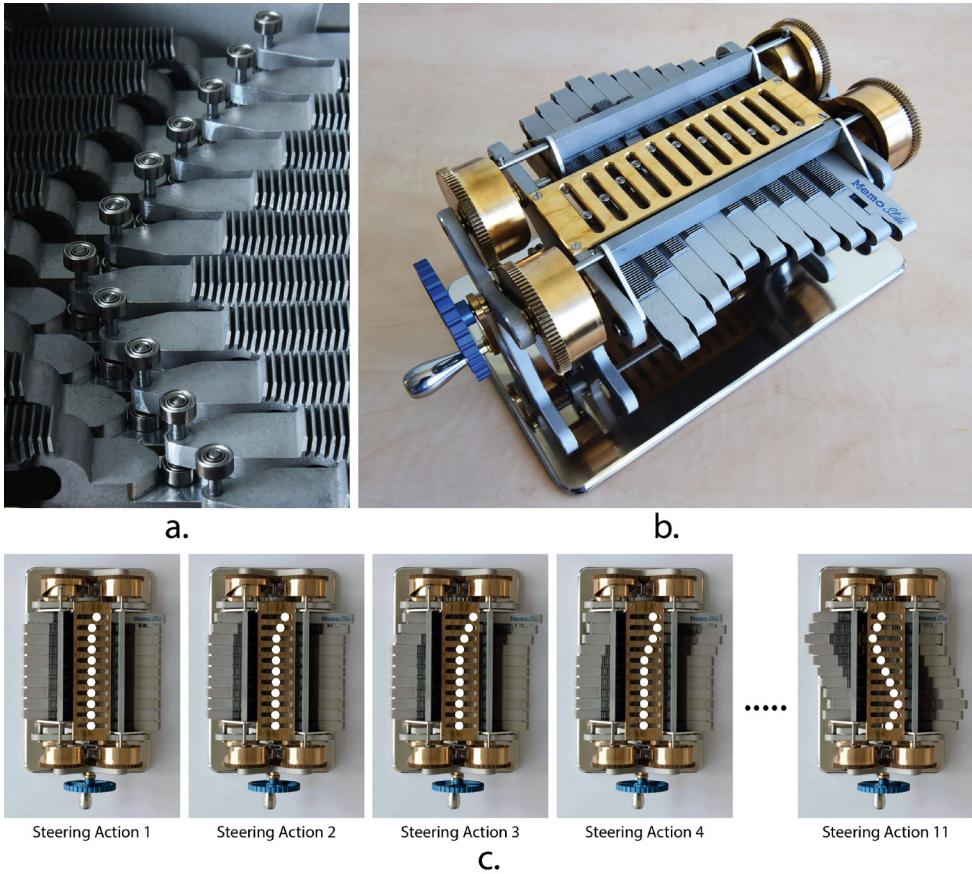


Figure 6.7: Finished MemoSlide. (a) Close-up of the interaction between the memory-elements (left) and the follower-elements (right), each follower-element containing two ball-bearings, one at the top and one at the bottom, the bottom one interacting with the wedge-shaped grooves. (b) Photo of the entire prototype with the top ball-bearings of the follower-elements guided through slots in a bronze plate and displaying – as an example – a triangular path. (c) Top view of the MemoSlide showing a triangular path propagating through the mechanism.

## 6.4 FUNCTIONAL EVALUATION

The MemoSlide was developed to prove the concept of the AM-mechanism. As an example, the serie of photos in Figure 6.7c shows a triangular path that is propagated through the MemoSlide. Initially, all follower control-points (denoted by white dots in Figure 6.7c) are aligned at the center of the prototype, which relates to a straight shape of an instrument shaft. The motion starts with a steering action to the right and continues with a series of other steering actions, creating a triangular path that is transported along the adjacent segments by alternately rotating the steering wheel and rotating the crank.

During the triangular path of Figure 6.7c, the torque on the crank was measured to be between 0.875 N/mm and 3.5 N/mm. The peak torque was measured during the sliding motion of the memory banks, while the lowest amount of torque was measured when only the cams were moving and can thus be credited to the friction between the bronze slide bushings of the cam system.

The *MemoSlide* mechanism works in two directions. By turning the crank clockwise, the positions of the control-points propagate downward in Figure 6.7c and by turning the crank counter-clockwise the positions of the control-points propagate upward in Figure 6.7c. This reversibility allows for the re-shaping of the shaft by retracting the shaft up to the point where a change of shape is desired. More importantly, it ensures that the instrument's shaft can be retracted along the same path over which it was propagated.

## 6.5 DISCUSSION

### 6.5.1 THE RANGE OF THE MEMOSLIDE

The elegance of the AM-mechanism in the *MemoSlide* is that it can create a large number of different paths with only steering and advancing actions as input. The number of paths can be calculated by:

$$\text{number of paths} = sr^N, \quad (6.3)$$

where  $sr$  is the steering range, i.e. the number of discrete positions one can choose from during a steering action, and  $N$  is the number of elements. The *MemoSlide* includes eleven elements ( $N = 11$ ) and its steering range is equal to nine discrete steering positions (four positions of the leader-element to the left, four positions of the leader-element to the right, and one position in the middle relative to the adjacent follower-element) ( $sr = 9$ ). As a result, *MemoSlide* has the potential to create a total of 911 different paths. In its current design, however, the array of 31 teeth on the elements is not enough to support all these paths. The next paragraph will discuss how the design choices of the AM-mechanism affect the functioning and range of motion for a cable-ring actuated shaft.

### 6.5.2 DESIGN CHOICES

The design choices that mainly affect the functioning of the mechanism are the size of the teeth, the play between interlocked teeth, and the angle of the wedge-shape grooves.

The size of the teeth determines the level of discretization of the steering action. Smaller teeth will increase the level of discretization but are weaker and more challenging to fabricate. The teeth were fabricated out of high strength aluminum (Al7075) using electric discharge machining that, as opposed to other machining techniques as milling or sawing, does not create any reaction force on the material preventing the teeth to deform during machining. The interval of the teeth was set on 1 mm, and the teeth were given a thickness of 0.45 mm while the gap between the teeth was set at 0.55 mm. As a result, there is a maximum of 0.1 mm play between interlocked teeth ensuring them to interlock smoothly, yet influencing the precision of the mechanism itself. The play between the teeth could be eliminated by giving the teeth a triangular shape instead of their current rectangular shape.

The overall dimensions of the AM-mechanism are mainly dictated by the width of the memory-elements, which is determined by the angle ( $\theta$ ) and width ( $w$ ) of the wedge-shaped grooves (Figure 6.6b). A larger wedge-angle would allow for thinner elements and thus a more compact AM-mechanism design, yet also increases the operating force of the AM mechanism. As the AM-mechanism is placed outside the patient, its size is less crucial, and smaller wedge-angles were therefore chosen for a smoother functioning of the mechanism.

### 6.5.3 THE MEMOSLIDE AS A SURGICAL INSTRUMENT

The schematic representation of Figure 6.8a illustrates how the MemoSlide's AM-mechanism can be integrated into a functional surgical instrument. The instrument is visualized by a cart, which holds the AM-mechanism and flexible shaft and runs over a gear rack that is fixed to the ground (Figure 6.8a). The leader and follower-elements of the AM-mechanism will be connected to the segments of the flexible shaft by cables, as illustrated in Figure 6.4 (cables not drawn in Figure 6.8a). A joystick is connected to the leader-element and used to steer the leader-element (top Figure 6.8a).

The movements of the AM-mechanism can be synchronized with the forward and backward movement of the instrument by including two sets of wheels on the cart. One set supports the leader & follower-elements and the shaft, and is connected to the corresponding locking mechanism. The other set supports the memory-bank and is also connected to the corresponding locking mechanism. In this way, the shaft can be moved forward or backward when the memory-bank is locked, corresponding to Step 2 in Figure 6.5. When the leader & follower-elements and thus the shape of the shaft is locked, the memory bank is free to slide back, corresponding to Step 4 in Figure 6.5.

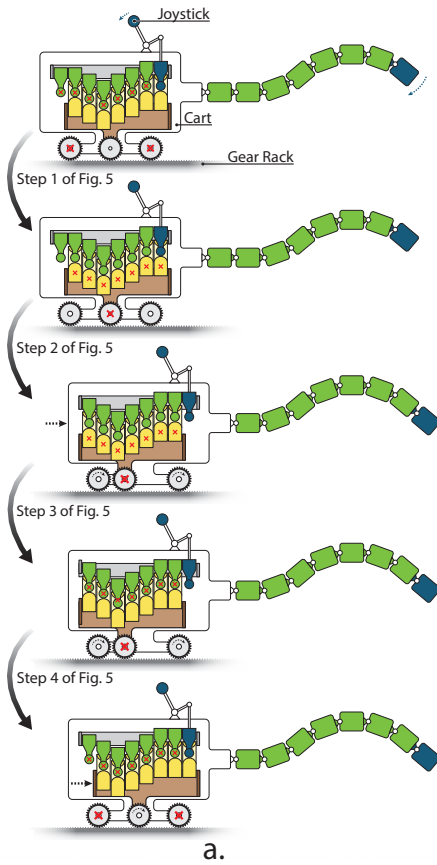


Figure 6.8: The MemoSlide as a surgical instrument. (a) Schematic representation of how the AM-mechanism can be integrated into an instrument. The AM-mechanism and shaft are placed on a cart, which runs over a gear-rack that is fixed to the ground. Cables connect the segments of the flexible shaft to the leader and follower elements as was illustrated in Figure 6.4 (cables not drawn). At the top, the leader segment is steered using a joystick. In the middle, the entire instrument is pushed one segment length forward whilst the memory-bank remains stationary to the ground (illustrated by the cross) and updates the shape of the shaft. At the bottom, the memory-bank slides back and the instrument regains its initial configuration. The transitions between the images represent steps 1 to 4 of Figure 6.5. (b) Artistic impression of an instrument capable of Follow-the-Leader propagation in 3D. Based on the MemoSlide, the instrument incorporates two 2D Alternating Memory (AM) mechanisms that separately control the movements in the vertical and horizontal plane. Steering the instrument is realized by a joystick, which connects to both AM mechanisms.



b.

During the advancing step of FTL-propagation as illustrated in Figure 6.4, the shaft is pushed one step forward during which its shape is transformed. This transformation can cause a temporary deviation from the path, especially when the step-size over which the shaft is moved forward or backward is large. In Figure 6.4, each step was set to be the length of one shaft segment. The forward step-size can, however, also be smaller, for example a fourth of the segment length. This will require that the cables of the shaft are not connected to every element of the AM-mechanism, but every fourth element. In that case four instead of one element embody the full steering range of a single shaft-segment.

An advantage is that the difference in position between adjacent elements will be smaller, resulting in a more fluent transition between steering steps. A drawback of this approach is the increasing number of elements in the AM-mechanism. The effect of the step-size of the advancing step on the path following accuracy will be investigated in future research.

Once integrated into a surgical instrument, the AM-mechanism will be subjected to loading caused by tension in the cables. Because antagonist cables are connected to the same element of the AM-mechanism as illustrated in Figure 6.4, an equal pre-tension in antagonist cables will balance out and therefore not cause any loading on the AM-mechanism. An unequal tension between antagonist cables caused by the weight and bending stiffness of the shaft, or external forces will cause loading of the AM-mechanism. When the leader & follower-elements are locked, this load is supported by the locking system and will not affect the functioning of the mechanism. The loading does come apparent during the sliding motion of the locked memory-bank (step 2 in Figure 6.5). At this point, the follower elements are momentarily unsupported and uneven tension between antagonist cables may cause them to shift. The range of this shift varies between zero and 4 mm, depending on the configuration of the mechanism, and the result is an undesired shape-change of the unlocked shaft. To prevent this undesired movement, there must be a force present that is higher than the difference in tension between the antagonist cables. The intrinsic friction on the cables and follower-elements might already be sufficient, e.g. the shaft of the MultiFlex of Figure 6.1a includes springs, yet remains in any bent position due to the intrinsic friction of the instrument. When the intrinsic friction is not enough, additional friction must be intentionally induced. Intentionally inducing friction will increase the operating force of the AM mechanism, making it only viable for small loads caused by light shafts with low bending stiffness, or low external forces. The AM mechanism therefore has the limitation that it cannot handle high loads during FTL-propagation without intentionally induced friction, which is a topic for future research. Nevertheless, once the shaft is at rest, its shape is locked and external loading is possible. Moreover, at this point, the leader segment of the shaft is free to be steered for changing the view of the endoscope or for manipulation purposes.

The schematic representation of Figure 6.8a still only functions in a two-dimensional plane, and the next step of this research will therefore be focused on developing an instrument capable of FTL-propagation in 3D space. An artistic impression of a 3D FTL-instrument is presented in Figure 6.8b. As the developed AM-mechanism can only control segments in a single plane, two separate AM-mechanisms will be incorporated into the design of this instrument. These two AM mechanisms will altogether control the 3D movements of the flexible shaft.

A strong benefit of constructing the 3D mechanism out of two 2D AM-mechanisms is that the control over the horizontal and vertical movement, as seen from an individual segment, is fully decoupled. The result is two relatively simple planar mechanisms that function completely independent from one another, i.e. an action in one mechanism does not affect the other. This decoupling allows for a design that is fully dedicated to a single function, allowing great freedom for design optimization and precise manufacturing.

Another advantage of using a set of two 2D AM-mechanisms is that a 2D mechanism allows easy implementation of a discrete locking system. Although limiting the motion of each DOFs to several discrete intervals, using discrete locking through teeth has an important advantage over using continuous locking through friction. With friction locking, small errors can occur in case of a mismatch between the memory-banks, i.e. one memory-bank not precisely copying the configuration of the other due to manufacturing inaccuracy. These small errors can accumulate as the copying process is being repeated, resulting in increasing deviations from the initial path and an unreliable system. As long as the manufacturing inaccuracy does not exceed the size of a discrete interval, with discrete locking, these small errors are automatically corrected as the memory-banks copy each other's discrete configuration exactly. For similar reasons, a few decades ago, the recording of video and sound switched from analog to digital as the latter proved to be much more resilient to the corruption of information.

## 6.6 CONCLUSION

In this paper, we introduced a new Alternating Memory mechanism for controlling Follow-the Leader (FTL) propagation of a flexible cable-driven shaft. This mechanism was successfully incorporated in a prototype called *MemoSlide*, including a discrete instead of a continuous locking mechanism, making it resilient against manufacturing inaccuracies or external disturbance forces. Tests have proven the mechanism to work well, being able to transfer any path initiated by the user along the body of the mechanism without error. The *MemoSlide* is, to our knowledge, the first fully mechanical control mechanism suited for FTL-propagation. Compared to a motor-driven instrument, it does not require sensors and actuators, overall resulting in a less complex and mechanically more robust control system. The *MemoSlide* sets the basis for a new direction in the development of snake-like surgical instrumentation, with a novel mechanical approach that opens new design pathways for minimally invasive surgery through compact anatomic environments.

## 6.7 REFERENCES

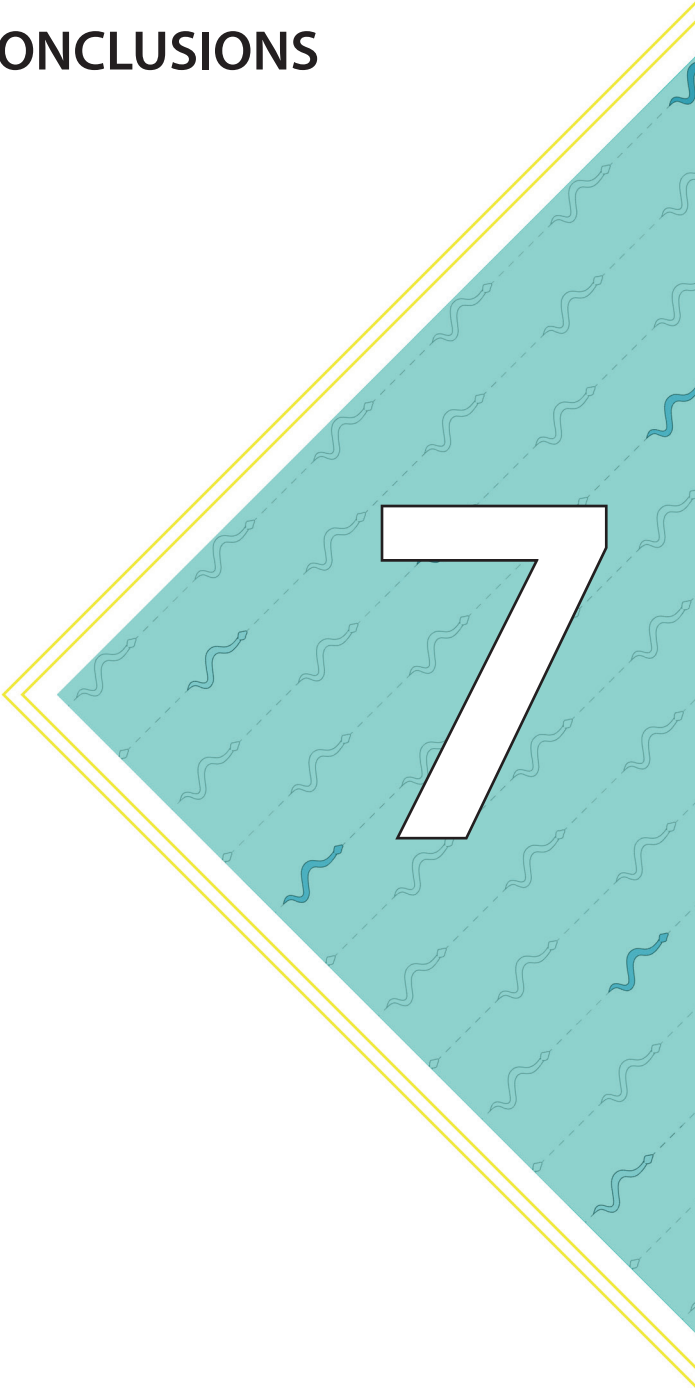
1. Roumm AR, Pizzi L, Goldfarb NI, Cohn H. Minimally invasive: minimally reimbursed? An examination of six laparoscopic surgical procedures. *Surg Innov.* 2005;12(3):261-87.
2. Targarona EM, Balague C, Knook MM, Trias M. Laparoscopic surgery and surgical infection. *The British journal of surgery.* 2000;87(5):536-44.
3. Dedemadi G, Sgourakis G, Karaliotas C, Christofides T, Kouraklis G, Karaliotas C. Comparison of laparoscopic and open tension-free repair of recurrent inguinal hernias: a prospective randomized study. *Surg Endosc.* 2006;20(7):1099-104.
4. Noguera Aguilar JF, Moreno Sanz C, Cuadrado García A, Olea Martínez-Mediero JM, Morales Soriano R, Vicens Arbona JC, et al. NOTES. Historia y situación actual de la cirugía endoscópica por orificios naturales en nuestro país. *Cirugía Española.* 2010;88(4):222-7.
5. Shrestha BM. Natural orifice transluminal endoscopic surgery (NOTES): an emerging technique in surgery. *JNMA; journal of the Nepal Medical Association.* 2011;51(184):209-12.
6. Fan C, Jelinek F, Dodou D, Breedveld P. Control devices and steering strategies in pathway surgery. *J Surg Res.* 2015;193(2):543-53.
7. Arkenbout E, Henselmans PJ, Jelínek F, Breedveld P. A state of the art review and categorization of multi-branched instruments for NOTES and SILS. *Surg Endosc.* 2015;29(6):1281-96.
8. Webster Iii RJ, Romano JM, Cowan NJ. Mechanics of pre-curved-tube continuum robots. *IEEE Transactions on Robotics.* 2009;25(1):67-78.
9. Gilbert HB, Rucker DC, Webster RJ, III. Concentric tube robots: The state of the art and future directions. *Springer Tracts in Advanced Robotics* 2016. p. 253-69.
10. Wu K, Wu L, Ren H, editors. Motion planning of continuum tubular robots based on centerlines extracted from statistical atlas. *IEEE International Conference on Intelligent Robots and Systems;* 2015.
11. Dupont PE, Lock J, Itkowitz B, Butler E. Design and Control of Concentric-Tube Robots. *Robotics, IEEE Transactions on.* 2010;26(2):209-25.
12. Gilbert HB, Webster RJ, editors. Can concentric tube robots Follow-the-Leader? *Proceedings - IEEE International Conference on Robotics and Automation;* 2013.
13. Gilbert HB, Neimat J, Webster RJ. Concentric Tube Robots as Steerable Needles: Achieving Follow-the-Leader Deployment. *IEEE Transactions on Robotics.* 2015;31(2):246-58.
14. Wayne JD. Quo Vadis: Another new colonoscope. *American Journal of Gastroenterology.* 2007;102(2):267-8.
15. Shang J, Noonan DP, Payne C, Clark J, Sodergren MH, Darzi A, et al., editors. An articulated universal joint based flexible access robot for minimally invasive surgery. *Robotics and Automation (ICRA), 2011 IEEE International Conference on;* 2011 9-13 May 2011.
16. Tappe S, Pohlmann J, Kotlarski J, Ortmaier T, editors. Towards a follow-the-leader control for a binary actuated hyper-redundant manipulator. *IEEE International Conference on Intelligent Robots and Systems;* 2015.
17. Tappe S, Kotlarski J, Ortmaier T, Dorbaum M, Mertens A, Ponick B, editors. The kinematic synthesis of a spatial, hyper-redundant system based on binary electromagnetic actuators. *ICARA 2015 - Proceedings of the 2015 6th International Conference on Automation, Robotics and Applications;* 2015.
18. Son J, Cho CN, Kim KG, Chang TY, Jung H, Kim SC, et al. A novel semi-automatic snake

- robot for natural orifice transluminal endoscopic surgery: preclinical tests in animal and human cadaver models (with video). *Surg Endosc.* 2015;29(6):1643-7.
19. Nguyen TD, Burgner-Kahrs J, editors. A tendon-driven continuum robot with extensible sections. *Intelligent Robots and Systems (IROS), 2015 IEEE/RSJ International Conference on; 2015 Sept. 28 2015-Oct. 2 2015.*
  20. Neumann M, Burgner-Kahrs J, editors. Considerations for follow-the-leader motion of extensible tendon-driven continuum robots. *2016 IEEE International Conference on Robotics and Automation (ICRA); 2016 16-21 May 2016.*
  21. Palmer D, Cobos-Guzman S, Axinte D. Real-time method for tip following navigation of continuum snake arm robots. *Robot Auton Syst.* 2014;62(10):1478-85.
  22. Prendergast JM, Rentschler ME. Towards autonomous motion control in minimally invasive robotic surgery. *Expert Review of Medical Devices.* 2016;13(8):741-8.
  23. Motor M. [www.maxonmotor.nl/maxon/view/catalog/](http://www.maxonmotor.nl/maxon/view/catalog/) 2017 [
  24. Kang B, Kojcev R, Sinibaldi E. The first interlaced continuum robot, devised to intrinsically Follow-the-Leader. *PLoS ONE.* 2016;11(2).
  25. Ota T, Degani A, Schwartzman D, Zubiato B, McGarvey J, Choset H, et al. A Highly Articulated Robotic Surgical System for Minimally Invasive Surgery. *The Annals of Thoracic Surgery.* 2009;87(4):1253-6.
  26. Rivera-Serrano CM, Johnson P, Zubiato B, Kuenzler R, Choset H, Zenati M, et al. A transoral highly flexible robot. *The Laryngoscope.* 2012;122(5):1067-71.
  27. Breedveld P, Sheltes JS, Blom EM, Verheij JEI. A new, easily miniaturized steerable endoscope. *Engineering in Medicine and Biology Magazine, IEEE.* 2005;24(6):40-7.
  28. Fan C, Dodou D, Breedveld P. Review of manual control methods for handheld maneuverable instruments. *Minimally Invasive Therapy and Allied Technologies.* 2013;22(3):127-35.
  29. Madhani AJ, Salisbury JK. Articulated surgical instrument for performing minimally invasive surgery with enhanced dexterity and sensitivity. *Google Patents; 1997.*
  30. Gerboni G, Henselmans PW, Arkenbout EA, van Furth WR, Breedveld P. HelixFlex: bioinspired maneuverable instrument for skull base surgery. *Bioinspir Biomim.* 2015;10(6):066013.
  31. Woodley BR, Oen J, Brown A, Julian C, Laby KP, Keller W, et al. System for managing bowden cables in articulating instruments. *Google Patents; 2009.*





# DISCUSSION & CONCLUSIONS



## 7.1 MAIN FINDINGS OF THIS STUDY

The goal of this research was to explore new mechanically-controlled Follow-The-Leader solutions suited for surgical purposes. This work was divided into two parts, Part 1 focusing on the construction of cable-driven hyper-redundant structures (Chapters 2-3) and Part 2 on mechanical control strategies of such structures to perform Follow-The-Leader motion (Chapters 4-6). In-line with the mechanical nature of this thesis, in every chapter new mechanical concepts were described, resulting in a physical prototype to test the proposed concepts and provide tangible hands-on experience.

Part 1 started with Chapter 2 that presented an investigation into the combined use of multi-directional cable-routes for the actuation of a compliant structure. The resulting design concept involves a manual actuation strategy that allows the user to control the position and angle of the tip by using a mechanical 4 DOFs joystick. The concept was successfully embodied in a prototype called the HelixFlex, and shows great potential for maneuvering the end-effector of a steerable instrument. The prototype was built using subtractive manufacturing techniques, which did require the design to be broken down into a chain of simple-to-fabricate parts and led to a considerable assembly time of several weeks.

Chapter 3 investigated the production of hyper-redundant shafts, with a special focus on decreasing the required time for fabrication and assembly. Know-how from fabricating the handle of the HelixFlex (Chapter 2) inspired the development of a 10 DOFs steerable instrument called the HelicoFlex. Apart from its cables, the hyper-redundant shaft of the HelicoFlex was additively manufactured from a single part without a need for support material. Moreover, the shaft included a friction-based locking system for easy fixation of the cables. This significantly reduced the assembly time to approximately four hours.

Part 2 started with Chapter 4 that introduced the concept for a mechanically-controlled FTL-instrument suitable for surgery. The concept involves a mechanism that captures the shape of a fixed 3D physical track and copies this shape to a cable-driven hyper-redundant shaft. The concept was embodied in the MemoFlex I prototype, which shows the feasibility of mechanical controlled FTL-motion. Mechanically capturing the shape of a 3D-track did, however, prove challenging, especially with the rigid-linked construction of the exoskeleton in the master. Moreover, the use of a 3D track means that the antagonistic cables need to be coupled to each other in the master, and cannot be individually controlled.

Chapter 5 presented a revised concept for a mechanical controlled FTL-instrument wherein the 3D track was broken up into four fixed 2D-tracks. As a result, the control over

the antagonistic cables could be separated. The concept was successfully incorporated in the MemoFlex II prototype, which also includes the compliant 3D-printed shaft design of Chapter 3. The MemoFlex II outperforms the MemoFlex I in the accuracy with which it can follow a predetermined path and shows more fluent motion.

In Chapter 6, the possibility of on-demand mechanically adjustable tracks was explored. This led to a novel concept that manages to capture the control algorithm for FTL-motion into a mechanism. The concept was implemented in the *MemoSlide* prototype; a mechanical memory-bank capable of creating a discretely adjustable track on-demand. The *MemoSlide* thus makes mechanical on-demand controlled FTL-motion feasible.

## 7.2 LIMITATIONS OF THIS STUDY

Although clinical purposes are envisioned, no actual clinical tests were performed. The main reason is that the developed platform technologies are not yet suitable for actual procedures. Moreover, the additively manufactured parts were constructed out of a resin that is toxic to humans and can thus not be used in a clinical setting. Biocompatible materials are available (E-Shell 600 biocompatible resin) and have been tried. These materials are more viscous than their non-biocompatible alternatives and clog up the grooves that guide the cables. Printable biomaterials are, however, still under development, and it can be expected that more suitable materials will become available in the coming years [1].

Before one of the mechanical solutions presented in the thesis can be useful for FTL-motion in a surgical setting, there is one major problem that still has to be addressed, which is the stiffness of the flexible shaft. Once in position, the FTL-instrument must be able to supply a stable base from which the instruments can extend and operate. The FTL-instrument must therefore be able to withstand the forces that arise during surgery. The applied forces can range from 0.1-0.8N for the resection of soft brain tumors, up to 16N for typical grasping and pulling tasks, and some references even report forces for cutting tissue ranging from 13-35N, depending on the organ [2-6]. In their current forms, the shafts of the MemoFlex I and II are not stiff enough to withstand such forces.

Stiffness can be interpreted as a joint's resistance to move due to external loading. One way of attaining a higher resistance is by increasing the actuation forces on the joints, which for a cable-driven solution means increasing the cable-tensions. This method works well for fully actuated constructions wherein each joint is actuated via an individual set of cables. However, when the shaft is based on a compliant structure, which is essentially a

continuous link of an infinite number of joints and therefore inherently under-actuated, this method will be less effective [7]. In this case, a solution can be found in an additional stiffening mechanism that can be switched on once the FTL-instrument is in position. A study of L. Blanc et al. provides a comprehensive overview of the possible solutions for enhancing the stiffness of a flexible shaft [3]. One of the presented solutions is called wire jamming and revolves around the use of a ring of cables [8]. Wire jamming is especially suited for a cable-driven shaft, as such a shaft already contains the required ring of cables. Moreover, it would be interesting to see if the multi-directional cable-configuration of Chapter 2 could be integrated into such a system. The helical direction of the cables could add a directional stiffness component, increasing the flexural and torsional stiffness.

### 7.3 MECHANICAL VERSUS MECHATRONIC PATH-FOLLOWING

This work started with the following question: can a mechanism control the high number of segments required to perform FTL-motion? The current answer to that question is that, up to a certain level of accuracy, mechanically-controlled FTL-motion along predetermined paths is possible. Moreover, mechanical on-demand control for FTL-motion seems feasible. As mechanically-controlled FTL-motion seems possible, an interesting follow-up question is whether mechanical control is preferable above mechatronic control.

Figure 7.1 shows the hypothetical mechatronic solution as was introduced in Chapter 1. This mechatronic solution has a couple advantages over a mechanical solution. Firstly, it can control each individual DOFs in its hyper-redundant shaft separately. Given a proper controller, this makes the mechatronic setup in theory more precise, being able to control each segment individually with an ability to fine-tune the overall movement. Secondly, separate control of each DOFs also means the shape of the shaft can be changed at any given moment. This makes the mechatronic solution a more versatile than a mechanical solution, which cannot deviate from the path it was given. Thirdly, as the instrument is not mechanically coupled to the control-side, the joystick and controller (surgeon console) can be positioned regardless of the position of the instrument, allowing a more ergonomic position for the surgeon and potentially enhancing the user experience.

It should be noted that the Flex System (Figure 1.9, also known as the HARP or CardioARM), currently the only commercially available FTL-system and discussed in Chapters 4, 5 and 6, is a mechatronic FTL-instrument with a significantly different construction as compared to the hypothetical setup of Figure 7.1. Instead of including one actuator for every individual DOFs in its shaft, the FTL-motion is based on a mechanism of two concentric shafts with

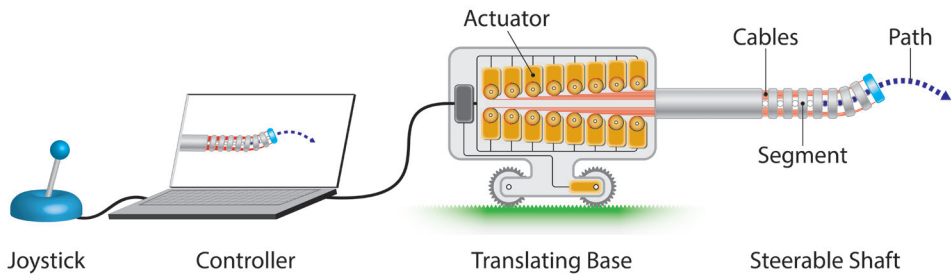


Figure 7.1: Hypothetical system providing mechatronic control over a cable-driven segmented shaft for performing follow-the-leader motion.

variable stiffness (for a more detailed description, see Section 6.2). The control over this mechanism is, however, realized via a mechatronic system. Although clear specifications about the precision of the Flex System's movements have not been found in literature, it can be stated that because the Flex System cannot separately control each individual DOFs in its shaft, it will not be able to deliver the potentially higher precision and versatility that the mechatronic system of Figure 7.1 has to offer. The added value of its mechatronic control strategy thus mainly revolves around an enhanced user-experience.

A mechatronic solution will also come with some drawbacks. For one, as already discussed in Section 1.6, surgical robotics tend to be relatively expensive compared to non-robotic alternatives, and attaining a sufficient level of reliability can be challenging. Another downside of using mechatronic components is that they can typically not withstand the temperatures (minimally 121°C) and moist conditions of the autoclaving sterilization process [9]. As a result, a mechatronic solution dictates that the sterile instruments can be decoupled from the non-sterile mechatronic components. Moreover, it requires a sterile barrier to be created between the non-sterile mechatronic components and the sterile instruments [10]. A mechatronic solution can thus increase the challenges for achieving a sterile working environment.

While the mechanical decoupling between the mechatronic control strategy and instrument may enhance the user-experience from an ergonomic point of view, it also decouples the user from the forces at the instrument, meaning the user will experience no haptic feedback [11]. In a mechanically-controlled cable-driven solution, the operator is directly coupled to the instrument via the cables. Although the resulting mechanical haptic feedback will be limited due to friction, it will be present to a certain extend. Regaining haptic feedback in a mechatronic system involves the use of additional mechatronic components. As such a system allows for the effects of friction to be filtered,

it can potentially deliver a higher quality of feedback compared to a mechanical solution, yet the additional components it requires will also further increase costs and challenge the system's overall reliability.

The answer to the question of whether mechanical control is preferable above mechatronic control will depend on the level of precision and versatility that is demanded by the application. If the mechanical solution is not precise or versatile enough, a mechatronic solution will be the preferred choice. Yet, if mechanical control along a predetermined path is sufficient for performing the task at hand, it is questionable whether the additional precision, versatility, and user-experience of the mechatronic system adds any significant clinical value to justify the additional costs.

## 7.4 CLINICAL IMPLEMENTATION

Figure 7.2 presents a hypothetical clinical setup that is based on the techniques presented throughout this thesis. The setup consists of a supporting base and an FTL-instrument for path-following containing internal lumens equipped with a flexible endoscope for vision, an optic fiber for illumination, tubes for irrigation and suction, and two flexible instruments for tissue interaction. The endoscope and instruments are given additional maneuverability, for example via a steerable segment based on the multi-directional cable-configuration of Chapter 2 or by using mechanical solutions used in steerable catheters [12]. All the DOFs of the setup are manually actuated. The optic fiber and tubes are controlled by simply sliding them forward or backward, whereas the endoscope and instruments are controlled via a joystick, similar to the one used in the HelixFlex (Chapter 2). The joysticks could include a locking mechanism to fix the position of the endoscope and instruments in position. The joystick of the instruments could include a scissor-like handle for actuating the functionality of the end-effector, e.g. to open and close the grasper.

The FTL-instrument (yellow in the figure) could involve one of the mechanisms for FTL-motion presented in Chapters 4, 5 and 6. Based on the level of control over the path that is required, three different setups could be used. In the first setup, the tracks are fixed, and the surgeon is presented with a range of generic tracks to choose from. In the second setup, the tracks are fixed and patient-specific, based on for example MRI or CT imaging. In the third setup, the tracks are adjustable and the path can be chosen and adjusted during the surgical procedure.

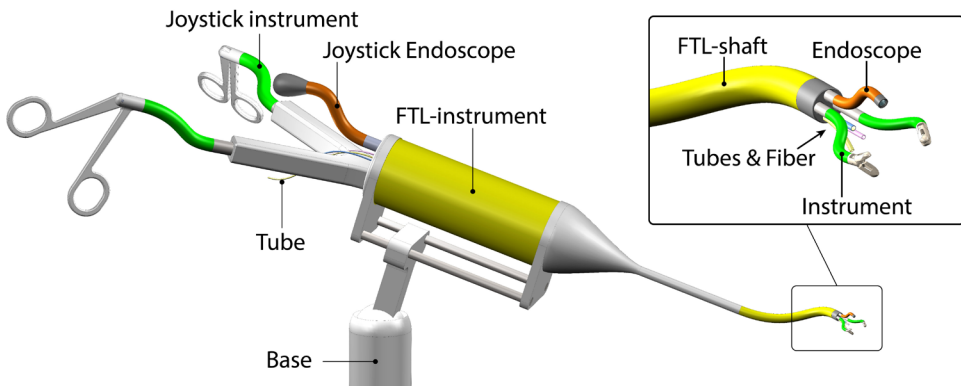


Figure 7.2: Hypothetical setup consisting of a supporting base, follow-the-leader instrument for path-following, an endoscope for vision, an optic fibre for illumination, two instruments for tissue interaction, and tubes for irrigation and suction.

Currently, the FTL-shaft used in the MemoFlex II (Chapter 5) has an outer diameter of  $\text{\O}8$  mm and four lumens of 1,75 mm. These lumens will be sufficient to fit a small flexible forceps, tubes and fiber optics, see Figure 3.8. Flexible endoscopes that fit these lumens are available, yet for better image quality, a 2-3 mm lumens would be better. Adding steerability to the instrument arms will also demand a larger lumen. Larger lumens can be achieved by simply increasing the entire diameter of the shaft, but might also be attainable by re-designing the shaft and including variable lumen sizes.

A remaining challenge concerns the sterility of the setup. Flexible and steerable instruments are difficult to sterilize for re-use [9, 13, 14]. The main reason is that these instruments have to be fitted with a flexible sealing to keep organic material away from the internal mechanism and provide a smooth outside surface. Current flexible sealings can, however, not reliably withstand the autoclaving process. To avoid any challenges and risks of sterilization, the parts that enter the body can, therefore, best be made disposable.

For a cable-driven shaft to function as a disposable, it must be cheap. This means that its advanced structure should at the same time be simple to manufacture. A first important step in this direction was the development of the compliant shaft that could be printed from a single part, disregarding the cables (Chapter 3). A next logical step is to include the cables in the printing process using embedded printing. This could, for example, be achieved by positioning off-the-shelf cables in the 3D-printing machine while the shaft is being printed. Another solution could be to also print the cables themselves, something that is already being explored in the development of non-assembly 3D-printed hand prosthesis [15].

When the shaft is made disposable, the question becomes how it will be coupled to the control mechanism. One option is to make the entire instrument disposable. This requires the entire instrument to be printed, preferably from a single part similar to the HelicoFlex (Chapter 3). The HelixFlex (Chapter 2) and MemoFlex I (Chapter 4) share a similar control-mechanism as the HelicoFlex, giving them the potential of 3D-printing from a single part. Instruments based on the concepts of Chapters 2, 3 and 4 could therefore in theory function as fully-disposable devices.

The control-mechanisms of the MemoFlex II (Chapter 5) and MemoSlide (Chapter 6) include a large number of sliding parts. Although a fully printable version of such mechanisms might be attainable, in their current forms they are not suitable for additive manufacturing. Setups based on the MemoFlex II or MemoSlide mechanisms could function as reusable solutions, in which the control-mechanism is re-usable and the cable-driven shaft disposable. Such a setup will require a (de-)coupling mechanism between the non-sterile control-mechanism and the sterile shaft, similar to the ones used in the Da Vinci system, yet including far more cables. Such a mechanism poses two main design challenges. For one, to ensure that the sterile shaft does not get contaminated by the non-sterile control mechanism, the coupling should include a sterile barrier [10]. The second design challenge will be a mechanism that can simultaneously couple all individual cables, preferably in one intuitive motion.

## 7.5 MEDICAL AND INDUSTRIAL APPLICATIONS

Path-following has potentially many applications in the medical field. Essentially, any procedure in which a tortuous surgical path can extend the reach and/or reduce the invasiveness of the procedure could benefit from FTL-instrumentation. One of the most prominent applications is skull base surgery. Brain tumors, and malignant tumors in particular, can extend through the dense anatomical area of the skull base, making them particularly hard to reach [16, 17]. Moreover, since the human face contains a network of important nerves and muscles that for example regulate facial expressions, skull base surgery is often restricted to entry-points through natural orifices such as the roof of the mouth (transoral), the eye-socket (transorbital) or nose (transnasal). Successfully targeting areas at the skull base through dense anatomy using a natural orifice is particularly challenging, and would benefit from path-following techniques.

Path-following is not only beneficial for weaving through dense anatomical areas, but could also be useful for following relatively broad and defined lumens. An interesting

application could be phonosurgery on the larynx (voice box), for example for vocal cord reposting in to maintain or improve the quality of the voice [18]. Currently, open surgery procedures using the front of the neck as entry point are used. Next to leaving a visible scar on the neck, there is a risk of damage to the integrity of the laryngeal cartilage, muscles and connective tissue [19]. FTL-motion could allow for a transoral (through the mouth) approach to the larynx, significantly reducing the invasiveness of the intervention.

Applications wherein the available lumens already offer support and guidance for the instrument could nevertheless also benefit from FTL-instrumentation. A typical diagnostic intervention in the lungs is a transbronchial biopsy for diagnosing cancer [20]. In this procedure, a steerable endoscope (bronchoscope) is inserted through the mouth and guided towards the trachea. In the lungs, the bronchoscope continues further through the bronchi. As the bronchi branch out they become thinner and increasingly delicate. As a result, the bronchi cannot supply the support needed for the precise positioning of the biopsy needle, which is a reason why effective targeting smaller lesions (< 20 mm) remains challenging [21, 22]. FTL techniques could provide additional support and guidance of the bronchoscope, extending its reach in the lungs. Another typical application wherein the instrument does get support from the environment is colonoscopy. In this procedure, a steerable endoscope (colonoscope) is inserted through the anus to reach up into the colon. The colon is, however, thin-walled and very flexible and is easily pushed away by the colonoscope, which can result in painful cramps [23]. Moreover, advancing the scope is a difficult task that involves combinations of twisting and steering the shaft, and requires extensive training. An FTL-mechanism could provide additional guidance, which could reduce the discomfort for the patient and make advancing the scope easier.

Applications can also be found in the cardiac realm of surgery. Transcatheter Aortic Valve Replacement (TAVR) is a relatively new alternative to heart valve replacement using open-heart surgery [24]. In TAVR, a catheter is inserted in the femoral vein (in the groin) and guided via the vessels towards the heart. Once inside the heart, the catheter no longer has support from the vessel wall, and needs to be steered towards the aortic valve [12]. This is a very tricky operation as the heart itself is beating, blood is flowing and the catheter is difficult to visualize. FTL-motion could prove useful for guiding the motion of the catheter through this dynamic environment towards the aortic valve.

The emerging field of intraoperative Magnetic Resonance Imaging (iMRI), involving the use of MRI images that are made during the surgical procedure, could provide another interesting application [25]. In this way, the surgeon can use MRI images to locate critical anatomy that needs to be avoided or to determine whether a procedure has been successful. The iMRI approach can, for example, be useful for the removal of brain

tumors that are located at difficult positions and hard to distinguish from normal brain tissue. These involve cases such as the endonasal approach towards the skull base that would in themselves already benefit from the additional reach that FTL-instruments can offer [26]. A major challenge with iMRI is the fact that the strong magnetic field of the MRI machine does not allow for the presence of any ferromagnetic materials. This makes iMRI-compatible instrumentation challenging to build and does not allow electromechanical robotic solutions. Mechanical solutions such as a cable-driven resin 3D-printed shaft do not require any magnetic or electric components. Although building the cable-driven mechanisms in this thesis completely from non-ferromagnetic materials will be challenging, such setups are in theory possible. The presented mechanical control strategies could therefore be particularly interesting for iMRI.

Although the developed technology is intended for surgical purposes, the presented platform technologies could also be useful in industry, for example for the assembly, maintenance and diagnostics of complex machinery, such as photolithography systems for chip-manufacture or advanced 3D-printing machines. In those machines, the internal components are packed closely together. As a consequence, diagnosing a fault within the assembly may require the machine to be (partly) disassembled to gain access, a labor-intensive and costly process. As the internal architecture of such machines is well documented, generic pathways to reach internal components can be defined and programmed in a mechanically-controlled FTL mechanism. In this way, an FTL-instrument could navigate through internal assemblies for a quick visual inspection to pin-point the exact location of the problem. Added functionalities such as a suction tube, gripper or a small soldering iron might even be added to handle simple tasks. The cable-driven mechanisms that were presented in this thesis could in this way speed up the diagnosis and prevent unnecessary disassembly of complex machinery.

## 7

### 7.6 RECOMMENDATION FOR FUTURE RESEARCH

Following a multi-curved path with a serially segmented shaft will inevitably lead to discrepancies from the path, the reason being that the path is a continuous curve, whereas the shaft is discretely segmented. Consequently, as is the case with every discretization process, information will get lost due to the discretization from path to shaft. The enhanced steerability of multi-directional cable-configurations (Chapter 2) might improve the accuracy of mechanically-controlled path-following. A preliminary study showed that shafts containing multi-directional cable-configurations have the potential to follow paths more fluently while using fewer segments than

cable-configurations using only parallel-routed cables [27]. Multi-directional cable configurations hold the potential to increase the quality of path-following, yet require control over multiple cables layers.

Mechanically controlling multiple cable-layers could pose a challenge for the MemoFlex II and MemoSlide mechanisms (Chapters 5 and 6). This is because every cable-layer would require its own set of tracks. Although such a setup is not impossible, it does require a large number of additional components and will expand the overall complexity of control, especially if the tracks require fine-tuning. In this regard, the MemoFlex I mechanism seems better suited for including a multi-directional cable-configuration as the additional cable-layers could be implemented in the already existing control-mechanism. This would require a redesign of the control-mechanism to accommodate the additional helical cable routes - something that could be achieved by adopting the printable guiding structure as used in the handle of the HelixFlex (Chapter 2). The MemoFlex I would therefore not require many additional components or tracks to implement the multi-directional cable-configuration. Regardless of the exact implementation, combining multi-directional cable-layers with one of the control-mechanism of Chapters 4, 5 or 6 would be an interesting topic for future research.

Another interesting combination between the different mechanisms would be the combination of the MemoFlex II (Chapter 5) and the MemoSlide (Chapter 6). In its current form, the tracks of the MemoFlex II are fixed, which means the path cannot be changed during the motion. The MemoSlide mechanism makes it possible to create adjustable tracks on-demand. A logical step would be to integrate the MemoSlide mechanism into the MemoFlex II allowing the operator to steer the shaft on the go as was illustrated in Figure 6.8.

Additive manufacturing, and particularly embedded printing, should play a key role in future developments of cable-driven hyper-redundant surgical instruments. For one, although 3D-printing machines capable of embedded 3D-printing are still in development, such techniques hold the potential to manufacture complex surgical instruments that are sufficiently cheap to function as a disposable. Secondly, the additive manufacturing process allows for the production of new designs without any additional costs of investments. Moreover, single unique parts can be produced without any significant change in the production line. This versatility opens the door towards procedure-specific, or even patient specific, instrumentation. Essentially, the surgeon could be given the possibility of defining the construction of an instrument, for example specifying the size, numbers, and configuration of the lumens within the instrument. This would allow the surgeon to experiment with different setups, or to optimize the length or configuration of

an instrument to fit the needs of a specific patient. Thirdly, additive manufacturing would allow for instruments to be printed locally, closer to the end-user. This could revolutionize the manufacturing of surgical instruments and holds the potential of bypassing the current manufacturing and distribution chains that increase the costs of surgical instrumentation and stimulate an oligopolistic market. Moreover, it might even allow for the instruments to be produced inside the hospital itself, further facilitating the surgeon's involvement in the development of surgical instruments and stimulating innovation.

## 7.7 CONCLUSIONS

The field of surgery continuously strives to reduce the invasiveness while simultaneously extending the reach of its procedures. Mechanical snake-like instruments that can follow tortuous pathways seem like a logical next step in this pursuit. This thesis aimed to explore mechanical control techniques for achieving follow-the-leader motion (FTL) of cable-driven hyper-redundant structures.

The first part of the work was focused on the construction of cable-driven structures for surgical applications. This resulted in a new mechanical control strategy wherein a compliant structure was manually actuated via multi-directional cable-layers. Next, the complexity of manufacturing hyper-redundant cable-driven instruments was addressed. Non-assembly additive manufacturing techniques were explored for the fabrication of complex instruments from a single 3D-printed component. The resulting complex yet simple hyper-redundant shaft contains a clever friction-based cable fixation system that led to a strong reduction of the effort needed for fabrication and assembly.

The second part of the work focussed on mechanical control strategies for these cable-driven hyper-redundant structures for performing FTL-motion. The MemoFlex I prototype showed its capability of following tortuous paths through free space based on a 3D track. Although the performance of the prototype is not yet up to the standards for medical applications, it does showcase the possibility of a mechanically-controlled cable-driven mechanism performing FTL-motion. Moreover, the flexible nature of its control mechanism in combination with additive manufacturing techniques shows great potential for a fully disposable solution. Dividing the 3D track into four 2D tracks in the MemoFlex II allowed the control of the antagonistic cables to be decoupled from one another, giving room for further fine-tuning and compensating for play in the mechanism. This decoupling had a major impact on the accuracy of path-following. The fixed tracks of the MemoFlex I & II require the path to be determined before it can be followed. The

MemoSlide mechanism managed to capture the control algorithm for cable-driven FTL-motion into a mechanism. Through this mechanism, tracks can be made adjustable and on-demand mechanically-controlled path-following has become feasible.

To conclude, this thesis work showed the potential of mechanically controlling cable-driven hyper-redundant structures to perform path-following motion. Furthermore, it presented important first steps towards complex yet affordable snake-like instrumentation that can extend the reach, while simultaneously minimize the invasiveness of surgery.

## 7.8 REFERENCES

1. Tappa, K. and U. Jammalamadaka, Novel biomaterials used in medical 3D-printing techniques. *Journal of Functional Biomaterials*, 2018. 9(1).
2. Bekeny, J.R., et al., Forces Applied at the Skull Base during Transnasal Endoscopic Transsphenoidal Pituitary Tumor Excision. *J Neurol Surg B Skull Base*, 2013. 74(6): p. 337-41.
3. Blanc, L., A. Delchambre, and P. Lambert, Flexible Medical Devices: Review of Controllable Stiffness Solutions. *Actuators*, 2017. 6(3): p. 23.
4. Tortora, G., et al., A Miniature Robot for Retraction Tasks under Vision Assistance in Minimally Invasive Surgery. *Robotics*, 2014. 3(1): p. 70-82.
5. Trejos, A.L., et al., Force sensing in natural orifice transluminal endoscopic surgery. *Surgical Endoscopy*, 2011. 25(1): p. 186-192.
6. Valdastri, P., et al., A scalable platform for biomechanical studies of tissue cutting forces. *Measurement Science and Technology*, 2009. 20(4): p. 045801.
7. Jelínek, F., et al., Attaining high bending stiffness by full actuation in steerable minimally invasive surgical instruments. *Minimally Invasive Therapy & Allied Technologies*, 2015. 24(2): p. 77-85.
8. Loeve, A.J., et al., Endoscope shaft-rigidity control mechanism: "FORGUIDE". *IEEE Trans Biomed Eng*, 2012. 59(2): p. 542-51.
9. Miner, N., *Cleaning, Disinfection and Sterilization of Heat-Sensitive Endoscopes, Endoscopy*, S. Amornyotin, Editor. April 30th 2013, IntechOpen.
10. Velsink, F., *Sterile barriers: Exploring possible design directions for barriers between the sterile and the nonsterile part of a cable-driven surgical instrument [Master's thesis]*, Delft University of Technology, Delft, the Netherlands, 2017. Available from <https://repository.tudelft.nl>.
11. Enayati, N., E.D. Momi, and G. Ferrigno, Haptics in Robot-Assisted Surgery: Challenges and Benefits. *IEEE Reviews in Biomedical Engineering*, 2016. 9: p. 49-65.
12. Ali, A., et al., Catheter steering in interventional cardiology: Mechanical analysis and novel solution. *Proceedings of the Institution of Mechanical Engineers, Part H: Journal of Engineering in Medicine*, 2019. 233(12): p. 1207-1218.
13. Rutala, W.A. and D.J. Weber, *Guideline for Disinfection and Sterilization in Healthcare Facilities*, C.f.D.C.a. Prevention, Editor. 2008.

14. Sabnis, R.B., A. Bhattu, and M. Vijaykumar, Sterilization of endoscopic instruments. *Curr Opin Urol*, 2014. 24(2): p. 195-202.
15. Cuellar, J.S., et al., Ten guidelines for the design of non-assembly mechanisms: The case of 3D-printed prosthetic hands. *Proceedings of the Institution of Mechanical Engineers, Part H: Journal of Engineering in Medicine*, 2018. 232(9): p. 962-971.
16. Snyderman, C.H., et al., What are the limits of endoscopic sinus surgery?: the expanded endonasal approach to the skull base. *Keio J Med*, 2009. 58(3): p. 152-60.
17. Liu, J.K., et al., Surgical nuances for removal of olfactory groove meningiomas using the endoscopic endonasal transcribriform approach. *Neurosurg Focus*, 2011. 30(5): p. E3.
18. Ford, C.N., Advances and refinements in phonosurgery. *Laryngoscope*, 1999. 109(12): p. 1891-1900.
19. Simaan, N., et al., Design and Integration of a Telerobotic System for Minimally Invasive Surgery of the Throat. *Int J Rob Res*, 2009. 28(9): p. 1134-1153.
20. Harrow, E.M., et al., The utility of transbronchial needle aspiration in the staging of bronchogenic carcinoma. *American Journal of Respiratory and Critical Care Medicine*, 2000. 161(2 I): p. 601-607.
21. Swaney, P.J., et al., Tendons, Concentric Tubes, and a Bevel Tip: Three Steerable Robots in One Transoral Lung Access System. *IEEE International Conference on Robotics and Automation : ICRA : [proceedings]*. *IEEE International Conference on Robotics and Automation*, 2015. 2015: p. 5378-5383.
22. Wang Memoli, J.S., P.J. Nietert, and G.A. Silvestri, Meta-analysis of guided bronchoscopy for the evaluation of the pulmonary nodule. *Chest*, 2012. 142(2): p. 385-393.
23. Loeve, A., P. Breedveld, and J. Dankelman, Scopes too flexible and too stiff. *IEEE Pulse*, 2010. 1(3): p. 26-41.
24. Leon, M.B., et al., Transcatheter or surgical aortic-valve replacement in intermediate-risk patients. *New England Journal of Medicine*, 2016. 374(17): p. 1609-1620.
25. Barone, D.G., T.A. Lawrie, and M.G. Hart, Image guided surgery for the resection of brain tumours. *Cochrane Database of Systematic Reviews*, 2014. 2014(1).
26. Schwartz, T.H., P.E. Stieg, and V.K. Anand, Endoscopic transsphenoidal pituitary surgery with intraoperative magnetic resonance imaging. *Neurosurgery*, 2006. 58(1 Suppl): p. ONS44-51; discussion ONS44-51.
27. Vieveen, S., Follow-the-leader motion simulation of a continuum manipulator with linear curvature segments, [Master's thesis], Delft University of Technology, Delft, the Netherlands, 2017. Available from <https://repository.tudelft.nl>.



# ACKNOWLEDGMENTS

Het schrijven van een proefschrift is dan wel een persoonlijk project, maar gelukkig sta je er niet alleen voor. Terugkijkend ben ik vooral erg dankbaar voor de grote diversiteit aan mensen waarmee ik de hoogtepunten kon delen en die me hielpen de dieptepunten te dragen. Ter afsluiting wil ik deze personen dan ook graag bedanken.

First I would like to extend my gratitude to the members of the promotion commission, who found themselves willing to read my thesis and take part in my defence. Thank you prof. dr. P. Valdastri, prof. dr. W.J.H.J. Meijerink, prof. dr. ir. J.L. Herder, prof. dr. J. Dankelman, dr. E. van der Poorten en prof. dr. H.E.J. Veeger.

Aan al mijn medeauteurs en de studenten die ik tijdens mijn promotie heb mogen begeleiden, bedankt voor jullie bijdrage aan dit proefschrift.

Gerwin, je opbouwende feedback en handige schrijftips waren een welkome toevoeging. Gezien Paul B. en uiteraard ikzelf erg intensief bij dit project betrokken waren, was het fijn dat jij zo nu en dan als neutrale partij wist op te treden.

Paul, bedankt voor je intensieve begeleiding en uiteindelijk je geduld. Ik heb genoten van onze ontwerp discussies en heb daarin veel van je mogen leren. Het was bijzonder hoe weinig woorden of penstrepen we nodig hadden om van gedachten te wisselen. Desalniettemin hielden de discussies vaak lang aan, iets dat onze betrokkenheid tot het project en gedeelde fascinatie voor mechanismen alleen maar onderstreept.

Aan mijn project-genoten; Ewout, Giada en Costanza. Bedankt voor jullie inhoudelijke bijdrage en prettige samenwerking. Ewout, je louter positieve instelling maakte het een waar genoeg om een bureau met je delen. Giada, starting my first project together with you was a lot of fun and I am grateful for the work we managed to do together. Costanza, it was very motivating to see you picking up where I left off, whilst giving it your own spin.

Aan de technische brigade van DEMO; Menno, David en Remi. Zonder jullie technische kennis en vaardigheden waren de ideeën uit dit werk ook enkel ideeën gebleven. Ontzettend bedankt voor jullie inzet en het vervaardigen van enkele prachtige prototypes! Verder heb ik de talloze flauwe grappen en onnozele geintjes altijd erg kunnen waarderen. Menno's opmerking dat ik liever bij hen in de werkplaats zat dan achter mijn bureau, had dan ook zeker een kern van waarheid in zich.

Aan mijn talloze andere collega's; Bram, Marta, Peter, Awaz, Juan, Frederique, Annetje, Teun, Eline, Bas, Jeroen, Ingrid, Tim, Nick, Tonke, Arjo, Roos, John, Henry, Nadia, Milton, Aimee en Marco, het waren een aantal prachtige jaren en wat hebben we gelachen! De vele te lange koffie pauzes, lunches, First-Fridays-of-the-Months, zinvolle en zinloze discussies,

nerfgun-battles, diners, team-prodent, stapavonden, pannen gin-tonics, promotie-videos, conferenties en de wintersport waren de beste secundaire arbeidsvoorwaarden die ik me ooit had kunnen wensen. Mijn kantoorgenoten, nog specifiek bedankt voor de gezellige en ontspannen werkplek. Eline, bedankt voor je de relativierende (zelf)spot, het managen van al mijn PR-gerelateerde zaken en de introductie tot de Science Battle. Jeroen, bedankt voor de kans bij DigiNova, ik ben erg benieuwd naar jullie ontwikkeling. Jullie allen hebben er aan bijgedragen dat ik me op de universiteit altijd erg op mijn gemak voelde. Hier heb ik me dan ook naar gedragen. Sorry, maar vooral bedankt daarvoor!

De Science Battle crew; Suzanne, René, Patrick en Richard. Het was erg leerzaam en vooral bijzonder leuk om in de Nederlandse theaters te mogen staan. Ga hier vooral mee door!

Aan mijn paranimfen; Bas en Renée. Hoewel de functie van paranimf in de loop der jaren sowieso al aardig wat aan gewicht heeft verloren, is deze in het corona-tijdperk wel erg magertjes. Desalniettemin wil ik jullie toch bedanken voor de geplande inzet. Bas, hoewel we in onze studententijd langs elkaar heen leefden, ben ik heel blij dat ik je post-toko alsnog heb leren kennen. BasEline is altijd welkom voor een diner voor 2+2! Renée, fijn dat je me wilde helpen bij het schrijfproces. Je feedback op mijn werk, en vooral je relativierende woorden hielpen enorm. Ik had je paranimf-droom graag in vervulling laten gaan, maar corona is een Engelse hond van het vrouwelijke geslacht zullen we maar zeggen.

Aan mijn vrienden binnen en buiten de universiteit die allemaal, op hun eigen unieke manier, totaal niets inhoudelijks aan dit werk hebben bijgedragen; jullie worden bedankt! De motorvakanties, Baltische campertour, squashwedstrijden, weekenden Center Parcs, de Dollars, visweekendjes, Rock Werchter, Geheime Liefde, dansfeesten en andere festivals, (3 koningen) borrels, spelletjes avonden, (loser-kerst)diners, Frühlingsfest, carnaval, geplande biertjes, random biertjes en goede gesprekken waren, en zijn, me van ongekende waarde. Dat er van dit alles nog maar veel mag volgen!

Aan mijn familie; Tineke en René, hoewel we de meest uiteenlopende paden bewandelen, weet dat ik altijd naar jullie gedrevenheid heb opgekeken.

Aan mijn ouders, bedankt voor jullie geloof in mij, dat jullie me altijd de ruimte geven om mijn eigen keuzes te maken, me daarin steunen en me op tijden ook de middelen gunnen die daarvoor nodig zijn. Verder ben ik trots op de normen en waarden die ik van huis uit heb meegekregen. In ben in Delft erg gegroeid, maar de basis is in Heeze gelegd.

Lieve Charlotte, woorden schieten me (wederom) tekort, en met deze kun je me écht niet helpen, om je te bedanken voor de manier waarop jij me gedurende mijn promoveren en hernia hebt ondersteund. Je bent het beste, leukste en liefste wat me deze jaren is overkomen. Bedankt dat je er bent.



# CURRICULUM VITAE

## PAULUS WILHELMUS JOHANNES HENSELMANS

*(Born 07-09-1987, Geldrop, the Netherlands)*

### EDUCATION

- 2013 – 2020      Ph.D. Mechanical Engineering  
Delft University of Technology, Delft, the Netherlands  
Department of BioMechanical Engineering,  
BioInspired Technology Group (BITE)
- 2018              Health Physics expert level 5B  
Faculty of Applied Sciences, National Centre of Radiation Protection
- 2016              Digital Operating Room Summer School,  
University Leipzig, Leipzig, Germany
- 2011 – 2013      MSc Mechanical Engineering  
Delft University of Technology, Delft, the Netherlands  
Specialization:      BioMechanical Engineering  
Internship:            Institute for Medical Science and Technology,  
Dundee, United Kingdom
- 2005 – 2011      BSc Mechanical Engineering,  
Delft University of Technology, Delft, the Netherlands  
Minor:                Management, Economics & Law

### AWARDS

- 2014              Innovative Medical Devices Initiative-talent award, first price

### RELEVANT WORK EXPERIENCE

- 2019              Lead Engineer  
DigiNova, Delft, the Netherlands
- 2017 – 2018      Engineer / Project Manager  
Dienst Elektronische en Mechanische Ontwikkeling - Reactor Institute Delft

# PUBLICATIONS

1. **Henselmans P.W.J.**, Culmone C., Jager D., Starkenburg R. van, Breedveld P. The MemoFlex: a non-robotic approach to Follow-the-Leader motion of a snake-like instrument for surgery, submitted to Medical Engineering & Physics.
2. Culmone C. **Henselmans P.W.J.**, Starkenburg R. van, Breedveld P. Exploring 3D-printing for novel compliant surgical devices, submitted to Additive Manufacturing.
3. Ali A., Sakes A., Arkenbout E.A., **Henselmans P.W.J.**, Starkenburg R. van, Szili-Torok T., Breedveld P. (2019). Catheter steering in interventional cardiology: mechanical analysis and novel solution. Proc. Inst. Mech. Eng. Part H: Journal of Engineering in Medicine, 12 p.
4. **Henselmans P.W.J.**, Smit G., Breedveld P. (2019). Mechanical Follow-the-Leader motion of a hyper-redundant surgical instrument: proof-of-concept prototype and first tests. Proc. Inst. Mech. Eng. Part H: Journal of Engineering in Medicine, 10 p.
5. Scali M., Veldhoven P. A. H., **Henselmans P. W. J.**, Dodou D., Breedveld P. (2019). Design of an ultra-thin steerable probe for percutaneous interventions and preliminary evaluation in a gelatine phantom. PLOS ONE Vol. 14, No. 9: e0221165.
6. **Henselmans P.W.J.**, Gottenbos S., Smit G., Breedveld P. (2017). The MemoSlide: an explorative study into a novel mechanical Follow-the-Leader mechanism. Proc. of the Institution of Mechanical Engineers, Part H: Journal of Engineering in Medicine. Vol. 23, No. 12, pp. 1213-1223.
7. Kreeft D., Arkenbout E.A., **Henselmans P.W.J.**, Furth W.R. van, Breedveld P. (2017). Review of techniques to achieve optical surface cleanliness and their potential application to surgical endoscopes. Surgical Innovation, Vol. 24, No. 5, pp. 509-527.
8. Sakes A., Wiel M. van der, **Henselmans P.W.J.**, Leeuwen J.L. van, Dodou D., Breedveld P. (2016). Shooting mechanisms in nature: a systematic review. Plos One, Vol. 11, No. 7, 46 p.
9. Gerboni G., **Henselmans P.W.J.**, Arkenbout E.A., Furth W.R. van, Breedveld P. (2015), "HelixFlex: A Bioinspired Maneuverable Instrument for Skull Base Surgery." Bioinspiration & Biomimetics, Vol. 10, No. 6, pp. 1-17.
10. Jelinek F., Arkenbout E.A., **Henselmans P.W.J.**, Pessers R., Breedveld P. (2015). Classification of Joints Used in Steerable Instruments for Minimally Invasive Surgery – a review of the state of the art. ASME Journal of Medical Devices, Vol. 9, No. 1, pp. 010801-1-010801-11.
11. Jelinek F., Gerboni G., **Henselmans P.W.J.**, Pessers R., Breedveld P. (2015). Attaining high bending stiffness by full articulation in steerable minimally invasive surgical instruments. Minimally Invasive Therapy & Allied Technologies, Vol. 24, No. 2, pp. 77-85.
12. Arkenbout, E.A., **Henselmans, P.W.J.**, Jelinek, F., & Breedveld, P. (2014). A state of the art review and categorization of multi-branched instruments for NOTES and SILS. Surgical Endoscopy, Vol. 29, No. 6, pp. 1281-1296.

## INVITED SPEAKER

1. **Henselmans P.W.J.** (2016). Extending the reach of surgery. Nederlandse Vereniging voor Klinische Fysica, Apr. 9, Woudshote Conferentiecentrum, Zeist, the Netherlands.
2. **Henselmans P.W.J.** (2015), An exciting new way of instrument steering, A day of wonder, Conference Center of Delft University of Technology, Delft, the Netherlands.

## INTERNATIONAL CONFERENCES

1. **Henselmans P.W.J.**, Krijger T., Breedveld P. (2017). A novel mechanism for Follow-the-Leader deployment of flexible surgical instruments. Proc. 6th Dutch Conference of Biomedical Engineering, Jan. 26-27, Egmond aan Zee, The Netherlands, 1 p.
2. **Henselmans P.W.J.**, Krijger T., Breedveld P. (2016). Follow-the-Leader deployment: a mechanical approach. Proc. 28th International Conference of Society for Medical innovation and Technology (SMIT), Oct. 05-08, Delft, the Netherlands, 1 p.
3. **Henselmans P.W.J.**, Gerboni G., Breedveld P. (2015). The HelixFlex: a dexterous instrument for minimally invasive surgery. Proc. 5th Dutch Bio-Medical Engineering Conference, Jan. 22-23, Egmond aan Zee, the Netherlands, 1 p.
4. **Henselmans P.W.J.**, Gerboni G., Arkenbout E.A., Breedveld P. (2014). The HelixFlex 2D: multi-actuation control. Proc. ASME Design of Medical Devices Conference – Europe Edition 2014, Oct. 22-24, TU Aula Conference Centre Delft, Delft, the Netherlands, Abstract 26, 2 p.
5. **Henselmans P.W.J.**, Jager D.J., Hoeven F.H. van den, Breedveld P. (2014). The IFlex: a steerable instrument for eye-surgery. Proc. 26th International Conference of Society for Medical innovation and Technology (SMIT), Sept. 18-20, Shanghai, China, p 96.